SPECIFIC HEAT AND OTHER STUDIES ON SOME PURE AND SUBSTITUTED HTSC CUPRATES

Thesis

Submitted in partial fulfilment of the

requirements for the degree of

Doctor of Philosophy

By

Deepak Varandani

Under the supervision of

Dr. A. K. Bandyopadhyay

BIRLA INSTITUTE OF TECHNOLOGY AND SCIENCE
PILANI (RAJASTHAN) INDIA

1997

BIRLA INSTITUTE OF TECHNOLOGY AND SCIENCE
PILANI (RAJASTHAN)

CERTIFICATE

This is to certify that the thesis entitled "Specific Heat and Other Studies on Some Pure and Substituted HTSC Cuprates" and submitted by Deepak Varandani (ID. No. 92PZYF008) for the award of Ph.D. Degree of the Institute, embodies original work done by him under my supervision.

Signature in full of
the Supervisor A.K. Bandyopadhyay

Name : Dr. A. K. BANDYOPADHYAY

Date: 6.5.97

Designation : Scientist EII
National Physical Laboratory
Dr. K. S. Krishnan Road
New Delhi 110 012

Abstract

The recent discovery of copper-oxide based high temperature superconductors has sparked unprecedented excitement and explosion of research in the field. Proper processing of these materials that will impart desirable properties and shapes is essential to realize significant technological applications. Remarkable advances have been made in understanding and improving the behaviour of high T_c superconductors, and development of prototype devices.

Specific heat is one of the most important parameters in solid state research. The specific heat data provide less dramatic evidence of superconductivity than the resistivity and magnetic measurements, but they show a remarkable anomaly at the transition temperature. In fact specific heat demonstrates unambiguously that the superconducting transition characterizes a sizeable fraction of bulk material and not merely small filamentary regions. The specific heat data of a solid can be used to calculate important parameters like the Sommerfeld constant, Debye temperature etc.

The thesis starts with a description of the various experimental setups used for the different measurements. A detailed account is given of the quasi-adiabatic calorimeter which has been employed for the specific heat measurements. The method of obtaining the temperature rise of the sample under study has been explained in this section and the improved post-heating driftline fitting procedure has been discussed as well.

The thesis is essentially based on the study of resistivity, susceptibility and specific heat of some well characterized high temperature superconductors. A set of erbium based 123 superconductors has been investigated in the pure form and also when Cu is partly (0.5 %) replaced by metallic dopants Ni^{2+}, Zn^{2+}, Fe^{3+}, Co^{3+} and Ga^{3+}. These substitutions are important because the first two dopants occupy the Cu(II) site (in-plane substitution) while the remaining three occupy the Cu(I) site (out-of-plane substitutions). With these substitutions the role of site-dependent substitutional disorder in conjunction with the fluctuation effects is investigated. The results show that, as compared to the in-plane, the out-of-plane substitutions exhibit a domination of fluctuation effects. This has been explained from the fact that out-of-plane disorder substantially decouples the interlayer links between CuO_2 planes across the adjoining unit cells in the c direction. This transforms the system more towards two-dimensions, thereby enhancing the contribution of fluctuations.

The other study is based on the investigation of the role of lead substitution in stabilization of the high T_c 2223 phase in the Bi-based cuprates. Different Pb substituted Bi-2223 samples where lead content is increased systematically have been prepared. These samples have been characterized by x-ray diffraction and high resolution scanning tunneling microscopy. From the resistivity measurements of these samples it is found that the zero resistance temperature shows a peak at a lead content of around 15 at % The susceptibility data of the samples indicate that the high T_c 2223 phase is present in the samples with Pb content (x) of 0.3 to 0.7. But the samples with lead content 0.3 to 0.5 show the presence of the low T_c 90 K Bi-2122 phase as well. The specific heat data indicate a clear anomaly around 90 K for the samples with x = 0.3

to 0.5 confirming the presence of both the phases in these samples with substantial volume fraction. Based on these results, the role of lead substitution in Bi samples, has been discussed.

Finally, a study of the mixed phase samples of Bi-2223 which have been characterized by x-ray diffraction and high resolution scanning tunneling microscopy, has been carried out. The substitutions are aimed to understand the role of disorder in the stabilized high T_c (Bi-2223) phase from the low T_c (Bi-2122) phase in conjunction with the fluctuation effects. It is found that the presence of the low T_c phase modifies the resistivity near T_c of the high T_c phase in a peculiar manner. Excess conductivity and specific heat due to fluctuations are obtained by subtracting the normal state values suitably. The main results of this study are: (1) disorder due to excess Cu reduces resistivity with an enhancement of T_c and also reduces the degree of two dimensionality of the system, (2) disorder in the Sr planes increases resistivity and T_c and also changes the dimensionality of the system a little towards three-dimensionality (3) reduced lead content shows the peculiar form of the resistivity near T_c.

Acknowledgements

I wish to express my deep sense of gratitude to my research supervisor Dr. A. K. Bandyopadhyay, who apart from initiating me into this reaserch field, also provided a constant and expert guidance in carrying out the experimental work as well as in developing an understanding towards the subject.

I am also grateful to Dr. A. V. Narlikar for his encouragement and timely support as the group leader of the Superconductivity Group. His valuable advice from time to time has helped me in bringing my thesis to the present shape.

I wish to thank Professor E. Gmelin, for his keen interest in my work during his visits to our laboratory. The stimulating discussions which I had with him helped me a great deal in understanding the experimental aspects of the specific heat measurements.

I wish to express my sincere thanks to Dr. B. V. Kumaraswamy, Dr. S. K. Agarwal, Dr. U. C. Upreti, Dr. Anurag Gupta, Dr. Ratan Lal, Mr. S. B. Samanta, Mr. V. S. Yadav, Dr. V. P. S. Awana, Mr. P. K. Dutta and Mr. Y. S. Sharma for their constant support and encouragement. Discussions with them helped me in overcoming some of the problems encountered during this period.

I am grateful to my friends V. N. Moorthy, E. P. Haridas, A. T. Nimal and Rajvir Singh for helping me in every possible way during my Ph.D work. I consider myself fortunate to have such devoted friends who have stood by me through thick and thin. I would also like to acknowledge the constant support of my colleagues Kaustav Chakravarty, N. Deepak Kumar, Yudhisther Kumar, D. Sarangi, C. Mukherjee and Mr. Maqsood Ahmed.

I express my gratefulness to the Director, National Physical Laboratory, New Delhi for providing laboratory facilities and also the Council of Scientific and Industrial Research for providing financial assistance during the tenure of my research work.

Words do not suffice to express my indebtedness to my parents and sister, who have stood by me throughout the research period.

Deepak Varandani

(Deepak Varandani)

Contents

List of Figures

List of Tables

Chapter 1

Introduction

1.1 Phenomenon of Superconductivity

Superconductivity is the phenomenon of sudden disappearance of electrical resistance of some materials when they are cooled below a characteristic temperature (T_c) called the transition temperature. This remarkable phenomenon was discovered by K. Onnes in 1911[1] while working to verify his earlier prediction that the resistance of high purity samples should approach zero at the boiling point of liquid helium. Onnes was investigating the behaviour of mercury, the only metal in those days that could be brought to a high degree of purity by multiple distillation. He found that though the resistance did become unmeasurably small, just below 4.2 K, the effect in no way corresponded to the expected reduction in resistance with temperature. It was actually a sudden fall in resistance within a few hundreths of a degree, due to mercury passing into a new state which Onnes called the superconductive state. Afterwards, many elements of the periodic table were found to be superconducting, though some of them become superconducting only under high pressure. Subsequently, many alloys and compounds were also found to be superconducting including the amorphous materials. It is beyond the scope of the present chapter to discuss all the topics relevant to the phenomenon of superconductivity. But some of them which are pertinent to the present work are reviewed briefly.

1.2 Conventional Superconductivity

The term conventional superconductivity is used in reference to the classic superconductors i.e., those studied before 1986, with critical temperatures not exceeding 23 K.

1.2.1 Superconductors in Magnetic Fields

If a superconductor is cooled below its transition temperature and then a magnetic field is applied which is lower than its critical magnetic field, the field is not allowed to penetrate inside it. This is known as the screening effect. In this phenomenon the application of field causes the flow of current due to the induction process in a manner similar to the eddy currents for a normal metal. This current flows as persistent current due to the fact that resistance is zero in the superconducting state and therefore unlike eddy currents it does not decay with time. These persistent currents prevent the penetration of the magnetic field inside the sample. On the other hand, if a superconductor is cooled below its transition temperature in the presence of a magnetic field, then no shielding current is expected to be present. However, it is observed that even in this case all the flux present inside the superconductor is expelled and the material exhibits perfect diamagnetism. This effect was first observed in 1933 by Meissner and Ochsenfeld[2] and is known as the Meissner effect. The phenomenon of Meissner effect along with zero resistance is necessary and sufficient condition to classify a material as a superconductor.

It has been observed that if the strength of the applied magnetic field is increased beyond a certain value, then the superconducting properties of the material are destroyed and it becomes normal. This value of the field is known as the critical magnetic field (H_c)[3]. The superconductivity of the material can also be destroyed by passing through it a current, the magnitude of which is greater than a certain critical value, which is called the critical current (I_c)[4]. The current density or the current per unit area corresponding to the critical current is known as the critical current density (J_c).

1.2.2 Type I and Type II Superconductors

The manner in which a superconductor responds to an externally applied magnetic field determines whether it is a type I or a type II superconductor. An ideal type I superconductor is a perfect diamagnet below its transition temperature. When such a superconductor is subject to a progressively increasing magnetic field, it remains a diamagnet upto its critical magnetic field. Above this, abrupt field penetration occurs and its negative diamagnetic moment increases to a small positive value and the material becomes normal. A typical magnetization curve for a type I superconductor is shown in Fig. 1.1. Generally, pure metals which show superconductivity are type

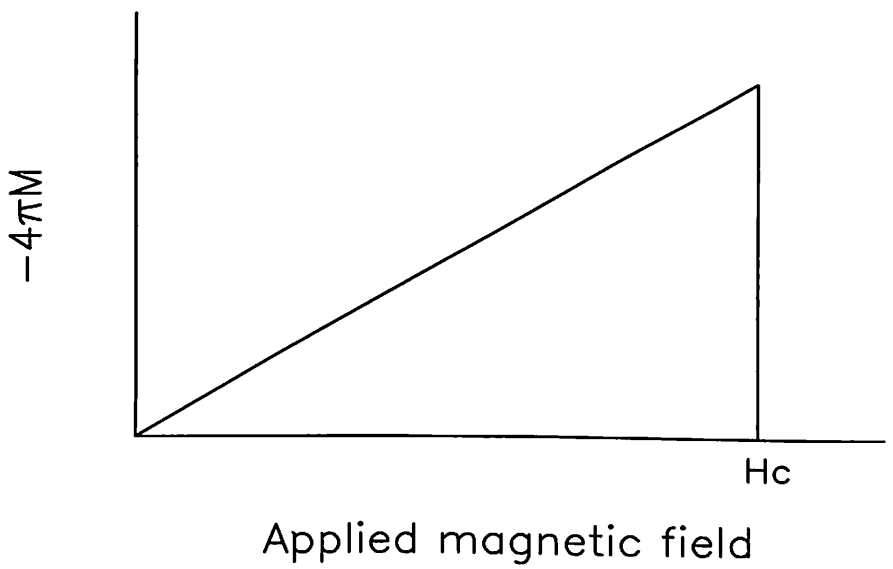

Figure 1.1: Magnetization curve for a type-I superconductor

I superconductors. Sometimes the geometrical shape of a homogeneous type I superconductor can be such that the external applied field though less than the critical field, exceeds the critical field value for some portions of the superconductor. The superconductor in this state, called the intermediate state, splits into superconducting and normalconducting regions.

In materials such as alloys and composite superconductors, on application of field greater than the critical field, superconductivity persists despite penetration of mag-

netic flux lines. These are the type II superconductors. In the superconducting state, the Meissner phase, with complete expulsion of magnetic field similar to that of type I superconductors, is observed only at and below a lower critical field H_{c1}. Above H_{c1}, the vortex state or Abrikosov state[5] in the form of a number of laminae of alternate superconducting and normal states parallel to applied field are observed[6]. In this state, the material shows superconductivity with partial expulsion of magnetic field and magnetization decreases monotonically with increasing external applied field. The fully normal state is restored only at a relatively higher value of external magnetic field, known as the upper critical field H_{c2}. The typical magnetization curve for a type II superconductor is shown in Fig. 1.2.

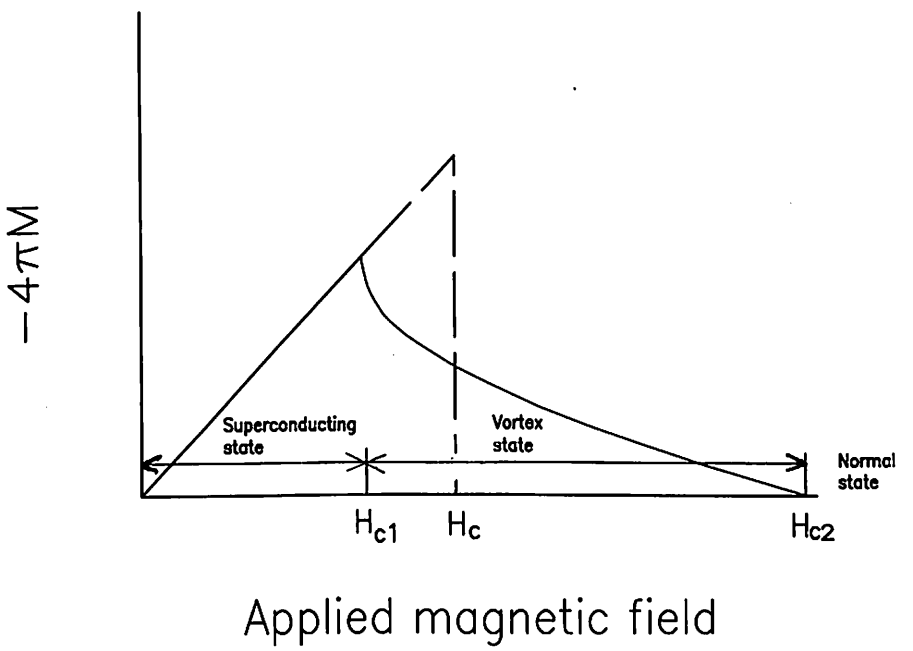

Figure 1.2: Magnetization curve for a type-II superconductor

1.2.3 Theories of Superconductivity

London's theory

This phenomenological theory was proposed by F. and H. London[7, 8] shortly after the discovery of Meissner-Ochsenfeld effect. The London theory is based on two

equations which describe the zero resistance and the Meissner effect.

$$\frac{dJ}{dt} = \frac{ne^2E}{m} \tag{1.1}$$

$$B = -\frac{m}{ne^2}\text{curl}J \tag{1.2}$$

In the above equations m, n and e are the mass, the number per unit volume and charge of the carriers of the supercurrent. In the London theory it was assumed that the current was carried by single electrons. Using the second of the London equations along with the Maxwell equation

$$\text{curl } B = \mu_o J \tag{1.3}$$

it was suggested that the magnetic behaviour of a superconductor might be described by

$$\nabla^2 B = \frac{1}{\alpha}B \tag{1.4}$$

where $\alpha = m/\mu_o ne^2$ and μ_o is the permeability of air. The differential equation has a simple solution

$$B(x) = B_a \exp\left(-\frac{x}{\lambda}\right) \tag{1.5}$$

where B_a is the applied flux density and λ is the penetration depth of the magnetic field into the superconductor.

Penetration depth

The field exclusion from the interior of the sample cannot take place exactly upto the surface of the sample. Because this would imply that the magnetic field at the surface changes from a finite value to zero. This would require infinite current density at the surface which is not possible. Thus, the magnetic field does penetrate inside the superconductor. The screening currents flow in a thin surface layer across which the magnetic field fall to very low levels. From Eq. 1.5 penetration depth can be defined as the distance inside a superconductor over which the magnetic field strength becomes 1/e of its value at the surface.

Ginzburg-Landau theory

A considerable insight into superconductivity on the basis of a two fluid model was obtained by the theory given by Ginzburg and Landau in 1950[9]. In two fluid model it was postulated that normal as well as superelectrons are present at any temperature $T < T_c$. By considering the Gibb's free energy of normal and superconducting states, Ginzburg and Landau found the solutions for order parameter and density of superconducting electrons. The solutions describe several features of superconductors, eg. a characteristic minimum length over which any perturbation in the superconducting order is smoothened out. This is called the coherence length (ξ) of the material. The magnetic field also penetrates the material with a characteristic penetration depth (λ) which is essentially the thickness of the material through which the shielding super currents flow. The most significant insight provided by the G-L theory was the difference between type-I and type-II superconductors. It was shown that if $\xi > \lambda$ and the surface energy between the normal and the superconducting states is positive, the material is type-I, while if $\xi < \lambda$ and the surface energy becomes negative at a field $H_{c1} < H_c$ the material is a type-II superconductor. The G-L theory also gives a dimensionless parameter κ, known as Ginzburg-Landau parameter, expressed as

$$\kappa = \frac{2\sqrt{2}H_c\lambda^2}{hc}.$$

For type-I superconductor $\kappa < 1/\sqrt{2}$ and for a type-II superconductor $\kappa > 1/\sqrt{2}$. It may be mentioned that for a type-II superconductor the parameter H_c is essentially hypothetical and determined by measuring the area of a reversible magnetization curve.

BCS theory

In search of a microscopic theory, Frolich in 1950 pointed out that an electron moving through a crystal lattice has a self energy by virtue of being 'clothed' with virtual phonons. This means that an electron moving through the lattice distorts the lattice, and the lattice in turn acts on the electron by the virtue of the electrostatic forces between them. The oscillatory distortion of the lattice is quantized in terms of the phonons. Thus, interaction between the lattice and the electron is basically a process

of constant emission and reabsorption of phonons by the latter. These are called the virtual phonons. An electron moving through a lattice can be thought of as being surrounded, even at 0 K by a cloud of virtual phonons. This contributes to the electron a self energy which is proportional to the square of the average phonon energy. In turn, this is inversely proportional to the lattice mass. Thus, the condensation energy which is equal to this self energy will have a mass dependence indicated by the isotope effect. Bardeen, Cooper and Schrieffer in 1957 developed the idea into a full theory[10]. They succeeded in showing that the basic interaction responsible for superconductivity appeared to be that of a pair of electrons by means of an interchange of virtual phonons. According to the BCS theory, at absolute zero an electron moving through the lattice with some momentum distorts the lattice and gets scattered, creating a virtual phonon. This phonon is absorbed by a second electron moving with a different momentum at some distance away when it is reached by the propagating fluctuation in the lattice charge distribution. The process being a virtual one, energy need not be conserved, and in fact, the resulting electron-electron interaction depends on the relative magnitudes of the electronic energy change and the phonon energy. If this latter exceeds the former, the interaction is attractive, and the charge fluctuation of the lattice is then such as to surround one of the electrons by a positive screening charge greater than the electronic one, so that the second electron is attracted by this net positive charge. The fundamental postulate of the BCS theory is that superconductivity occurs when such an attractive interaction between two electrons by phonon exchange dominates the usual repulsive Coulomb interaction. The two electrons which form a bound state due to the weak attractive interaction are said to form a cooper pair. The electrons constituting a cooper pair have equal and opposite spin and momentum. In the BCS model the cooper pair formation gives rise to superconductivity. As the temperature is increased, the lattice vibrations acquire sufficient energy to break the pairs and at T_c all the pairs are broken.

According to the theory the Cooper pair formation lowers the energy and the resulting state of lowest energy is referred to as the BCS ground state. The minimum energy required to break a Cooper pair into quasi-particles is found to be 2Δ. Thus,

there exists an energy gap, $E_g = 2\Delta$ in the excitation spectrum of the superconductor, and a radiation of frequency ν is absorbed only if $h\nu > 2\Delta$. From the variation of the energy gap with temperature, the theory also predicts a simple relation between the critical temperature and energy gap given by

$$E_g(0) = 2\Delta(0) = 3.5k_BT_c. \tag{1.6}$$

At temperatures below about $0.6T_c$, the energy gap is substantially independent of temperature. The number of pairs broken up at a finite temperature T is proportional to $\exp[-\Delta(0)/k_BT]$.

Coherence length

The difference between the normalconducting and the superconducting region of a material lies in the fact that the Cooper pair density in the normalconducting region is zero and it is finite in the superconducting region. This density is dependent on the temperature and the nature of the material. The Cooper pair density $n_c(T)$ cannot change suddenly from a finite value to zero at the phase boundary of the normal and the superconducting region. The strong correlations between Cooper pairs requires them to vary spatially. This can occur only over a distance that is larger than a characteristic length, which is known as the coherence length ξ_{GL}.

1.2.4 Fluctuations

The superconducting transition is characterized by a mean non zero value of the order parameter below the transition temperature. Above the transition temperature the mean value of the order parameter is zero. There are fluctuations in the order parameter about the values both above and below the transition temperature. Thus there is a probability of Cooper pair formation even above the transition temperature. The static properties like diamagnetism and specific heat and the dynamic properties like electrical conductivity both are affected by these fluctuations both above and below T_c. The effect of thermodynamic fluctuations on most of these properties is around T_c and the region very close to and above T_c is known as the dynamical

critical fluctuation regime.

Because of the large coherence length and low T_c the fluctuation contribution in the conventional superconductors is reduced and the temperature range over which this contribution can be detected is limited. In fact in conventional superconductors the dynamical critical region is very close to T_c and is inaccessible experimentally.

1.3 High Temperature Superconductors

J. G. Bednorz and K. A. Muller in 1986 were working on the hypothesis that substances with pronounced Jahn-Teller effect (which signifies the displacement of an ion from a highly symmetrical state with respect to its surroundings) could be superconducting with particularly high transition temperatures. They began with a study of compounds based on Nickel and Aluminium containing perovskites, such as mixed crystals of $LaNiO_3$ and $LaAlO_3$, since Ni^{3+} and Al^{3+} in an octahedron of oxygen atoms exhibit a large Jahn-Teller effect. However, superconductivity was not observed in these groups of substances. Then they started working on copper oxides, such as $LaCuO_3$, since Cu^{2+} also shows a large Jahn-Teller effect in an octahedron of oxygen atoms. They began with an investigation of the compound with formula $Ba_xLa_{5-x}Cu_5O_{5(3-y)}$ by changing its Ba content. After a few months they succeeded in making a sample which showed a steep drop in resistance above 30 K. They were able to identify the phase responsible for the peculiar behaviour as having the composition La_2CuO_4 and also found out that the resistance drop shifted to lower temperatures on passing larger currents[11]. The possibility of superconductivity in this compound was confirmed by Takagi et al.[12]. The compound $La_{2-x}Ba_xCuO_4$ which has K_2NiF_4 structure, was confirmed to be superconducting. These studies triggered a flood of research in HTSCs to understand the origin of high value of T_c and to find out other superconducting materials. It was found that the superconductors with transition temperatures above 40 K could be prepared from the system La-Sr-Cu-O which is essentially the composition used by Bednorz and Muller, with Sr replacing Ba[13]. Attempts on substitution of Y at La site led Wu et al.[14] to discover the su-

perconducting Y-Ba-Cu-O system with a transition temperature of around 90 K. The identification of the superconducting phase was performed by Siegrist et al.[15] and it was found to have the composition $YBa_2Cu_3O_{7-\delta}$ (Y-123 or YBCO) with a oxygen deficient triple perovskite structure. The superconductors of the systems La-Sr-Cu-O and Y-Ba-Cu-O were also discovered simultaneously and independently in Beijing by Z. X. Zhao and his co-workers[16]. The studies of substitutions in the 123 structure established[17, 18] that all but a few (cerium and terbium) of the lanthanide series could be incorporated fully in the structure at the yttrium site. Out of the structures that could be formed only $PrBa_2Cu_3O_{7-\delta}$ is not superconducting[19, 20]. For the remaining structures transition temperatures of the order of 91-95 K have been reported for the fully substituted structures. Following the observations of superconductivity in the Y-123 system, this phenomenon was observed in rare earth free ceramic oxides like Bi-Sr-Ca-Cu-O (BSCCO)[21] and Tl-Ca-Ba-Cu-O (TBCCO)[22]. Structural investigation by Sunshine et al.[23] in Bi-based compounds and Hazen et al.[24] in Tl-based compounds showed the presence of multiple phases (all with layered structure), with one, two or three Cu-O layers. It was observed that T_c depended on the number of Cu-O layers present in these systems. Recently Hg-based compounds Hg-Ca-Ba-Cu-O[25, 26] with T_c of 135 K have been discovered. The discovery of mercury-based compounds exhibiting such high T_c values has stirred considerable interest. These compounds have compositions $HgBa_2Ca_{n-1}Cu_nO_{2n+2+\delta}$. At atmospheric pressures they have T_c values of 94 K, 128 K and 134 K for n = 1, 2 and 3 respectively. The highest value of the transition temperature currently is 164 K, shown by the n = 3 compound under pressure.

The High Temperature Superconductors (HTSCs) share a common phenomenology with the conventional superconductors, eg., zero resistance, diamagnetic effects (HTSCs are type II superconductors), specific heat anomaly etc. In addition, they do possess some distinct and characteristic properties of their own. These superconductors are anisotropic in character in contrast to the isotropic conventional superconductors. The Bi-based cuprates are highly anisotropic while in $Y_1Ba_2Cu_3O_{7-\delta}$ and $La_{2-x}Sr_xCuO_4$ anisotropies are doping-dependent. These properties lead to certain

phenomenon not generally observed in conventional superconductors, such as superconducting fluctuations, 2D-3D dimensional crossover effects and 2D pancake vortex formation. The coherence length of the HTSC materials (0.5-30 Å) is much smaller than that of the conventional superconductors ($10^3 - 10^4$ Å). Also, the HTSC materials have a granularity on a length scale of 1 micron. In general, these compounds have a orthorhombic or tetragonal crystal structure. The common feature in the structure of these superconductors is the presence of the highly conducting CuO_2 planes, where superconductivity is supposed to reside. It is generally assumed that the normal and superconducting state properties of the layered high T_c cuprates derive from the charge and the spin dynamics in the CuO_2 planes, while the other structural components in the unit cell function either as inert spacers or as charge reservoirs that regulate the charge density in the CuO_2 planes. Among the HTSC materials the 123 superconductor has been investigated the most as it is a stable and a single phase system. The presence of anisotropy in transport properties (resistivity and transport J_c), coherence length, penetration depth and H_{c2} is a unusual feature of the HTSC cuprates. In the case of YBCO the resistivity near the transition temperature in c direction has been reported to be nearly two orders of magnitude larger than that in the ab plane[27, 28]. On the other hand, for Bi-2212 the c-axis resistivity is around 10^5 times larger than the ab-plane resistivity[29, 30]. The observed value of anisotropy of J_c and H_{c2} is also as high as 1:10 in the two perpendicular directions even in polycrystalline samples, whereas most conventional superconductors are nearly isotropic[31]. A large J_c is observed for single crystals as compared to the polycrystalline materials whereas in a conventional type II superconductor like Nb_3Sn, a high density of crystal defects is the prime requirement for high J_c.

1.3.1 Structure of RBaCuO (R=Y or rare earths) system

The structure of $R_1Ba_2Cu_3O_{7-\delta}$ (R = Y or rare earths) is shown in Fig. 1.3. The superconductor has a layered oxygen deficient triple-perovskite structure. It can be viewed as ($BaCuO_3$)-($RCuO_3$)-($BaCuO_3$), with oxygen vacancy ordering. The copper atoms occupy two different positions with respect to their oxygen environment. One of

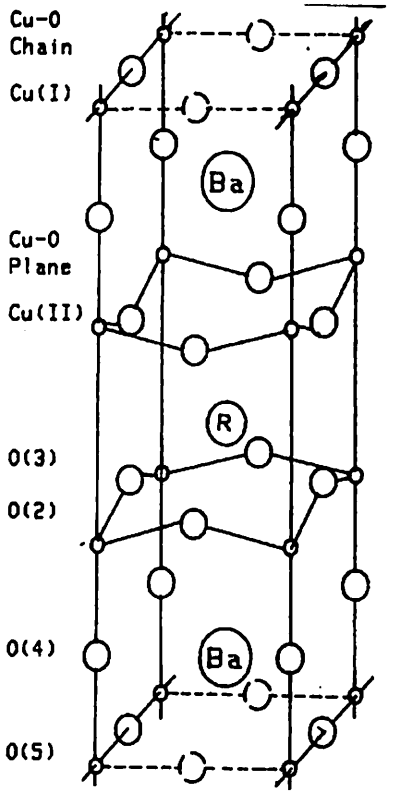

Figure 1.3: Crystal structure of $R_1Ba_2Cu_3O_{7-\delta}$ (R=Y or rare earths) unit cell

the copper positions is at the base of a square-pyramidical arrangement where oxygen atoms form the edges of the pyramid. The sixth position of the oxygen octahedron is not occupied (along the yttrium plane). These pyramids are joined at the corners forming layers. The other copper position is at the centre of a square pyramidical arrangement with four oxygen atoms at the corners. These form the Cu-O-Cu-O chains along the b axis. But there are no oxygen atoms between the copper ions along the a axis. This causes the structure to be orthorhombic with the b parameter slightly larger than the a parameter. The copper atoms of the Cu-O chains are designated as Cu(I) and those in the planes are referred to as Cu(II). In addition to the highly conducting CuO_2 planes and the CuO chains, the RBaCuO structure also has the insulating BaO and R planes. The apparent mixed valence of Cu and the two dimensional CuO_2 networks have been identified as important ingredients responsible for superconductivity in the ceramic oxides and in particular for the RBaCuO system. The copper valence is controlled by the oxygen content in the 123 system, and as such, oxygen vacancy and

order is related directly with the transition temperature. The variation of transition temperature with δ is shown in Fig. 1.4. The behaviour is very interesting as there are two plateaus corresponding to transition temperature values of 90 K and 60 K. The first plateau is in the oxygen content range of 7 to 6.8 and second in the range 6.6 to 6.4. The 90 K phase is known as the ortho-I phase and the 60 K phase is referred to as the ortho-II phase. As oxygen content decreases, the transition temperature

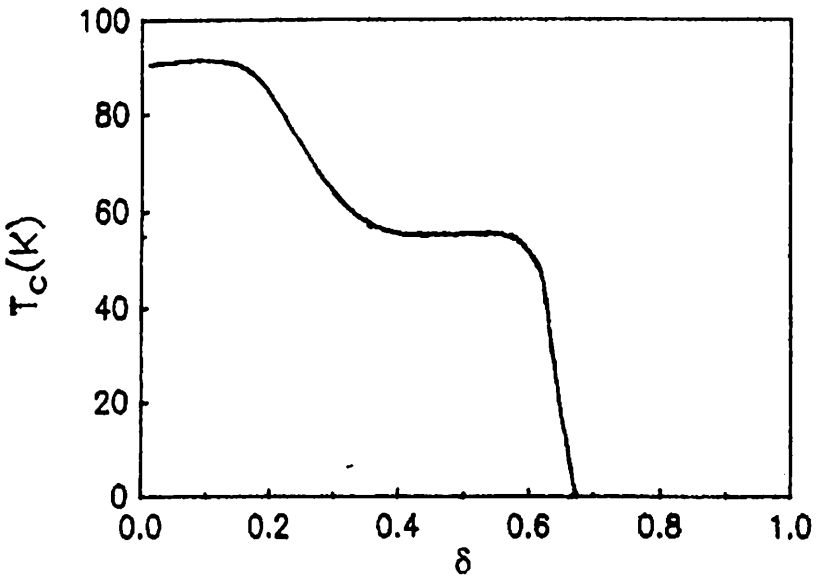

Figure 1.4: T_c vs δ in $R_1Ba_2Cu_3O_{7-\delta}$

drops from its upper limit of about 90 K (at $\delta = .05$) and the superconductivity gets quenched at a oxygen content of around 6.4. The variation in the oxygen content can be brought about by heating in vacuum or in presence of gases like nitrogen or argon at appropriate temperatures. The mobile oxygen is rapidly inserted or extracted from the Cu(I) chains and the structure changes smoothly with oxygen concentration through orthorhombic-tetragonal transition at the oxygen content of 6.27. The coordination number of the Yttrium ion is 8 (due to missing oxygen in the Y-plane), unlike in the case of a ideal perovskite where its coordination number should be 12. Similarly, in a fully oxygenated sample the coordination number of barium is 10.

1.3.2 Structure of Bi-2122 superconductor

The idealized crystal structure of Bi-2122 compound is shown in Fig. 1.5. The structure is built up of different layers of atoms. The two Bi-O layers form a rock salt (NaCl) type structure. These layers are quite weakly bonded together to form the cleavage planes of the material. The rock-salt arrangement is extended on either sides by the additional layers of SrO. Between the two rocksalt structures there is

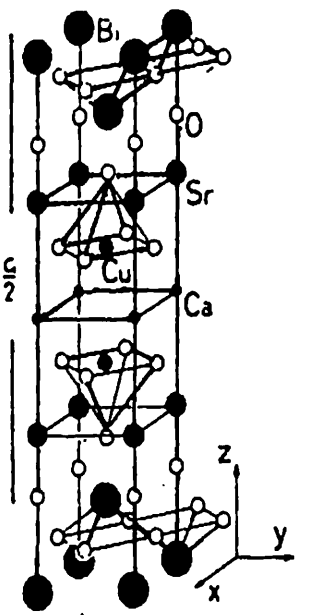

Figure 1.5: Unit cell of $Bi_2Sr_2Ca_1Cu_2O_8$

a perovskite block containing two CuO_2 planes and a Ca plane in the middle. Each copper atom has four coplanar oxygen neighbours. Another more distant oxygen atom in the adjacent SrO plane completes the square pyramidal arrangement. The double copper layers are very similar to those found in RBaCuO system. Unlike the 123 system there are no CuO chains in Bi-2122. The Bi atoms have octahedral coordination with the neighbouring oxygen atoms. The structure of the system is pseudotetragonal with a=b=5.4 Å and c=30.67 Å. The structure essentially comprises two demi unit cells of c/2=15.3 Å, each containing single molecule of Bi-2122. The two demi unit cells are displaced with respect to each other by b/2. The real structure of Bi-2122 as revealed by electron diffraction studies shows departures from the idealized structure

discussed above. One of the important deviations is the presence of structural features (modulation) along the b direction having a much greater length scale than the 5.4 Å repeat distance of the basic building block. These are related to a superstructure with a lattice spacing five times larger (27 Å) in the b direction.

1.3.3 Structure of Bi-2223 superconductor

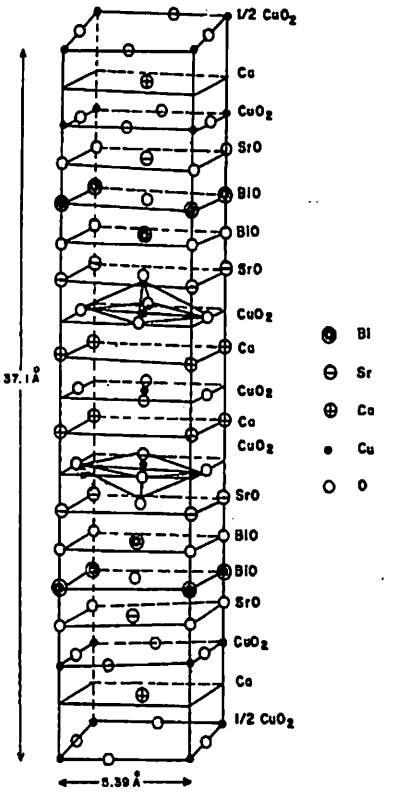

Figure 1.6: Unit cell of $Bi_2Sr_2Ca_2Cu_3O_{10}$

The structure of Bi-2223 is shown in Fig. 1.6. Compared to Bi-2122 this structure possess an additional CuO plane and a Ca layer. The additional Cu in this system has square planer coordination with the neighbouring oxygen atoms. The structure of the compound is pseudotetragonal with a=b=5.4 Å and c=36 Å . Other features of the system are similar to the Bi-2122 compound.

1.4 Heat Capacity of Solids

The heat capacity C of a system of arbitrary mass m is defined in terms of the following limit

$$C = \lim_{\Delta T \to 0} \frac{\Delta Q}{\Delta T} \tag{1.7}$$

where ΔQ is the quantity of heat that must be added to the system to raise its temperature by an amount ΔT. In order to obtain a quantity that is independent of mass, the above equation is divided by the system mass to yield the specific heat capacity, or more simply the specific heat

$$c = \frac{C}{m} = \frac{dq}{dT}, \tag{1.8}$$

where dq is the quantity of heat required to raise the temperature of a unit mass of the system by an amount dT. In general, the required quantity of heat will depend upon the temperature of the system as well as the changes that may occur in other physical properties of the system during the temperature rise. There are two principal specific heats, one defined at constant pressure and the other at constant volume:

$$c_p = \left(\frac{dq}{dT}\right)_p \tag{1.9}$$

and

$$c_v = \left(\frac{dq}{dT}\right)_v \tag{1.10}$$

respectively. In most theoretical calculations, the natural quantity to calculate is the 'heat capacity per mole' since this refers to a fixed number of particles. This quantity is also a 'specific heat capacity' and, consequently, it is also referred to as the specific heat or molar specific heat. The molar specific heats will be denoted by upper case symbols and are defined as:

$$C_p = \left(\frac{dQ'}{dT'}\right)_p \tag{1.11}$$

and

$$C_v = \left(\frac{dQ'}{dT'}\right)_v \tag{1.12}$$

where dQ′ is the quantity of heat required to raise the temperature of one mole of a substance by an amount dT′ under conditions of constant pressure and constant volume respectively. Though C_v is a more fundamental quantity than C_p, but from the experimental point of view C_p is easier to determine. They are related by $C_p - C_v = 9\alpha^2\beta VT$ where α is the temperature coefficient of thermal expansion, V is the volume and β is the bulk modulus of the solid. The difference between C_p and C_v is small for solids and may be neglected.

In a solid the contribution to the heat capacity arises both from the vibrations of the lattice and from the free electrons. Thus, the total heat capacity is a sum of the two contributions. It must be mentioned that in the case of magnetic solids there is a large contribution to the heat capacity over the temperature range in which magnetic moments become ordered. This is because a change in the degree of order means a change in entropy and thus a contribution to the heat capacity. Below 0.1 K the ordering of the nuclear moments may give rise to very large heat capacities as well.

The measurement of heat capacity is a major technique of physical investigation for the understanding of materials, because heat capacity can be calculated ab initio from the model of a physical system. Ruhemann[32] suggests that more significance can be attached to heat capacity measurements than to any other investigation, at least at low temperatures. Even at high temperatures, these measurements are useful in understanding many physio-chemical phenomenon. The heat capacity is the temperature coefficient of the average energy of the system and can be readily used as a test for any model or theory, though C_p is an averaged quantity so that its measurement cannot directly shed any light on the finer details of the model[33].The specific heat (heat capacity per unit mass) reflects the distribution of energy levels of a physical system. The ensemble of energy levels, expressed by the density of states, leads directly to the partition function from which the heat content is derived by differentiation with respect to temperature. The inverse of this procedure is not possible even for most accurate measurements. But information can be obtained on the level structure by experimental specific heat data.

1.4.1 Lattice Specific Heat

Dulong and Petit[34] measured the specific heat of 13 solid elements near room temperature and found out that the product of specific heat per unit mass at constant pressure and the atomic weight of the element is approximately a constant, and is about 6 cal.(g-at)$^{-1}$deg^{-1}. Thus, based on these observations they formulated the 'Dulong-Petit law' which states that the heat capacity per atom is about the same for different elements. This law was generalized in the form of 'Kopp-Neumann law' according to which the heat capacity per gram molecular weight of a chemical compound is equal to the sum of the heat capacities per gram atomic weights of the constituent atoms. Thus the diatomic and triatomic solids were expected to have specific heats of about 12 cal.(g-at)$^{-1}$. deg^{-1} and 18 cal.(g-at)$^{-1}$ deg^{-1} respectively.

A theoretical explanation of the Dulong and Petit's law was first given in 1871 by Boltzmann[35] on the basis of his law of equipartition of energy. This law states that for a system in thermal equilibrium, each degree of freedom contributes 1/2 k_BT to the average energy of the system. If an atom is considered to be a three dimensional harmonic oscillator then its average kinetic energy is 3/2 k_BT. According to Virial theorem, a particle moving in a parabolic potential well has an average total energy twice its kinetic energy, in this case $3k_BT$. Hence, the specific heat of a atom at constant volume is $3k_B$ and per mole it is $3Nk_B$ (N is the Avogadro number) or 3R ($\approx$ 6 cal.(g-at)$^{-1}$deg^{-1}). For a compound containing n atoms per molecule, the above argument can be extended to yield $C_v = 3nR$. Thus, for diatomic and triatomic solids with n equal to 2 and 3 respectively, the molar specific heat has the value 12 and 18cal.(mol)$^{-1}$deg^{-1} respectively. Nevertheless, exceptions to the Dulong-Petit rule do exist like in the case of silicon, boron and diamond which have specific heats of about 20, 11 and 8 J.mol^{-1}.K^{-1}, respectively, near 300 K. Later measurements by Weber[36] on diamond over a temperature range of 200 to 1300 K established that specific heat of all the substances approaches the Dulong-Petit value at sufficiently high temperatures. Experiments at low temperatures led Nernst[37] and others to suggest that specific heat of solids must tend towards zero as the absolute zero of temperature

is approached. It was thus realized that the classical theory which predicts a constant specific heat down to low temperatures was not sufficient to describe the behaviour of a solid. This must be explained by the quantum theory. Einstein[38] assumed that a crystal containing N atoms can be treated as a combination of 3N one dimensional harmonic oscillators. He assumed that the atoms vibrate independently of each other and with the same frequency because of the assumed identical surroundings. Einstein's theory gave the specific heat at constant volume as,

$$C_v = 3R(\theta_E/T)^2 \exp(\theta_E/T)[\exp(\theta_E/T) - 1]^2 \qquad (1.13)$$

where $\theta_E = \hbar\omega/k_B$ is the characteristic temperature known as the Einstein temperature, ω is the frequency of the oscillating atom, k_B is the Boltzmann's constant and $\hbar$ is the reduced Planck's constant. At high temperatures Eq. 1.13 reduces to the Dulong-Petit value. Further, at low temperatures the expression for specific heat reduces to

$$C_v = 3R\left(\frac{\hbar\omega}{k_B T}\right)^2 \exp\left(-\frac{\hbar\omega}{k_B T}\right) \qquad (1.14)$$

Therefore, as $T \rightarrow 0$, $C_v \rightarrow 0$ because of the exponential term. This theory was able to explain the decrease in specific heat with temperature, but the work of Nernst and others[39] showed that while the low-temperature behaviour predicted by Einstein model was qualitatively correct, the specific heat of real solids did not decrease as rapidly with decreasing temperature as predicted by Einstein. The major drawback in this theory was that Einstein had assumed each atom to be an independent harmonic oscillator, oscillating with a frequency ω. But, actually, the atoms oscillate relative to their neighbours in the lattice. For wavelengths which are long relative to lattice spacings, the motion of atoms is hardly independent and large regions of crystal move together coherently. The long wavelength motions have low frequencies and these are particularly important at low temperatures.

Debye[40] considered this situation and realized that it was possible to propagate waves through solids covering a wavelength region extending from low frequencies (sound waves) upto short waves (infrared absorption). The essential difference between the Einstein and the Debye model is that Debye considered the vibrational

motion of a crystal as a whole. He assumed that the continuum model could be employed for all possible vibrational modes of the crystal. For wavelengths which are long as compared to the interatomic spacings the crystal can be considered as a elastic continuum from the point of view of the wave. The fact that crystal consists of atoms is taken into account in Debye theory by limiting the total number of vibrational modes to 3N. Thus, the frequency spectrum corresponding to perfect continuum is cut off so as to comply with the condition of the total number of modes being 3N. The cut off procedure leads to a maximum frequency ω_D common to the transverse and longitudinal waves. The frequency distribution function in the Debye theory is given as $f(\omega)d\omega \sim \omega^2 d\omega$. Debye obtained the specific heat per gram-atom as

$$C_v = 9R(T/\theta_D)^3 \int_0^{x_{max}} \frac{e^x x^4}{(e^x - 1)^2} dx \qquad (1.15)$$

where $\theta_D = \hbar\omega/k_B$ is known as the Debye temperature and $x_{max} = \theta_D/T$. At high temperatures, $x = \hbar\omega/k_B T$ is small, and so the integral reduces to $\int x^2 dx$ yielding the Dulong and Petit value of 3R for the specific heat. At low temperatures, x is large and so the upper limit x_{max} can be considered to be infinity. The integral in Eq. 1.15 with ∞ as the upper limit has the value $4\pi^4/15$. Accordingly, the following expression is obtained for the low temperature specific heat

$$C_v = \frac{12}{5}\pi^4 R\left(\frac{T}{\theta_D}\right)^3 \qquad (1.16)$$

The cubic expression should hold up to a temperature of about $\theta_D/10$. As mentioned, in the Debye treatment the range of frequencies is limited to some maximum or cut-off frequency ν_D and corresponding to this frequency is defined the Debye temperature $\theta_D = h\nu_D/k_B$. According to the Debye theory the Debye temperature should have a constant value. However, in order to accurately fit the Debye model to the experimental specific heat data of a solid, the θ_D value has to be varied with temperature which implies that one or more of the approximations made in the derivation of the Debye theory may not be valid. In general the $\theta_D(T)$ functions for different solids exhibit a number of similar features. At temperatures below $\theta_D/50$, the Debye temperature becomes essentially constant and is approximately equal to its limiting value

at absolute zero. At very high temperatures, all the vibrational modes are excited and thus, θ_D is expected to be constant. In many solids, this is approximately true at temperatures above $\theta_D/2$. At intermediate temperatures, however, θ_D varies somewhat, often passing through a minimum.

1.4.2 Electronic Specific Heat

The conduction electrons in normal metals are Fermions and they obey Fermi-Dirac statistics. These statistics play a fundamental role in determining the temperature dependence of the electronic contribution to the specific heat. As the temperature is decreased, only those electrons which have energy very close to the Fermi energy E_F are able to change their state. Therefore, there is only a very slight increase in the electron energy distribution, implying thereby that electronic specific heat is very small. Thus, the contribution of electrons to the total specific heat of a metal is negligible at room temperatures when the lattice contribution is quite high. The electronic specific heat may be expressed to a first approximation as

$$C_e = \frac{\pi^2}{3} n(E_F) k_B^2 T \equiv \gamma T \tag{1.17}$$

In the above equation $n(E_F)$ is the electron density of states (EDOS) at E_F and γ is called the Sommerfeld constant. A linear variation of electronic specific heat is observed in all normal metals. At room temperature electronic specific heat is only about 1 per cent of the lattice specific heat. But, at low temperatures it becomes quite important because then the lattice specific heat has a T^3 variation. Thus, the lattice specific heat decreases much faster than the linearly varying electronic specific heat.

1.4.3 Specific Heat at Low Temperatures

In the liquid-helium region the two specific heats are usually comparable with one another. So, the total specific heat can be written as,

$$C_v = \gamma T + \beta T^3. \tag{1.18}$$

In the above equation $\beta = 12\pi^4 R(\theta_D)^{-3}/5$. At low temperatures there is no significant difference between C_p and C_v. Thus, the experimental results are usually analyzed

by fitting the values of C_p/T vs T^2 to a straight line by the method of least squares, yielding values of slope β (and hence the Debye temperature) and intercept γ.

1.5 Specific Heat of Superconductors

A system is completely determined thermodynamically if we can specify a suitable thermodynamic function for it, called the Gibbs function. Internal energy (U), free energy (F) and free enthalpy (G) are important Gibbs functions which are given by:-

$$dU = TdS - PdV$$

$$F = U - TS$$

$$G = U - TS + PV$$

In the above listed equations U is the internal energy, V is the volume, P is the pressure, S is the entropy, F is the free energy and G is the free enthalpy of the system. Entropy (S) is one of the most important parameters associated with the thermodynamic treatment of a solid. It is defined as $S = -\left(\frac{\partial G}{\partial T}\right)_{H,P}$, where H is the applied magnetic field. Also the specific heat is related to the entropy by the relation $C_p = T\left(\frac{\partial S}{\partial T}\right)_{P,H}$. Thus

$$C_p = T\left(\frac{\partial S}{\partial T}\right)_{P,H} = -T\left(\frac{\partial^2 G}{\partial^2 T}\right)_{P,H} \tag{1.19}$$

The difference between the free enthalpy of a material in the superconducting (G_s) and the normal (G_n) states is given by

$$G_n - G_s = V\frac{H_c^2}{2\mu_o} \tag{1.20}$$

In the above equation H_c is the critical field which is given by $H_c(T) = H_c(0)[1 - (T/T_c)^2]$, where $H_c(0)$ is the critical field at T = 0 K and V is the volume of the material which is regarded as a constant. Thus, using Eqs. 1.19 and 1.20 the relation between the normal state and superconducting state specific heats (C_n and C_s respectively) is obtained, and this is given by

$$C_n - C_s = -\frac{VT}{\mu_o}\left[\left(\frac{\partial H_c}{\partial T}\right)^2 + H_c\frac{\partial^2 H_c}{\partial^2 T}\right] \tag{1.21}$$

From the expression for the critical field it is clear that at $T = T_c$ the critical magnetic field is zero. Therefore, at the transition temperature Eq. 1.21 gives

$$(C_s - C_n)_{T = T_c} = \frac{VT_c}{\mu_o}\left(\frac{\partial H_c}{\partial T}\right)^2_{T = T_c} \tag{1.22}$$

This relationship is called Rutgers formula[41]. It is clear from this relation that at T_c, $C_s > C_n$ and so on going from the normal to the superconducting state the specific heat shows a discontinuity or a jump at the transition temperature. On the other hand, from the definition of the entropy it is clear that the difference between the normal state entropy (S_n) and superconducting state entropy (S_s) is given by

$$S_n - S_s = -\frac{V}{\mu_o}H_c\left(\frac{\partial H_c}{\partial T}\right). \tag{1.23}$$

Thus since at the transition temperature the critical magnetic field $H_c = 0$, therefore, from Eq. 1.23 it is apparent that the entropy is invariant at the point of transition from the normal to the superconducting state. The specific heat, on the other hand, shows a jump in the specific heat. This can be expressed by the two equations:

$$\left(\frac{\partial G}{\partial T}\right)_n = \left(\frac{\partial G}{\partial T}\right)_s \text{ and } \left(\frac{\partial^2 G}{\partial T^2}\right)_n \neq \left(\frac{\partial^2 G}{\partial T^2}\right)_s \tag{1.24}$$

A phase transition which satisfies the above two equations, is called a second order phase transition. Thus, the superconducting phase transition is a second order phase transition.

Since $\partial^2 H_c/\partial T^2 < 0$ and $(\partial H_c/\partial T)^2$ becomes ever smaller as the temperature is reduced we have a temperature $0<T<T_c$, where $C_s = C_n$. The specific heat of a conductor in the normal state is due to two different contributions. First is the contribution of the conduction electrons C_{ne} and second is the contribution due to the lattice vibrations C_{ng}. Similarly in the superconducting state there is a contribution of the electrons C_{se} and a contribution due to the lattice C_{sg}. The jump in the specific heat observed for the superconductors can be ascribed to the electron system, because the lattice contribution is practically invariant across the superconducting transition. Thus, from Eq. 1.21 the relation

$$C_{se} - C_{ne} = \frac{VT}{\mu_o}\left[\left(\frac{\partial H_c}{\partial T}\right)^2 + H_c\frac{\partial^2 H_c}{\partial T^2}\right] \tag{1.25}$$

is obtained. The temperature dependence of the specific heat in the superconducting state is very well approximated by a parabola of third order $C_s(T) \propto T^3$. This dependence yields the parabolic law for temperature dependence of the critical magnetic field. For T→0 the BCS theory predicts $C_{se} = 9.17\gamma T_c \exp\left(-\frac{1.5T_c}{T}\right)$. This exponential dependence has actually been observed and it is a direct proof of the existence of energy gap in the superconductors.

1.6 General Features of Specific Heat of HTSCs

In the case of the cuprates the transition temperatures are quite high as compared to the conventional superconductors. Thus, near the transition temperature the lattice specific heat is high as compared to the electronic specific heat. Consequently, the jump in the specific heat at the transition temperature is only a small percent of the total specific heat. Furthermore, the value of the upper critical field H_{c2} is very high for the HTSCs. It is therefore not possible to quench superconductivity and measure the normal state specific heat down to liquid helium temperatures, a method which has been routinely used in the case of conventional superconductors for the determination of important parameters like the Sommerfeld constant and the Debye temperature. The result is that the analysis of the experimental specific heat into C_{en}, C_{ng} and C_{es} is not possible for the HTSCs.

1.6.1 Specific Heat in The Low Temperature Region

There are two contributions to the low temperature specific heat that set the cuprates apart from the conventional superconductors. These are :

(i) Low temperature upturn in the specific heat data.

(ii) Linear term in the low temperature data.

The low temperature upturn in the specific heat at zero applied magnetic field is the high temperature tail of the Schottky anomaly. The magnetic field (H) and temperature (T) dependencies of this upturn are those expected for the Cu^{2+} magnetic

moments which for H = 0 order in the vicinity of 0.1 K under the influence of internal interactions. When a field is applied which is large enough compared to the internal interactions, the upturn becomes a Schottky anomaly. The concentration of the Cu^{2+} moments associated with this feature can be determined by the in-field-data. Since the distribution of the internal field broadens the anomaly relative to a Schottky anomaly, the high temperature tail is not well represented by the T^{-2} dependence characteristic of a magnetic anomaly and requires additional terms in negative powers of T.

The linear term for the HTSCs is given by $\gamma(H)T$. The field dependence of this term is represented by

$$\gamma(H)\ T\ =\ \gamma(0)\ +\ \left(\frac{d\gamma}{dH}\right) H \tag{1.26}$$

In the above equation $\frac{d\gamma}{dH}$ is independent of H within experimental uncertainty. The measurements on $La_{2-x}Sr_xCuO_{4-y}$ and on $Y_1Ba_2Cu_3O_{7-\delta}$ have revealed the existence of a linear term in the temperature range of 1-10 K. In YBCO $\gamma(0)$ is reported to vary from 20 mJ/mole K^2 to as low as 3 mJ/mole K^2[42–45]. The low temperature specific heat of $Y_1Ba_2Cu_4O_8$ has been studied by Junod et al.[46] and they have shown that the specific heat of this material in the range 1.4 K to 7 K can be fitted to a formula $C_v\ =\ \gamma\ T\ +\ \beta\ T^3\ +\ \delta\ T^5$ to give a γ value of about 4.9 mJ/mole K^2. The authors, however, stress that there is no clear evidence that the linear term exists in the material. In case of Bi- based superconductors various authors have concluded that there is no linear term in the low temperature specific heat data[47–49]. In the TBCCO system the $\gamma(0)$ values range from 0 to 63 mJ/mol. K^2.

Thus, within experimental error $\gamma(0) = 0$ for nearly all the BSCCO samples (single crystal or polycrystalline), while $\gamma(0)$ is finite for YBCO, LMCO (M = Ca, Ba, Sr) and for some, but not all, TBCCO samples. For YBCO it has been shown[50] that $\gamma(0)$ can be interpreted as arising partly due to[51] presence of some form of $BaCuO_2$, present as a impurity phase, and partly because of normal material interspersed with superconducting material. For La-Sr-Cu-O system, $\gamma(0)$ is associated entirely with the normal material[52]. Structurally, the TBCCO and BSCCO compounds are alike. However, one significant difference is that the former contains Ba, and hence there is

a possibility of the presence of $BaCuO_2$ phase, which could contribute to $\gamma(0)$. This view is supported by the fact that for the single crystals of TBCCO (Tl-2223)[48] which have relatively small amount of the $BaCuO_2$ phase, $\gamma(0) = 0$.

1.6.2 Specific Heat anomaly at T_c

According to BCS theory, the relation between the specific heat jump at T_c and γ (electronic heat capacity coefficient) is given by

$$\frac{\Delta C}{\gamma T_c} = \alpha. \tag{1.27}$$

For the weak coupled superconductors α has the value 1.43 (BCS value), though it can be as high as 2.5 for the case of strong coupled superconductors. In the case of the HTSCs the determination of Δ C is rather difficult due to the following reasons:

(a) The transition temperature of these materials is high and so the jump in the specific heat is only a few percent of the total heat capacity. This is because the lattice heat capacity dominates the electronic heat capacity at such high temperatures.

(b) The jump in the specific heat is quite broad in HTSCs as compared to the conventional superconductors. There are two basic reasons for this and both are related to the short value of the coherence length, ξ, although otherwise they are quite different in origin. One reason is sample inhomogeneity and the atomic scale defects in the HTSCs. Since in these materials the coherence length ξ is of the order of the lattice parameters, therefore these defects can produce regions differing in superconducting properties. However, in the conventional superconductors the greater value of the coherence length has an averaging effect. The second reason is that due to the small value of coherence length the fluctuation effects are strong in the HTSC materials. This causes an intrinsic broadening of the anomaly. In conventional superconductors these effects are much less in magnitude.

(c) Since the fraction 'f' of superconductor is not known with any degree of certainty, it is difficult to deduce the specific heat jump for the fully superconducting sample from the measured jump.

(d) As previously mentioned, the critical field H_{c2} of these materials is very high and so it is impossible to drive the material into the normal state by application of a magnetic field to determine γ (which can be used to calculate ΔC) from the low temperature specific heat.

The quality of the sample also has an effect on the specific heat anomaly at the transition temperature. Junod et al.[46] carried out a study on the effect of sample quality on the specific heat anomaly and found out a positive correlation between the Meissner fraction and $\Delta C/T_c$. For a sample of better quality the specific heat anomalies are higher and narrower. The shape of the specific heat anomaly is also influenced by coupling effects.

1.6.3 Fluctuation Contribution to Specific Heat near T_c

The coherence length in HTSCs is small. Therefore, there are contributions to the specific heat both above and below T_c from thermodynamic fluctuations in the order parameter. Outside of the critical region (i.e.,. as long as the contribution of fluctuations to the specific heat is small compared to the mean field specific heat jump) fluctuations can be described by the Gaussian approximation. Around the transition temperature the critical behaviour becomes important especially for oxide superconductors because they have a very short coherence length. It is useful to note Ginzburg criterion

$$\left(1 - \frac{T}{T_c}\right) \gg \epsilon_G = \left(1 - \frac{T_G}{T_c}\right) = \left(\frac{8\pi\, k_B T_c}{H_c^2(0)\xi^3(0)}\right)^2 \qquad (1.28)$$

At temperatures that satisfy the above equation, critical fluctuations do not dominate, and the mean field theory provides a reasonable approximation to the thermodynamic behaviour of the superconductor. For a typical type II superconductor, ϵ_G = 2e-11. The HTSCs have a very small value of ξ and a large value of T_c. Therefore, ϵ_G becomes larger. For YBCO, ϵ_G = 0.01 which is in the experimentally accessible temperature

range. According to the Gaussian fluctuation theory[53–56] the extra specific heat caused by fluctuations is expressed as

$$C_{fl}^{+}(T) = C^{+} \ (-\epsilon)^{-2 + d/2} \qquad T > T_c \tag{1.29}$$

$$C_{fl}^{-}(T) = C^{-} \ (\epsilon)^{-2 + d/2} \qquad T < T_c \tag{1.30}$$

for $\epsilon = \left(1 - \frac{T}{T_c}\right)$ less than and greater than zero respectively. Here d is the dimensionality in the sense of superconductivity. Also

$$\frac{C_{fl}^{+}}{C_{fl}^{-}} = \frac{n}{2^{\frac{d}{2}}} \tag{1.31}$$

where n is the number of components of the order parameter.

1.7 Techniques of Measurement of Specific Heat

The basic experimental techniques of heat capacity measurements are quite old. The systems based on isothermal calorimetry and the method of mixtures are extensively used even today with little change in the principles of operation. The idea of adiabatic calorimetry was developed by Nernst[57] more than seventy years ago. These classical methods generally provide very good accuracies; but newer work has been taken up, where the classical techniques cannot be used. The following are the major methods employed in calorimetry:-

(a) Method of mixtures

(b) Method of cooling

(c) Methods based on change of state or latent heat calorimetry

(d) Electrical methods

The principles of operation of these methods are quite straight forward. A certain quantity of energy Q is supplied to the sample, usually in the form of electric power, which is accurately determined. The resultant change in the temperature of the sample is accurately monitored and possible heat losses are evaluated. Then

$$Q = \int_{T_1}^{T_2} C_p dT + \int_t k dt. \tag{1.32}$$

Here k represents a parameter of heat leak and T_1 and T_2 represent the initial and the final temperatures of the sample.

It must be mentioned that the temperature range in which the heat capacity measurements are to be made determines the exact technique to be used for the measurement and for the precautions to be taken. The temperature ranges and the particular techniques used are listed below:

Calorimetry below 1 K

The techniques used in this temperature range are : (a) Adiabatic calorimetry (b) Continuous heating calorimetry (c) Transient calorimetry (d) a.c. calorimetry

Calorimetry in the range 0.3-3 K

The techniques commonly used in this temperature range are : (a) Isoperibolic calorimetry (c) Adiabatic calorimetry (c) Continuous heating calorimetry (d) Steady state a.c. temperature calorimetry (e) Temperature wave method (f) Diffuse temperature pulse method (g) Temperature relaxation method (h) Resistive squid calorimetry (i) Differential calorimetry with small samples

Calorimetry in the range 5-300 K

Various techniques involved are: (a) Adiabatic and isoperibolic calorimetry (b) Inverse temperature drop calorimetry (c) calorimetry at high pressures (d) calorimetry in magnetic fields (e) Thermal relaxation calorimetry (f) Laser flash calorimetry (g) Flow calorimetry

Calorimetry above 300 K

The techniques involved are: (a) Adiabatic calorimetry (b) Drop calorimetry

The electrical methods shall be discussed briefly.

1.7.1 Electrical Methods

The electrical method was developed by Joule in his attempts to determine the mechanical equivalent of heat. Though the method was initially applied to liquids, the present discussion is limited to the case of solids only. The electrical method was first applied to solids by Gaede[58] in 1902. E.H. Griffiths and E.Griffiths[59] determined the specific heat of many metals over the temperature range -160°C to 100°C. The

substance to be measured was used in the form of a calorimeter and was cooled below the desired temperature. Electrical energy was utilized in heating the calorimeter and the temperature was measured by a resistance thermometer. The calorimeter was enclosed in a constant temperature bath whose temperature was kept constant to 1/100 th of a degree by cooling the vessel with the aid of a spiral tube through which previously cooled air was allowed to flow at a regulated rate. Correction was applied for the heat lost by radiation and hence the heat capacity evaluated. A different form of the apparatus, known as the vacuum calorimeter, was used by Nernst and Lindemann[60] for measuring specific heat at very low temperatures. This differed from the foregoing one essentially in having the calorimeter suspended in vacuum.

1.7.2 Adiabatic Technique

In many thermophysical calorimetric measurements, determination of the energy lost by heat leak is the factor that most severely limits the accuracy. Therefore, decision usually must be made between retaining a significant but calculable heat leak or endeavoring to eliminate the heat leak to the point where it is insignificant. For this purpose a thermal shield (with a heater wound around it) is usually used. If the controlled-temperature shield is designed to have a heat capacity to retain an essentially constant temperature during a measurement cycle, the technique is described as one involving essentially a isothermal jacket. This is the isothermal or isoperibolic technique which was first used by Nernst and his colleagues. If, on the other hand, the temperature of the shield is so regulated as to be nearly identical with the sample temperature, the technique is called the adiabatic technique. This method at cryogenic temperatures has been credited to Southard and Andrews[61].

1.7.3 Special Techniques

In addition to the above mentioned methods certain specialized techniques are also used. These include Levitation calorimetry, Differential scanning calorimetry, Calorimetry at very high pressures and calorimetry of the radioactive materials. We shall discuss only Differential scanning calorimetry briefly.

Differential Scanning Calorimetry

The DSC is a high accuracy, versatile, commercial instrument for thermal measurements. This method is used for chemical measurements involving the precise measurement of enthalpy, though it can also be used for heat capacity measurements. It is used to measure the heat capacity of chemically stable, non-volatile, condensed phases. In this technique the differential signal (between the sample and the reference) is monitored to obtain the calorimetric data while scanning (in temperature). This technique was introduced by Watson et al.[62]. Essentially, the calorimeter consists of a sample chamber and an identical chamber for the reference. The system has independent heaters and sensors for the two chambers. There is provision for heating both the chambers at an identical, pre-programmed rate (Fig. 1.7). The heating power

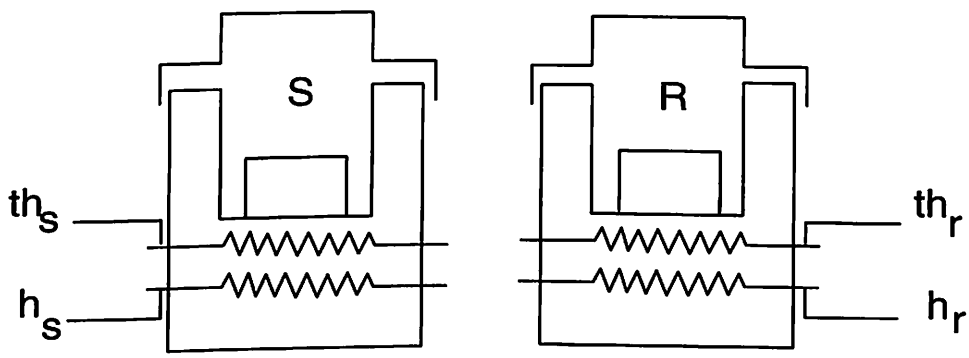

Figure 1.7: Schematic diagram of the DSC apparatus (s-sample, r-reference, hs-sample heater, hr-reference heater, ths- sample thermometer, thr-reference thermometer).

input to the two parts is continuously varied to maintain the heating (or cooling) rate. The difference in the power input to the standard and sample is caused by any exothermic or endothermic transformation occurring in the sample and the reference and by difference in their heat capacities. This difference is continuously plotted. The plot

can be analyzed to give the heat capacity values, enthalpy changes, etc. The quantity of sample required is very small ($\approx$ 10-50 mg). The system is used with aluminium or gold containers. Special containers for volatile samples are also available. Unlike other heat capacity measurements, the DSC is fast. The normal rates of heating in a DSC experiment vary between 5 and 50-K/min. This places a serious limitation on the DSC. Since the temperature is continuously changed at such rapid rates, there is a possibility of sample temperature lagging behind indicated changes. Also, the lag may depend upon the sample thermal conductivity and the internal relaxation time. The packing of the sample in the container and the thermal conduction barrier between the sample and the container have also to be considered. The variation of the absolute temperature calibration from run to run and calibration of enthalpy scale are other factors to be considered in obtaining high accuracy heat capacity data.

1.8 Aim Of The Work

The aim of the present study is to carry out dc electrical resistivity, ac magnetic susceptibility and specific heat measurements on some well characterized good quality polycrystalline superconducting samples. The specific heat data are used to evaluate certain important parameters of a solid like Sommerfeld constant, Debye temperature etc. Further, on some of these samples paraconductivity and excess specific heat studies have been made. These are used to gain an insight into the fluctuation effects which are significant in the high temperature superconductors.

1.9 Outline Of The Work

The present chapter includes a detailed discussion of the basic aspects of superconductivity with special emphasis on the specific heat studies.

Chapter 2 includes the preparation techniques of rare earth and bismuth based high temperature superconductors (polycrystalline bulk samples). This chapter also includes the description of experimental setups used to study the different properties of the superconducting samples.

Chapter 3 deals with a systematic study of resistivity, ac magnetic susceptibility and specific heat in Er-123 system for both the pure phase and when Cu is partly (0.5%) replaced by Ni, Zn, Fe, Co and Ga. These substitutions are used to study the role of site dependent in-plane and out-of-plane disorder, in conjunction with fluctuation effects.

Chapter 4 contains in detail the resistivity, ac susceptibility and specific heat measurements carried out on samples $Bi_{2-x}Pb_xSr_2Ca_2Cu_3O_{10+y}$ ($0 \leq x \leq 0.7$) samples that were characterized by x-ray diffraction and high resolution scanning tunneling microscopy. Based on the results obtained from these experiments, the role of lead substitution in bismuth samples, particularly in stabilization of the high T_c phase is investigated.

Chapter 5 includes the results of resistivity, ac susceptibility and specific heat measurements on samples $(Bi)_{2-x}Pb_xSr_{2-x'}Ca_{2+x'}Cu_{3+x''}O_{10+y}$ (x = 0.1-0.4). These samples were characterized by XRD and high resolution STM. The study concentrates on the role of disorder in the stabilized high T_c (Bi-2223) phase from the low T_c (Bi-2122) phase in conjunction with fluctuation effects.

Finally in **Chapter 6** the conclusions from the overall study have been drawn.

Chapter 2

Experimental Techniques

In this chapter we have mainly concentrated on the sample preparation techniques and the different characterization methods. The sample preparation is an art of any solid state research. In particular, in the high T_c superconducting samples the method of preparation plays an important role as far as phase purity is concerned[63, 64]. We shall only discuss the topics pertinent to our studies. We have used the solid state method to prepare the samples and so we have begun by reviewing the preparation of different samples by this method. Thereafter, we have discussed the various methods of characterization. The characterization of a sample for phase purity started with the structural studies, namely, X-ray diffraction (XRD), and microstructural studies, like, Scanning Electron Microscopy (SEM), Scanning Tunnelling Microscopy (STM) etc. After characterization of the sample for the presence of the desired phase through these methods, we carried out the electrical (dc resistivity) and magnetic (ac susceptibility) measurements to ascertain the transition temperature and the volume fraction of the superconducting phase in the sample. Finally, specific heat measurements were carried on these well characterized samples.

2.1 Sample Preparation

Since the discovery of high-T_c superconductivity in the La-Ba-Cu-O system, a wide variety of cuprate superconductors have been synthesized and characterized. Several methods of synthesis have been employed for preparing these cuprates, with the object-

ive of obtaining pure monophasic systems with good superconducting properties[65, 66]. These studies have clearly established that the superconducting properties, like, T_c, critical current density J_c, etc, depend crucially on the processing method and the conditions of preparation[67]. The most common method of synthesis of cuprate superconductors is the traditional Ceramic or Solid State Reaction method which has been employed for the preparation of a large variety of oxide materials[68]. Although the Solid State Reaction method has yielded many of cuprates with satisfactory characteristics, different strategies have become necessary in order to control factors, such as, cation composition, oxygen stoichiometry, cation oxidation states and carrier concentration. Other than the Solid State method, some specially noteworthy methods being used are Chemical or Solution routes. These methods permit better mixing of constituent cations in order to reduce the diffusion distances in the solid state[68]. Coprecipitation, use of precursors, the sol-gel method and the use of alkali fluxes may be cited as examples of these methods. The other reported method is the Combustion or the Self Propagating High Temperature Synthesis (SHS) method.

2.1.1 Solid State Method

The most common method for synthesizing inorganic solids is by reaction of the component materials at elevated temperatures. If all the components are solids, the method is called the Solid State Reaction or Ceramic method. If one of the constituents is volatile or sensitive to the different constituents of the atmosphere, the reaction is carried out in sealed evacuated capsules. Platinum, silica or alumina containers are generally used for synthesizing metal oxides. The starting materials are metal oxides, carbonates, or other salts, which are mixed, homogenized and heated, at a given temperature, sufficiently long for the reaction to be completed. A knowledge of the phase diagram is useful in fixing the compositions and conditions in such a synthesis. This method generally requires relatively high temperatures which are attained by resistance heating using different kinds of furnaces. In case of cuprate superconductors the steps carried out are described below:

a) Powder preparation

The Solid State Reaction method involves mixing and grinding of the various component oxides, carbonates or nitrates in the appropriate stoichiometric ratios. For quantities of powders which are less than around 10 grams, grinding is carried out using an agate mortar and pestle. In case of larger quantity of material, another technique, viz, ball milling, is used. Since the quality of the sample is crucially dependent on the homogeneity of this mixture, adequate precautions are taken in this regard.

b) Calcination

The calcination of the mixture is carried out either in the powder or the pellet form at the desired temperature. The purpose of the calcination is to decompose the carbonates and inter-diffuse the starting materials for the phase formation and chemical homogenization. In general, two to three calcinations are carried out. Each calcination is followed by a thorough grinding and mixing of the sample.

c) Forming

The ground powder is pelletized with the help of a die and hydraulic press. A pressure of about 9 kbar is applied on the powder. After a few minutes the pressure is released and the pellet taken out. Sometimes, 1 to 3% by weight of an organic solvent binder, such as, poly-vinyl-alcohol (PVA), can also be added to the powder to enhance the strength of the pellet.

d) Sintering

The final treatment of the samples is carried out in the form of the pellets. The pellets are kept in a furnace at the required temperature. The sintering process involves heating at a temperature higher than the calcination temperature in air or oxygen, depending on the material to be synthesized.

Preparation of Er-123 system

The ingredients used in the preparation of $ErBa_2Cu_3O_{7-\delta}$ were mainly taken in the form of oxides and carbonates, namely, Er_2O_3, $BaCO_3$ and CuO of 5N purity (99.999%), which were mixed in the stoichiometric ratio of 1:2:3. These raw materials were thoroughly ground and the calcination of the mixture was carried out in air in the temperature range 900-920°C for 15-20 hrs for removal of carbon or any other

volatile impurity. Two or three intermediate grindings were carried out during the calcination process to ensure better homogeneity. The calcined material was crushed again and ground to get a fine powder. This powder was pelletized into a tablet and sintered at a temperature of about 940°C for 15 hrs in a continuous flow of oxygen followed by slow cooling to 600°C. The annealing of the samples was done in oxygen atmosphere at 600°C for 6 hrs followed by furnace cooling. The annealing temperature was optimized at around 600°C because at this temperature there is a maximum intake of oxygen into the 123 lattice[69].

Preparation of Bi-2223 system

The synthesis of the pure and substituted Bi-2223 samples was carried out by the solid state reaction method. The ingredients used (purity better than 4N) were Bi_2O_3, Pb_3O_4, $SrCO_3$, $CaCO_3$ and CuO. The starting powders were mixed thoroughly in the stoichiometric ratio and calcined three times for 12hrs each at 820°C 830°C and 840°C respectively, in succession, and finally quenched to room temperature. Each calcination was followed by a proper mixing of the powder. The sintering of the samples was carried out in the pellet form at a temperature of 860°C for around 100hrs and finally the samples were cooled down to the ambient temperature. The annealing for a long time is essential to the formation of the 2223 phase[70, 71].

2.2 Sample Characterization

2.2.1 Structural Studies

X-Ray diffraction

This technique provides information about the phase purity and lattice parameters. We obtained the X-ray diffraction (XRD) patterns of materials with the help of a Siemen's D-500 diffractometer. The instrument is fully computer-controlled and has been regularly used for routine measurements. The sensitivity of this instrument is around 2% for phase identification. The principle of diffraction of X-ray through crystal lattice, following the Bragg's law, has been used. The sample is rotated very slowly

and the diffracted beam is recorded at each angle. Cu-Kα radiation of wavelength 1.5417 Å was used as the X-ray source.

The XRD patterns of the samples were usually recorded for Bragg angle in the range of 10°-70°. The phases were identified by matching the main reflection peaks of XRD patterns with the ASTM data. All peaks of XRD patterns were indexed and lattice parameters of the unit cell calculated through refinement technique and a computer program developed for the calculation. The presence of foreign phases in the material can easily be identified.

Microstructural studies

Scanning electron microscopy

The principle of this technique is based on the ionization of the material under high energy electron beam having energy in the range of 30-50 Kev. The secondary electrons and back scattered electrons are produced by this electron beam. These secondary electrons coming from different portions of the sample surface provide the information about surface topography, i.e, grain morphology. The grain shape, size and distribution can be studied by using the fractured surface of the material.

The scanning electron micrographs for different samples were recorded in the secondary-electron-emission mode with a 0° tilt using a JOEL JSM 35 CF instrument.

Scanning tunnelling microscopy

The technique of scanning tunnelling microscopy (STM) is a versatile tool to reveal the atomically resolved nanostructures of the sample surface. The technique has an equally powerful spectroscopic component, namely, the scanning tunnelling spectroscopy (STS), which allows one to explore the electronic structure of the surface layers with the atomic level resolution.

All the samples were freshly cleaved before mounting them on STM (Nanoscope II, Digital Instruments Inc. U.S.A), which was operated at ambient temperature using nanotips of Pt-Ir. Real space gray scale images were obtained in the constant current

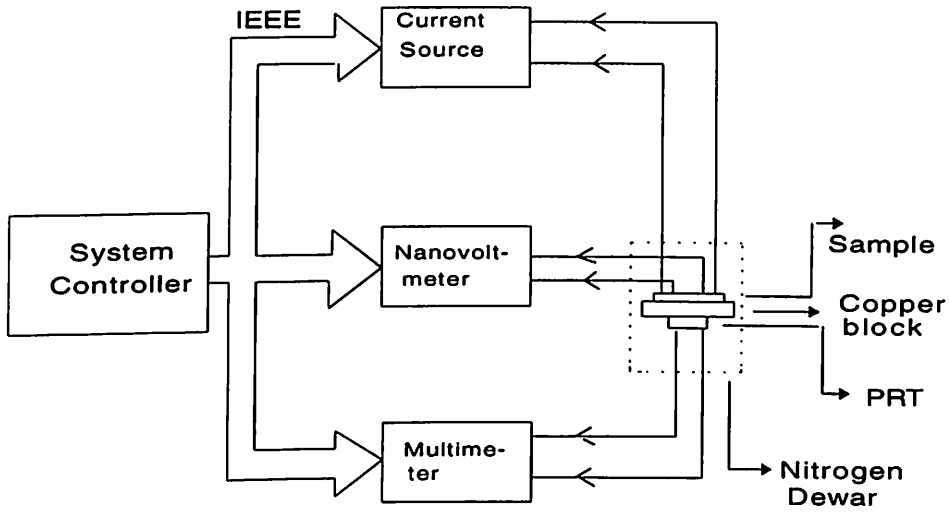

Figure 2.1: Block diagram of dc resistivity measurement setup

mode with the bias voltage (negative) in the range of a few millivolts to about 500 mV.

2.3 Electrical and Magnetic properties

2.3.1 DC electrical resistivity

The simplest way to characterize any superconducting sample is to study the resistivity of the sample as a function of temperature both in the normal as well as the superconducting state. The major problem in the resistivity measurement of the ceramic samples comes from the contact resistance. The most commonly used method to avoid the contact resistance is the four-probe method[72]. This method was used in measuring the dc resistivity of all our samples. Fig. 2.1 shows the block diagram for the measurement of dc resistivity of a sample. For dc resistivity measurements, the samples were pelletized in the form of rectangular bars before sintering. The dimensions of the rectangular bars were measured with the help of a travelling microscope. Silver paste was used for making the current and the voltage contacts. Generally, the current contacts are provided with adequate silver paste, while the voltage contacts are obtained by using a thin layer of equipotential silver paste surface. Fig. 2.2 shows the

schematic view of the sample pasted on a PCB with its four contacts. The temperature

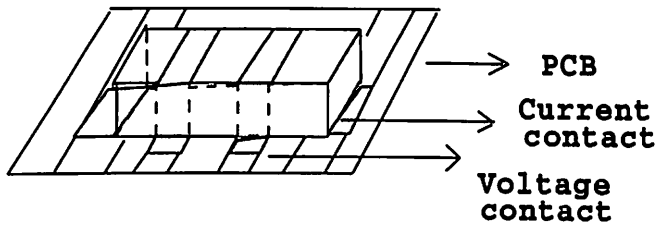

Figure 2.2: Sample on a PCB

variation was obtained by dipping the sample in liquid nitrogen. The sample temperature was monitored using a standard platinum resistance thermometer (PRT-100) in conjunction with a digital multimeter (*Keithley DMM model 195A*) with an accuracy of 0.1 K in the temperature range of 77-300K. A current of around 1mA was passed through the sample from a programmable current source (*Keithley model 224*) and the voltage across the sample was measured with the help of a nanovoltmeter (*Keithley model 181*). For each reading the current was allowed to pass in both the directions and the corresponding voltage drops were recorded. The thermoelectric voltages were nullified since the current is passed in both the directions. The average voltage V was used to determine the sample resistance R from the known current I at a particular temperature value. From the resistance value, the resistivity was calculated using the sample dimensions. We have automated the entire measurement procedure, including the data acquisition and the instrument control, using a PC-486 or a HP-9220 series computer.

2.3.2 AC susceptibility measurements

These measurements involve ac susceptibility χ as a function of temperature. Magnetic measurements are essential in the characterization and analysis of superconducting materials. Measurement of the dynamic or ac susceptibility $\chi =$ dM/dH yields information that is not easily obtained from static or dc magnetization measurement. The ac susceptibility measurements provide useful information about the behaviour of

real and imaginary components of magnetic susceptibility (χ' and χ'') as a function of temperature and the variation of χ' and χ'' support the nature of the superconducting state in the sample. χ' gives information about the presence of other phases and Tc, while χ'' provides information about intergranular coupling in the sample. From the variation of χ'' with temperature one can estimate important parameters like, Jc, grain boundary pinning strength, etc. The ac technique is as sensitive as static alternative measurements. Further, with the small amplitude of the ac field and the ability to vary the measurement frequency, information about the magnetic microstructure and magnetodynamics of the system can be obtained. The ac susceptibility measurements were done on a Lake Shore Model 7000 AC Susceptometer, which is an integrated unit consisting of an ac current source, a phase sensitive detector, a temperature controller and a comprehensive cryogenic testing system. These are all software-controlled through a Hewlett Packard Vectra-CS Series PC. It can adjust the variables for temperature (4K to 330K), frequency (5Hz to 1000Hz) and a magnetic field (.005 to 10 Gauss RMS) in variable combinations. The block diagram of the ac susceptibility setup is shown in Fig. 2.3. The ac susceptibility is very useful for studying high

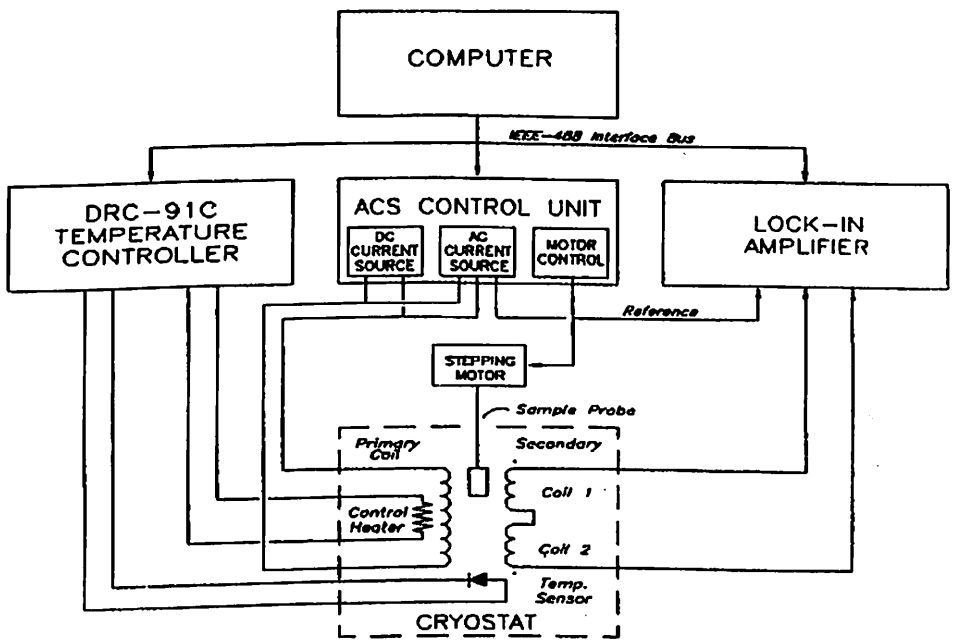

Figure 2.3: Block diagram of ac susceptibility measurement setup

Tc superconductors. These materials are characterized by superconducting grains or inclusions that have a relatively high Tc. Often two peaks in the imaginary part of susceptibility are observed, corresponding to the intra-grain and inter-grain current components respectively. χ' represents the supercurrent shielding and a non-zero χ'' is a manifestation of losses in the material.

2.4 Specific Heat Measurements

Specific heat is one of the fundamental thermal measurements and has been used extensively as one of the tools to determine bulk superconductivity. Since the measurement of specific heat is the theme of the present work, an exhaustive analysis has been made to highlight the different features of the calorimeter and its supporting system developed in our laboratory. The heat capacity can be studied by using any one of the variety of available methods. In most of these experiments the only limitation is that these are very slow and time consuming, a condition which has to be strictly followed in order to achieve a high degree of accuracy. The use of computers for controlling the instruments and automatic data acquisition has partially compensated this limitation. The basic requirement is for a high precision calorimeter which is easy to handle and, if possible, of a low cost.

The design of the calorimeter is based on the classical Nernst step heating method under quasi-adiabatic or isoperibolic conditions. In this method, the temperature difference between the sample and the thermal shield is made as small as possible in order to avoid heat loss to the surroundings[73–75]. However, strict adiabatic conditions are difficult to achieve for any sample. Adiabatic shield control,in practice, is utilized only for samples with a large heat capacity, that is, for a sample weighing 2 gm or more. With decreasing sample mass, which means decreasing heat capacity, however the experimental conditions deviate more and more from adiabacy. Therefore, isothermal shields have been used with a suitable correction for the heat loss. Such quasi-adiabatic calorimetry has been extensively used, attaining a resolution of better than 1% with samples weighing from 0.5 to 1 gm[76].

The basic problem in any calorimetric measurement is the lack of adiabacy and thermal equilibrium leading to systematic errors. Some classes of compounds, such as, the high temperature superconductors, polymers, ceramics, etc are characterized by low thermal conductivity and partially by low reflection coefficients. Therefore, serious problems arise, which are listed below:

(i) Uncontrolled heat exchange by heat radiation ($\propto T^3\Delta T$) between the sample and the surroundings resulting from non-adiabatic conditions, specially during the heating at temperatures above 60K.

(ii) Temperature gradients along the thermal shield

(iii) Unusually long internal relaxation time τ_i, comparable to the external relaxation time (between the sample and the heat shield) τ_e, leading in conjunction with an eventual small drift of the heat shield to non-exponential post-heating curves.

(iv) In some cases (for e.g., superconducting transition) there are strong variations in specific heat with temperature during external thermal relaxation period.

2.4.1 Cryostat Design

Figure 2.4 depicts the calorimeter. It consists of a double walled polished upper tube made out of thin walled cryogenic grade stainless steel (SS), which being a bad thermal conductor, reduces the thermal losses. The inner tube is used to take out the electrical connections and the outer tube is used for evacuating the cryostat. At the top of the tube both the parts are separated and split into the electrical and the vacuum ports, respectively. The electrical port has a sixteen pin D-connector to which are connected the electrical connections coming out of the sample chamber. These are then fed through to the different measuring instruments. The tube at the lower end is connected to two coaxial cylindrical chambers made out of copper. To avoid radiation losses the outer surface of both the chambers are nickel plated and polished. The supporting top plate of the outer chamber is soldered directly to the SS tube.

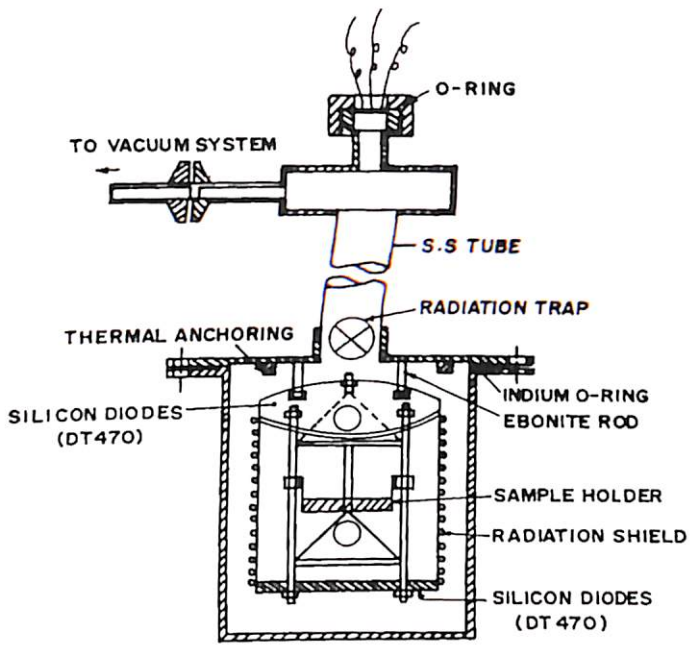

Figure 2.4: A schematic view of the calorimeter

Thermal shield

The outer surface of inner cylindrical chamber (sample chamber) acts as the thermal shield. As mentioned in the previous section, the thermal shield plays an important and crucial role in maintaining the true adiabatic conditions. Therefore, it is mandatory to have a better and efficient construction of the thermal shield. By definition, an ideal thermal shield is an equithermal surface around the sample whose temperature is almost identical to the sample temperature. Since the sample is placed in a evacuated chamber, there is no heat loss due to convection and conduction. Besides, because of the thermal shield, the radiation losses should also be negligible. But, as these ideal conditions cannot be realized in practice, efforts have been made to obtain the conditions in which the radiation losses could be minimized . This has been done by using a isothermal shield, a technique referred to as the quasi-adiabatic or isoperibolic technique.

During the last few years, we have improved upon the construction of the thermal shield, in particular in regard to the material of suspension, the adhesive and the material used as the heating element. For example, we observed that ebonite rods

performed better than the stainless steel rods when used for suspending the sample chamber.

As mentioned in the preceeding paragraphs, the sample chamber is suspended through the top flange of the cryostat. The sample chamber is made from a copper block. A demountable threaded screw arrangement has been made. The top plate of the sample chamber is suspended from the fixed upper plate of the outer chamber using ebonite rods, while the lower portion of the chamber is connected through a screw and thread arrangement to the top plate. This demountable arrangement allows easy removal of the bottom portion and mounting of the sample. The temperature of the thermal shield is regulated using a heater which is wound around the sample chamber. To facilitate a better thermal connection between the chamber and the heater, GE varnish is used. The heating element is made out of Nicrome wire which is flattened by pressing in a wire extrusion unit. A thin layer of the epoxy is spread on the chamber and then mylar sheet is wound around it. The whole system is allowed to dry completely and then the flattened heater wire is wound around the chamber tightly and another layer of epoxy spread over it. Finally, a thin layer of teflon tape is wound around the heater wire and the assembly is allowed to dry for a couple of days. As the space between the inner surface of the outer chamber and the outer surface of the inner chamber is very small, adequate precautions have been taken to optimize the heating element, for obtaining maximum performance from this arrangement. Flattening of the heater wire helps in getting a larger surface area of the heater in contact with the chamber and hence improves the performance of the thermal shield. The combination of mylar and teflon layers minimizes the thermal losses very efficiently and thus, maintains the isoperibolic conditions effectively.

It is pertinent to mention at this stage that the heating element is distributed in such a way that the top plate of the sample chamber is also heated equally. This reduces the possibility of a temperature drift in the thermal shield. Since the top plate and the bottom portion are connected through threads, therefore, for facilitating better thermal connection, GE varnish is used in the threadings.

The temperature monitoring and controlling of the thermal shield is carried out

by two temperature sensors (*Silicon diodes-DT 470*). One of the diodes is placed at the top, while other is placed at the bottom of the chamber. Both of these sensors detect the temperature of the shield simultaneously to compensate for any drift in the temperature due to thermal lag between the top and bottom portions of the chamber.

Sample holder

Fig. 2.5 shows the schematic view of the sample holder. The sample holder consists of a demountable triangular shaped platform which can be inserted inside three tubes attached to the top plate of the inner chamber. A three screw arrangement is used to fit in the platform tightly. The tripod platform is made out of copper with nickel electroplating and has two triangular plates soft soldered to it. These triangular plates have central holes in them through which electrical leads can be conveniently taken out of the sample holder and through the SS tube to the external D connector. The

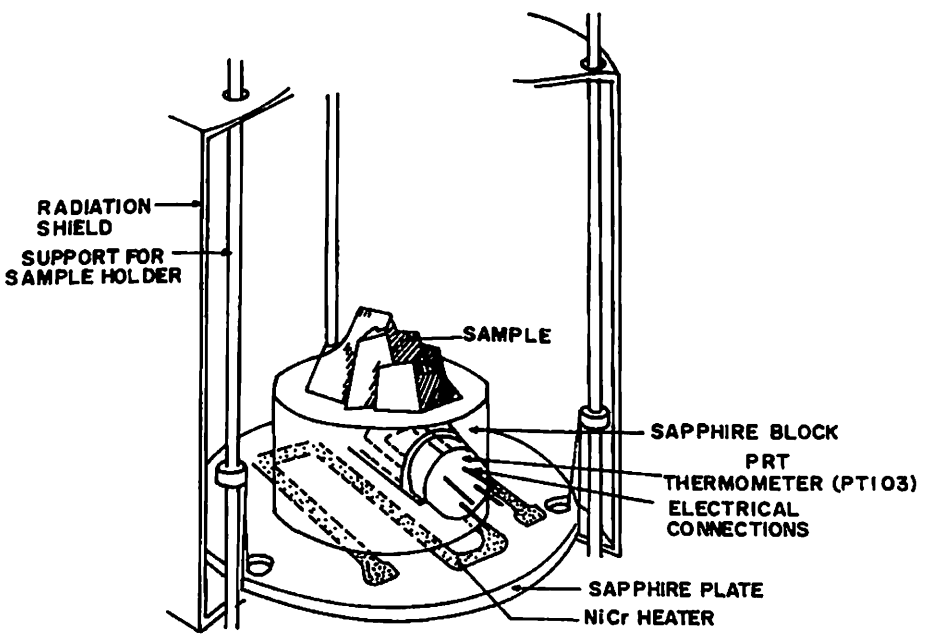

Figure 2.5: The sample holder

sample holder also comprises of a sapphire plate (diameter=14mm, thickness=0.1mm) on which a NiCr film heater is evaporated. The approximate resistance of the heating element is 1440 Ω. A sapphire block (diameter=8mm, thickness=6mm) is kept over

the sapphire plate. The sample is placed over the sapphire block. The heating element is wound in such a way that the total energy is distributed uniformly over the sapphire block. The sapphire block has an ultrasonically drilled central hole, in which a platinum resistance thermometer (PRT) is inserted for measuring the sample temperature. Apiezon N grease is applied between the sapphire plate and the block and also between the block and the sample to have a good thermal contact between all the components. The diameter of the hole in the block is made close to the outer dimensions of the PRT, so that with the application of little apiezon grease it can slip inside the block. This method enables measurement of the block temperature accurately. In our case the samples to be measured were all high temperature superconductors, which are also bad thermal conductors. Therefore, we used one more PRT at the top of the sample with the proper application of apiezon N grease on the sample. We took the average of the temperatures recorded by the two thermometers, to take care of any variation in the temperature across the sample surface. The sapphire plate with the heating element is suspended inside the tripod stand (depicted in Fig.2.5) by three nylon threads. The electrical connections coming from inside the sample holder are anchored suitably so that heat losses due to the thermal gradient along the wires can be minimized.

Thermometry

Two types of thermometers were used. The first one, to measure the sample temperature and the second one, to measure the shield temperature. The sample temperature is measured using the PRT and the shield temperature by using the silicon diode thermometer (DT-470). The PRT was calibrated in our temperature standards laboratory and the coefficients obtained as per the IPTS 90[77]. Thus, a polynomial relation was obtained between the resistance of the PRT and the temperature. The four probe method was used to measure the resistance of the PRT and thereby, the absolute value of the temperature known. Generally, a current of around 0.5mA is passed through two terminals of the PRT using a current source (*Keithley model 224*) and the resultant voltage developed is measured across its other two terminals using a nan-

ovoltmeter (*Keithley model 181*). After changing the direction of the current to nullify the thermal emf, and measuring the resultant voltage the resistance of the PRT is obtained. By using the polynomial function, described above, the temperature of the sample is ascertained. The coefficients of the polynomial function were checked from time to time so that the measurement of temperature is as accurate as possible. The DT-470 diodes were obtained from Lakeshore cryotronics, initially calibrated by them and later by us from time to time in the laboratory, using fixed points. Since these thermometers are small in size and respond quickly to the temperature controlling system even at low temperatures, the same were preferred to other thermometers.

Thermal Isolation

In an isoperibolic calorimetry, the calorimeter has to be isolated as much as possible from the surroundings so that the loss or gain of heat energy from or to the sample is minimum. Ideally, the sample temperature should rise only due to the heat energy supplied to it. To minimize the heat losses due to conduction and convection, the experiment is carried out under high vacuum of the order of 10^{-6} Torr or better. In addition, the sample is surrounded by a thermal shield the temperature of which is kept quite close to the sample temperature. Because of the presence of this thermal shield, the loss of heat energy due to radiation can be minimized to a large extent. Also, the use of ebonite rods helps in isolating the sample holder from the surroundings to a large degree.

Thermal Contact

A proper thermal contact is needed in the calorimeter between the different components in order to reduce heat leak as far as possible. Therefore, apiezon N grease is applied between different thermal components where the occurrence of heat loss is possible. For example it is used between the sapphire plate and the sapphire block and between the block and the sample. Also, as stated earlier, grease is applied at the screwed connection between the top plate and the bottom portion of the sample chamber. Similarly, we used a film heater for sample heating which helped in ensuring

a better thermal contact between the sapphire block and the heater and resulted in a uniform distribution of heat to the sample.

Vacuum System

The sample chamber has to be evacuated to a pressure of around 10^{-6} Torr to ensure accurate measurements. For this purpose we used a diffusion pump backed by a rotary pump in conjunction with a liquid nitrogen cryotrap. The pressure in the chamber was measured using pirani and penning gauges. These gauges were calibrated from time to time.

Application of Heat

Heat energy is required to be applied to the sample to raise its temperature. In order to maintain the shield temperature as close as possible to the sample temperature, i.e, to maintain quasi-adiabatic conditions, heat energy is to be supplied to the thermal shield as well. The heat energy ΔQ was supplied to the sample through a current source (*Keithley model 224*). The shield current was provided by a temperature controller (*Lakeshore model 91C*).

Supporting System

The cryostat is kept inside a commercially available (Oxford Instruments) double walled liquid nitrogen metal dewar. The schematic view of the dewar is shown in Fig. 2.6. The bath is also evacuated to minimize liquid refrigerant losses. This bath has a provision to put liquid refrigerant in both the chambers. As per observation, the loss of liquid refrigerant is very low.

2.4.2 Method of Measurement

The block diagram of the specific heat measurement setup is shown in Fig. 2.7. The standard method of obtaining specific heat data consists of measuring the temperature (T) of the sample as a function of time (t). The T-t plot is referred to as the driftline.

The cryostat was dipped inside the liquid nitrogen bath and the sample allowed

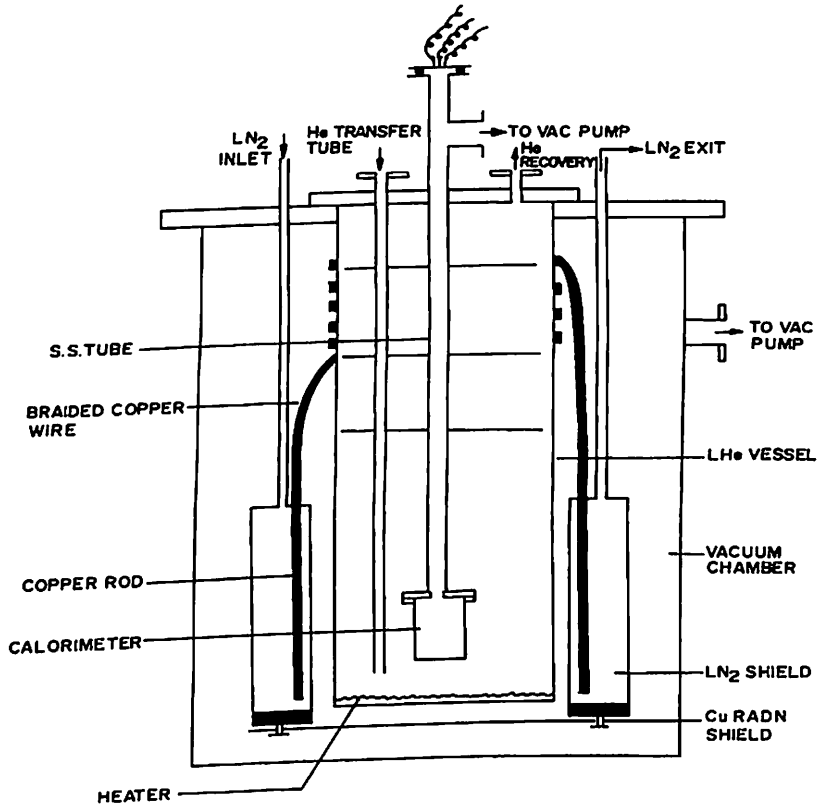

Figure 2.6: A schematic view of Nitrogen dewar

to attain the bath temperature before commencing the measurement cycle. Since the sample holder was under vacuum, helium was used as an exchange gas to facilitate the attainment of liquid nitrogen temperature. Later, when the sample stabilized at 77 K, helium was flushed out before commencing the measurement.

The first step after the temperature stabilization of the sample was to ensure that the temperature of the thermal shield was within 0.5 K of the sample temperature. If this was not so, then from software control the temperature controller passed appropriate current through the thermal shield. This continued till the shield temperature was within $\pm$ 0.5 K of the sample temperature. After the shield attained the desired temperature, it was made to follow the sample temperature with the help of the temperature controller as per the software. Once the temperature of the sample as well as the shield stabilized, the preheating driftline measurement started. The usual method for obtaining T-t curve is to measure n successive T_{sam} (sample temperature) at a constant time interval t_p. Thereafter, stepwise pulsed heat is provided to the sample

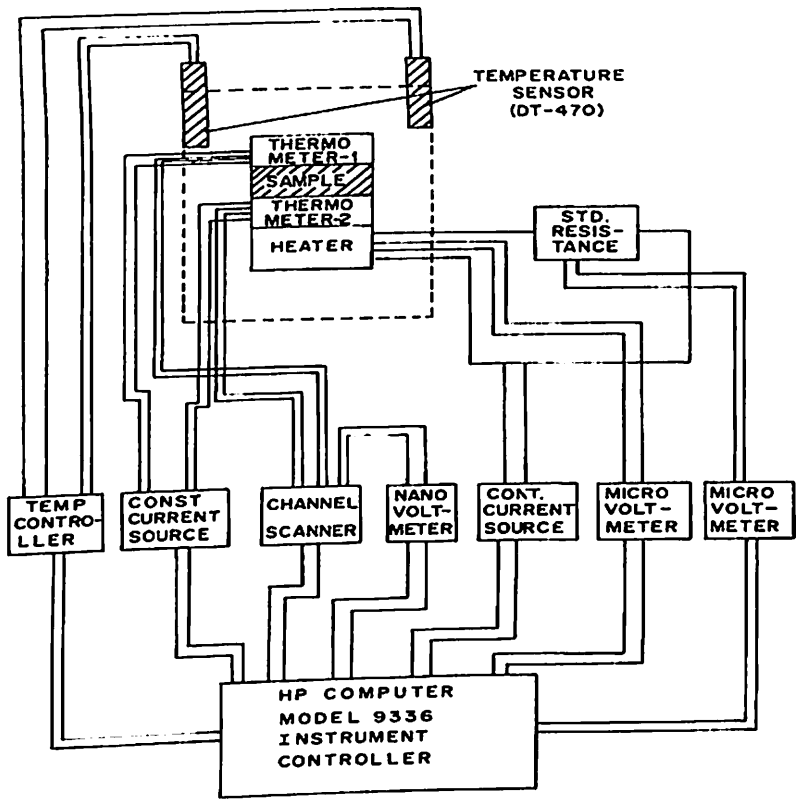

Figure 2.7: Block diagram of specific heat measurement setup

for a predetermined definite time interval $t_h = t_e - t_s$, where t_s is the time of start of heating which is taken as 0s and t_e is the time when the heating ends. This raised the sample temperature by an amount ΔT. After waiting for a delay time of t_d in order to allow for internal temperature equilibrium of the sample/sample-holder assembly, again n successive T_{sam} were measured at the time interval t_p. Fig. 2.8 shows such a typical driftline plot where n = 25 and t_p = 19s. The variation of the shield temperature (T_{shield}) is also depicted in the Fig. 2.8. The determination of specific heat of the sample requires the calculation of two parameters, namely, the heat ΔQ supplied to the sample and the consequent rise in the temperature ΔT.

Determination of ΔQ

It is assumed that the total amount of heat energy dissipated by the heater is used to heat the sample without any losses. To have a precise knowledge of the energy supplied to the sample we used a standard resistance ($R_s = 100\Omega \pm 0.0005\%$) and two precision microvoltmeters. The first, a nanovoltmeter (*Keithley model 181*) was

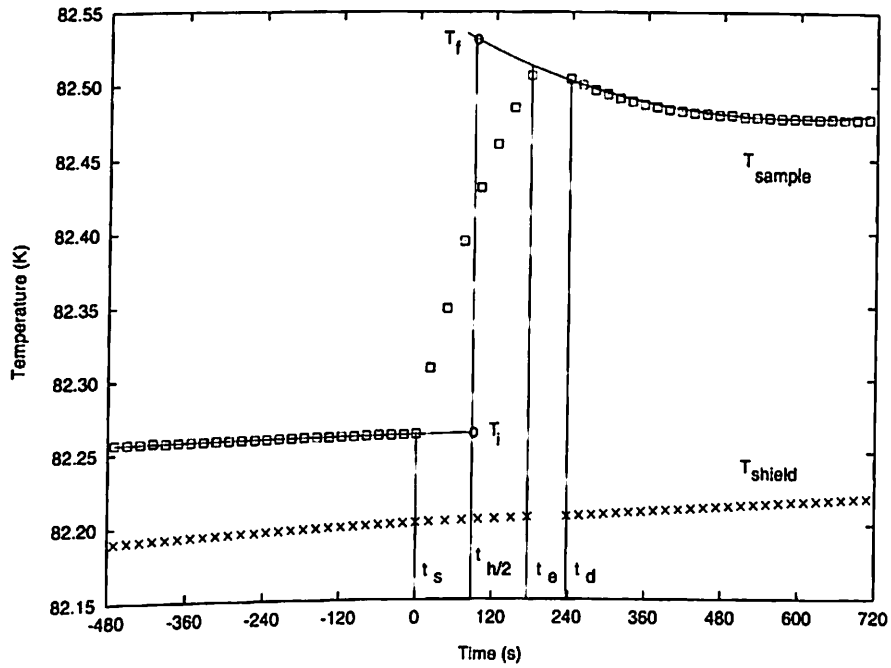

Figure 2.8: A T-t plot with the quasi-isothermal shield

connected in parallel across the sample heater and the second, a Autocal standard multimeter (*Datron model 1081*) was put across the standard resistance and operated in the dc voltage mode. The voltage drop across the sample heater V_h was measured by the former, while the latter determined the current through the film heater by measuring the voltage drop V_s across the standard resistance. The computer program is developed in such a way that it automatically nullifies the thermoelectric emf developed across the sample heater by passing the current in both the directions. Therefore, by definition, the current i_h through the heater is given by V_s/R_s and since the current was passed for a definite time interval t_h, the heat energy ΔQ fed to the sample heater is given by $i_h V_h t_h$. The option was kept to have a constant heating time or set the time on the basis of the heat capacity found in the previous cycle. The real time provision of the computer provided the start/stop signals and measured the duration of heating.

Determination of ΔT

The isoperibolic technique for heat capacity measurement, requires a suitable correction for heat losses. The usual method of correction for the heat loss is to linearly extrapolate the pre and post-heating temperature drift curves to the middle of the heating period to obtain the temperature rise.

The thermal equation describing the calorimeter is :

$$C \frac{dT_s}{dt} = P - k(T_s - T_o) \tag{2.1}$$

In the above equation, P is the heating power, C is the heat capacity and T_s is the sample temperature. The parameter T_o denotes the sample temperature in the absence of heating and can be determined by a linear extrapolation of the pre-heating temperature drift curve. Keesom and Kok[78] used the above expression to derive the analytical expressions for the heating and cooling curves in the operation of the calorimeter. As a first step of approximation, they neglected any time lags in the temperature measurement, which implies, among other things, that the thermal conductivity of the specimen is extremely large. Further, they assumed that the rate of heat exchange between the calorimeter and its surroundings, in accordance with Newton's law of cooling, is related to the temperature difference between them. The respective results for heating and cooling curves are as follows:

$$\Delta T(t) = \frac{P}{C\beta} (1 - e^{-\beta t}) \tag{2.2}$$

$$\Delta T(t) = \frac{P}{C\beta} (1 - e^{-\beta t_h}) \; e^{-\beta(t - t_h)} \tag{2.3}$$

In the above equations, $\Delta T(t) = T_s - T_o$, $\beta = \frac{1}{\tau_e}$ and τ_e is the external thermal relaxation time constant of the calorimeter. Based on this derivation, Keesom and Kok[78] gave a graphical method of analysis. Subsequently, Kouvel[79] elaborated a more realistic arithmetic method by computing the area under the post heating temperature drift curve to determine the heat capacity. Above about 150K, the thermal radiation loss becomes significant and in contrast to experiments at low temperatures, quite often a short external relaxation time constant $\tau_e = C/k$ is encountered. This is

comparable to the heating time t_h. Here C is the heat capacity of the sample assembly and k is the integral thermal conductivity of the heat leak between the sample assembly and the surroundings. When τ_e is comparable to heat pulse duration t_h, the linear approximation of the temperature drift curve (especially the post heating one) results in significant errors. This gives rise to a large scatter in the heat capacity data, because:

(i) the coefficients of the linear least-squares fit drastically differ depending on the position of the temperature drift curve used for the fit procedure, and

(ii) due to the random variation of the thermal radiation, which modifies k and τ, respectively, as a function of time.

By fitting the $\Delta T(t)$ vs t data for $t \geq t_h$ with the exponential expression and extending it down to $t = (1/2)\ t_h$ the following expression is obtained:

$$\Delta T(\frac{t_h}{2}) = \frac{P}{C\beta}\ (1 - e^{-\beta t_h})\ e^{\beta \frac{t_h}{2}} \tag{2.4}$$

Thus,

$$\Delta T(\frac{t_h}{2}) = \frac{P}{C\beta}\ (e^{\beta \frac{t_h}{2}} - e^{-\beta \frac{t_h}{2}}) \tag{2.5}$$

$$\Delta T(\frac{t_h}{2}) = \frac{2P}{C\beta}\ \sinh(\frac{\beta t_h}{2}) \tag{2.6}$$

Therefore ,

$$\Delta T(\frac{t_h}{2}) = \frac{P t_h}{C}\ (1 + \frac{(\beta t_h)^2}{24} + \ldots) \tag{2.7}$$

Cheung[80] used the above equation in the temperature range 1-20K, and in their particular case $\beta t_h \ll 1$. Thus they obtained

$$\Delta T(\frac{t_h}{2}) = \frac{P t_h}{C} \tag{2.8}$$

Since β and $\Delta T(t_h/2)$ are obtained from the fit of the equation and P and t_h are known experimentally, C is easily calculated. In confirmation of the above work Ota and Gmelin[81] extended their method to the case when $\tau_e \approx t_h$ and hence $\beta t_h \approx 1$, which consequently cannot be neglected. Based on the above arguments, they showed:-

$$\Delta T(t_h/2) = \frac{P t_h}{C}\ (1 + \frac{(\beta t_h)^2}{24}) \tag{2.9}$$

They calculated C from the above equation iteratively and, by retaining the $(\beta t_h)^2/24$ term, also took into account the variations of the external thermal relaxation time with temperature.

In our measurement of the driftline (Fig. 2.8), we took adequate care to keep the temperature drift rate as small as possible so that the pre-heating driftline could be approximated by a linear fit. The drift rate is $12\mu Ks^{-1}$ in the particular example shown in Fig. 2.8. However, we found from a number of experiments above 70 K on HTSC in recent years[82–84] that the post heating driftline is nonlinear in a logarithmic scale (unlike Eq. 2.3). Similar observations have been made by others in different laboratories. Consequently, Eq. 2.9 is not sufficient to represent the T-t behaviour of the sample holder assembly. However, no exact numerical solution to the problem is possible. Systematic errors obviously occur in the determination of C. They must be attributed to the unstable or slightly drifting shield temperature, nonlinear heat exchange by radiation and/or heat capacity changing as a function of temperature, as well as, intermixing of τ_i and τ_e for certain class of materials.

For further improvement we introduced a corrective term C_{corr}[85] in Eq. 2.3 to fit the data in a polynomial function, i.e., :-

$$\ln(\Delta T(t)) = A + B(t - t_h) + C_{corr}(t - t_h)^2 \qquad (2.10)$$

where $A = -\{\ln(\frac{P}{C\beta}) + \ln(1-e^{-\beta t_h})\}$, $\beta = 1/\tau_e$ and C_{corr} constitutes a exponential second order correction. Instead of using an iterative method for calculating the heat capacity, we calculate the parameters A, B and C_{corr} through a second order polynomial fit in the program itself. The typical values for the present case are: A = 1.390576, B = 0.043357 min^{-1}, C_{corr} = -0.00304 min^{-2} and τ_e = 1384s. Using Eq. 2.10, ΔT turns out to be 0.2675K for the present case.

2.4.3 Determination of C

The values of ΔQ and ΔT having been calculated, the heat capacity $C = \Delta Q/\Delta T$ is evaluated at the average temperature $T_a = (T_f + T_i)/2$. The manner in which the

initial temperature T_i and the final temperature T_f are chosen, is shown in Fig. 2.8.

The specific heat of the sample is obtained by subtracting the heat capacity of the addenda (the sapphire sample holder including a small preweighed amount of grease) from the raw data. Once the heat capacity value is obtained using, the molecular and actual weight of the sample, we can easily determine the specific heat from it. Having obtained the specific heat value for a particular temperature, we return to driftline measurements and each such cycle gives us the specific heat value at a particular temperature.

2.4.4 Sources of Error

The main sources of error are:-

(i) Errors in temperature measurement

(ii) Errors in electrical measurements

(iii) Errors due to departure from isoperibolic conditions.

We have taken adequate precautions to minimize the errors arising due to the above mentioned factors. The thermometer calibration was performed at out Temperature Standard Group, with an estimated accuracy within 10^{-4}. Similarly, the calibration of electrical components at room temperature has an accuracy of better than 10^{-4}. We have also, through software control ensured that the thermal shield follows the sample temperature accurately. Thus, isoperibolic condition is maintained. Another important feature is that the sample should reach complete thermal equilibrium before commencing a new heating cycle, for which special care has been taken in the software.

2.4.5 Accuracy

The overall accuracy of our calorimeter and of the evaluation procedure according to Eq. 2.10 was tested by measuring the heat capacity of a 1.5 gm OFHC (oxygen free high conductivity) copper standard sample, obtained from our Vacuum Standards Laboratory. The results are displayed in Fig. 2.9. The continuous line indicates the

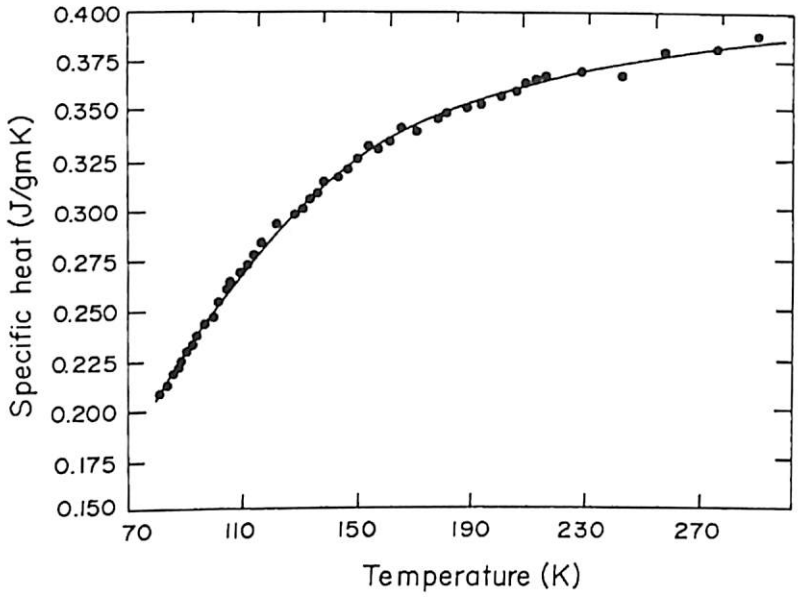

Figure 2.9: Specific heat as a function of temperature of OFHC copper

C_p values as listed in literature[86]. The standard deviation amounts to 0.72% and the maximum mean C_p value deviation does not exceed 0.8%. The scattering of the individual measured points is within 1% of the accepted value. The achieved accuracy essentially results from the improved post-heating drift line fitting procedure. There is no limitation to the use of the calorimeter down to liquid helium temperatures or to measure samples with high thermal conductivity.

Chapter 3

Site Dependent Substitutional Disorder in Er-123 system

3.1 Introduction

The oxygen deficient superconducting perovskites of general formula $RBa_2Cu_3O_{7-\delta}$ (where R= Y and the rare earths) exhibit a transition temperature of around 90 K. The first report on such a superconductor is credited to Wu et al.[14] who were investigating a compound with formula $(Y_{1-x}Ba_x)_2CuO_{4-\delta}$ with x = 0.4. The compound turned out to be superconducting with a transition onset temperature of 90 K, though the actual transition temperature was around 80 K. This result prompted them to conclude that superconductivity occurs in the Y-Ba-Cu-O system with a transition temperature between 80 and 90 K.

Following the discovery of superconductivity in the Y-Ba-Cu-O system, numerous researchers began to explore the feasibility of substituting different elements into the $Y_1Ba_2Cu_3O_{7-\delta}$ structure. Early studies[17, 18] on substitutions concentrated on replacement of Y by the different rare earth ions. These surveys found that all but a few of the lanthanide series ions could be incorporated in the $Y_1Ba_2Cu_3O_{7-\delta}$ structure. In fact, all the lanthanides except Ce and Tb can fully replace Y in the $Y_1Ba_2Cu_3O_{7-\delta}$ structure. Of the structures that have been synthesized, only $Pr_1Ba_2Cu_3O_{7-\delta}$ is not superconducting. For the remaining structures, transition temperatures of the order of 91-95 K are reported for the fully substituted structures[87].

In addition to the substitution at the Yttrium site, copper site substitution by the

metallic dopants such as nickel, zinc, iron, cobalt, gallium and aluminium has also been investigated extensively. These studies have established that each of the metallic dopants suppresses T_c albeit to a different extent . It is now generally agreed[88–91] that T_c is most strongly suppressed by zinc. Iron, cobalt and gallium, which act similarly, have a lesser degree of effect while nickel reportedly has the least effect on T_c.

The fluctuations in the superconducting order parameter, just above T_c, is an important effect responsible for a host of interesting phenomena, such as paraconductivity (excess conductivity), field induced broadening of resistivity curves, precursor diamagnetic susceptibility and excess specific heat etc., as reviewed by various authors[92, 93]. The thermodynamic fluctuations of the superconducting order parameter play a more important role in high temperature superconductors as compared to the conventional low-temperature superconductors. This is primarily due to both the high value of the superconducting-normal transition temperature (T_c), and the small value of the Ginzburg-Landau coherence length ξ_{GL} in the case of the high temperature superconductors.

As stated above, substitutional effects have been studied in considerable detail for the rare earth based 123 systems. A need was felt to study the fluctuation effects arising in conjunction with chemical substitutions in these systems, an area where there is a need to probe further. It is well established[92, 94] that owing to their quasi two-dimensional nature, coupled with their intrinsically very small coherence length ($\approx$10 Å), the fluctuation effects tend to become significantly pronounced in high-T_c cuprates in comparison to the conventional low-T_c superconductors which form three dimensional systems with large coherence lengths of about 1000 Å. The low dimensionality of the cuprate superconductors essentially stems from their unusual layered structure which comprises of one or more planar CuO_2 layers intervened by other cationic-oxide (or pure cationic) layers. With the exception of epitaxial thin films of these cuprates prepared under stringent conditions, the majority of samples[95] even in pure form generally exhibit significant resistive transition widths ΔT. The origin of the large ΔT is considered to be a manifestation of superconducting fluctuations in the

form of excess conductivity at temperatures just above T_c. Secondly, a comparatively broad specific heat anomaly at T_c depicted by the high T_c cuprates, is also believed to be a direct consequence of fluctuations in the order parameter around T_c[96, 97].

This chapter presents a systematic study of the dc resistivity, ac magnetic susceptibility and specific heat measurements in the Er-123 system for both the pure phase and when Cu is partly (0.5%) replaced by Ni, Zn, Fe, Co and Ga. It is reported that the nominally trivalent elements like Fe[89, 98, 99], Co[89, 99] and Ga[89, 99, 100] substitute at the Cu(1) site and cause a moderate reduction in T_c, while nominally divalent dopants like Zn[98, 99, 101] and Ni[89, 99, 102] primarily occupy the Cu(2) site. Divalent substitution would be referred to as in-plane disorder and trivalent substitution as out-of-plane disorder. Purely from superconductivity considerations the main difference between the two substitutions is that the former interrupts the CuO_2 planes where superconductivity is supposed to reside, while the latter affects the chains and thereby influences the interlayer coupling between the successive stacks of CuO_2 planes of the neighboring unit cells along the c-direction. The former has the effect of lowering the T_c while the latter tends to broaden the resistive transition. The role of the interlayer coupling in broadening the resistive transition of Bi-2122 system has been elaborated by Samanta et al.[103]. A comparative study of the effects of the in-plane and out-of-plane substitutions in Er-123 system on the resistivity, ac magnetic susceptibility and specific heat anomaly should provide a useful insight into the possible role of fluctuations associated with the site dependent disorder in the system.

3.2 Experimental Details

The bulk polycrystalline samples of composition $ErBa_2(Cu_{1-x}M_x)_3O_{7-\delta}$ [(M:Ni, Zn, Fe, Co and Ga) and $x = 0.005$] were prepared by solid state reaction using ingredients of purity 99.999%. The different samples (Pure, Cu/Ni, Cu/Zn, Cu/Fe, Cu/Co and Cu/Ga) are designated as (1) Er-123 (pure), (2) Er-123 (Ni), (3) Er-123 (Zn), (4) Er-123 (Fe), (5) Er-123 (Co) and (6) Er-123 (Ga). The synthesis procedure has already been described in chapter 2. It must be mentioned that because of simultaneous

oxygen annealing of all the samples and the low doping level, their oxygen contents are assumed to be nearly identical.

The characterization of the samples for phase purity was carried out by X-ray diffraction (XRD), using a Siemen's D-500 diffractometer with Cu-K_α radiation. The scanning electron micrographs (SEM) for different specimens to study the grain size distribution were recorded in a secondary-electron-emission mode with a 0°C tilt using a JOEL JSM 35 CF instrument. Electrical resistivity measurements were carried out from the room temperature to 77 K. In the ac susceptibility measurement the samples were cooled in a low field of .02513 Oe (rms) superimposed with a dc field of 6.033 Oe, and a frequency of 111.1 Hz through their transition temperatures (T_c) and χ' and χ'' were measured while warming up slowly. Suitable demagnetization factor for each sample taken from the instrument manual, was used to calculate the absolute value of susceptibility. The specific heat of the samples was measured in the temperature range 77-120 K. The details of the measurement techniques are described in chapter 2.

3.3 Results

3.3.1 XRD

Figure 3.1 shows the XRD patterns of the samples Er-123 (pure), Er-123 (Ni) and Er-123 (Zn). It is clear from the figure that all the important and major peaks of the 123 structure namely (110)/(103), (104), (113), (123)/(213) etc. (reflections for the orthorhombic structure) are found in these samples. The expected orthorhombic splitting associated with (110), (103) and (123), (213) peaks can clearly be observed in all the three samples. This indicates that all the three samples are essentially orthorhombic as has been reported for the pure, Ni and Zn substituted rare earth based 123 samples[104]. Fig. 3.2 shows the XRD patterns of the samples Er-123 (Fe), Er-123 (Co) and Er-123 (Ga). Here also all the prominent peaks corresponding to the 123 structure namely, (103), (104), (113), (123)/213) etc. (reflections of the orthorhombic structure) are present. In case of these samples also we find the orthorhombic split-

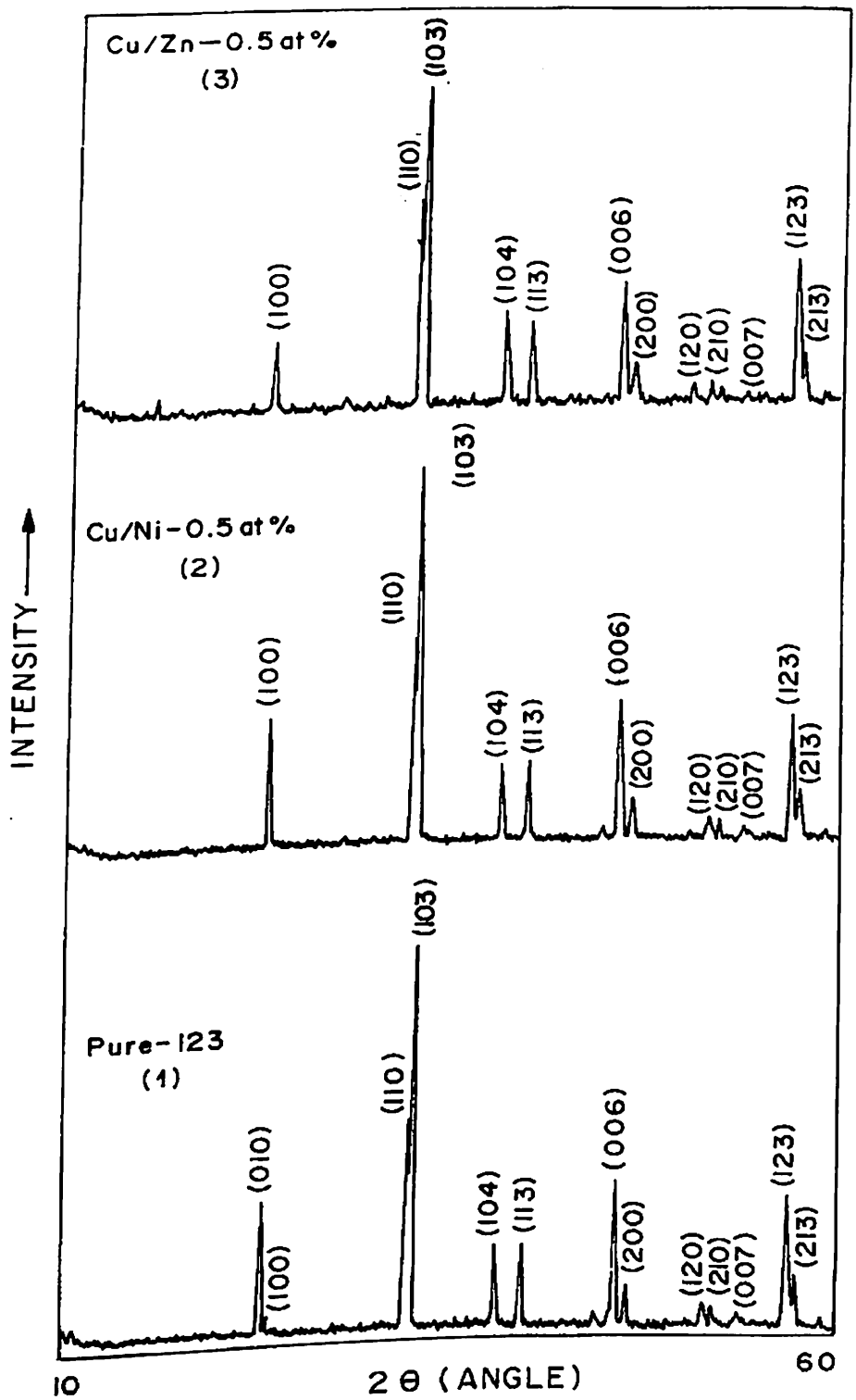

Figure 3.1: XRD patterns of (1) Er-123 (pure), (2) Er-123 (Ni) and (3) Er-123 (Zn).

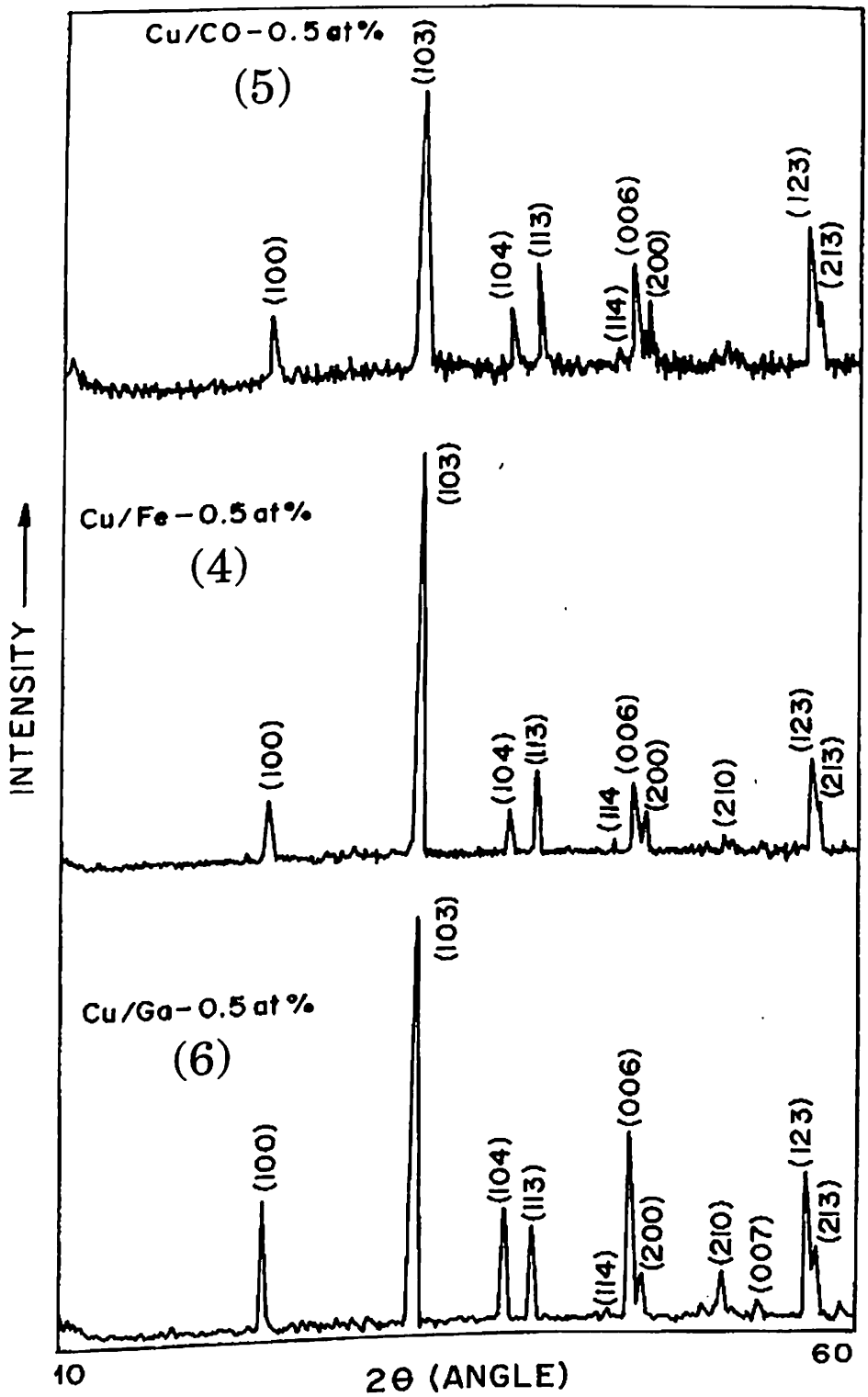

Figure 3.2: XRD patterns of (4) Er-123 (Fe), (5) Er-123 (Co) and (6) Er-123 (Ga).

Table 3.1: Lattice parameters of the six samples

Sample	a (Å)	b (Å)	c (Å)	(b−a)/(b+a) (X 10^{-3})
Er-123 (pure)	3.82	3.89	11.63	9.08
Er-123 (Ni)	3.82	3.89	11.62	9.08
Er-123 (Zn)	3.82	3.89	11.63	9.08
Er-123 (Fe)	3.83	3.86	11.64	3.90
Er-123 (Co)	3.83	3.87	11.63	5.19
Er-123 (Ga)	3.84	3.86	11.64	2.60

ting in case of the peaks (123) and (213). Thus these three sample also seem to be orthorhombic but the degree of orthorhombicity is less as compared to the former three samples. This is evident as in the latter three samples the peak with maximum relative intensity has no orthorhombic splitting. Furthermore, all the six samples are single phase materials because no impurity peaks have been observed in their XRD patterns. This suggests the upper limit of 1-3% for the level of any impurity phase that may be present in these samples. Further there is no reason to believe that the effect of the impurity phase, if any, is more in the case of Fe, Co and Ga substituted samples.

The lattice parameters for these six samples (shown in Table 3.1) are obtained by our optimization programme taking into account all of the peaks. The observed d values are compared with the calculated d values and the difference ($d_{obs} - d_{cal}$) occurs in the third decimal place. As is apparent from the lattice parameter values, all the samples are orthorhombic. In case of Er-123(Fe), Er-123(Co) and Er-123(Ga) samples though, the degree of orthorhombicity is lower in comparison to the Er-123(pure), Er-123(Ni) and Er-123(Zn) samples which is apparent from the values of a and b parameters for these samples. This variation in the degree of orthorhombicity is shown in the form of a plot of the spontaneous strain (b−a)/(b+a) (values listed in Table 3.1) for all the samples in Fig. 3.3.

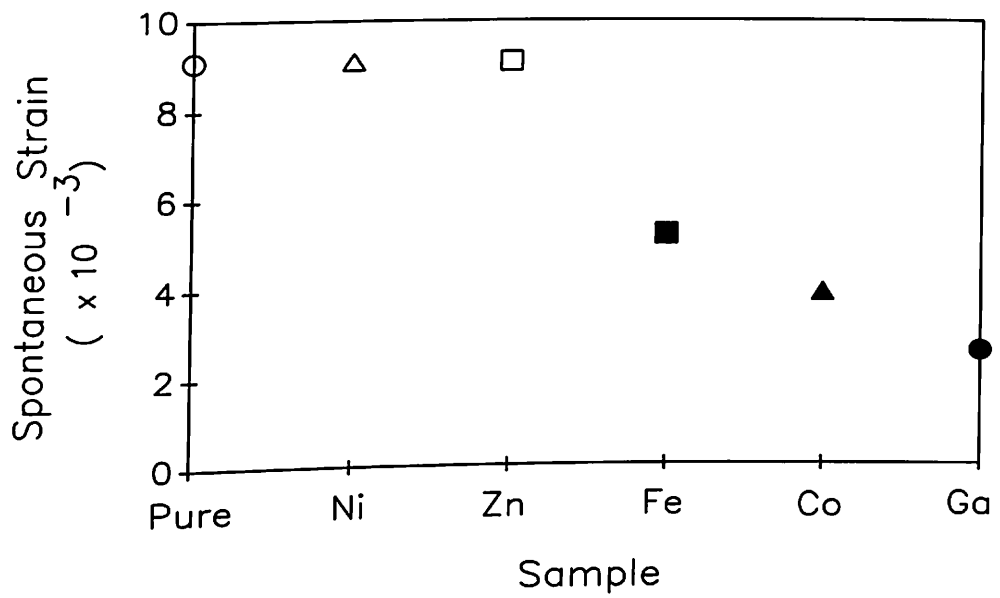

Figure 3.3: Spontaneous strain plot for all the six samples.

3.3.2 SEM

SEM studies reveal that there is a homogeneous and uniform distribution of grains with sizes ranging between 2 and 6 microns for all the samples. The SEM micrographs for the pure and Co substituted sample are shown in Figs. 3.4 and 3.5 respectively.

3.3.3 Resistivity

Figure 3.6 shows the variation of resistivity (ρ) with temperature (T) in the range 77 K - 290 K for all the six samples. The inset shows a view of the resistivity plot in a temperature range close to the transition temperature. $T_c(R = 0)$ is 92.5 K, 89.1 K, 86.2 K, 88.5 K, 89.9 K and 89.5 K for the samples Er-123 (pure), Er-123 (Ni), Er-123 (Zn), Er-123 (Fe), Er-123 (Co) and Er-123 (Ga), respectively. The normal state behaviour of resistivity of all the samples is essentially analogous because of the low substitution level of the dopant. Interestingly though, the absolute value of normal state resistivity for the substituted samples shows a distinctly higher value as compared to the pure sample. It is clear from the inset of Fig. 3.6 that T_c (onset) in comparison to the Er-123(pure) sample decreases with different substitutions and

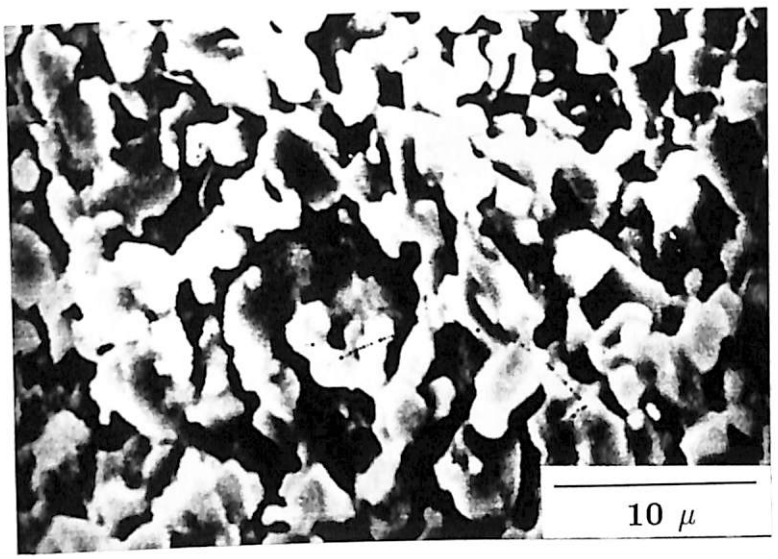

Figure 3.4: SEM micrograph of Er-123 (pure).

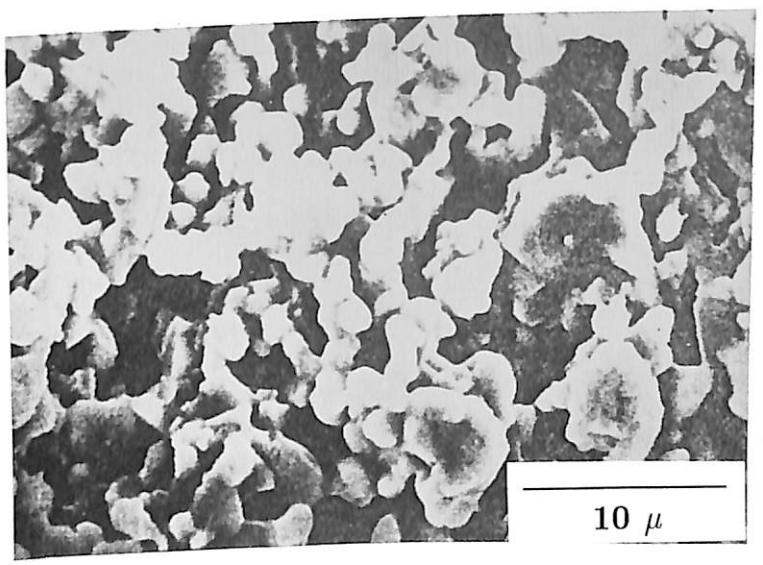

Figure 3.5: SEM micrograph of Er-123 (Co).

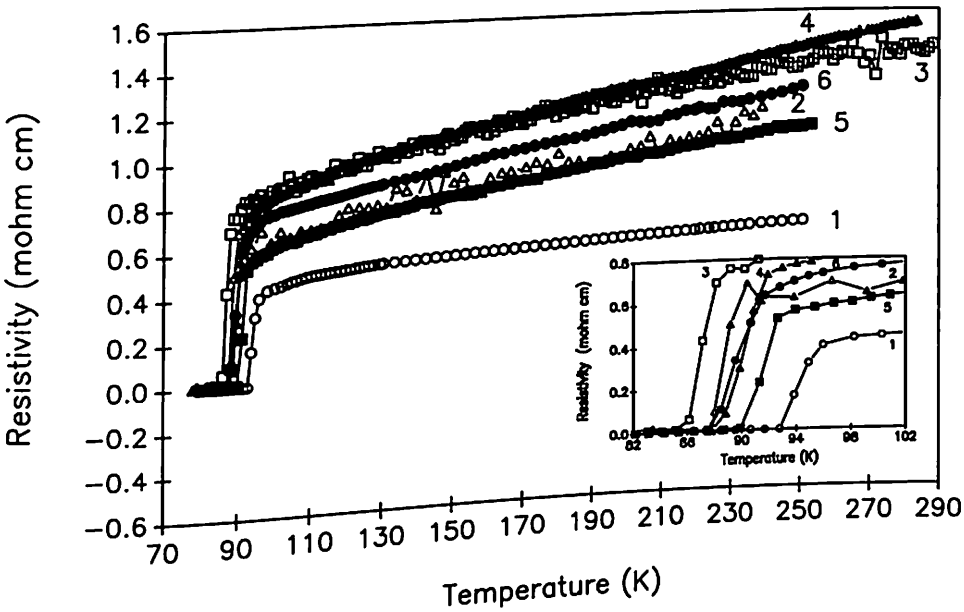

Figure 3.6: Resistivity (ρ) vs Temperature (T) curves for (1) Er-123 (pure), (2) Er-123 (Ni), (3) Er-123 (Zn), (4) Er-123 (Fe), (5) Er-123 (Co) and (6) Er-123 (Ga).

$T_c(R = 0)$ shows a significant change with substitutions as well. The maximum depression ($\approx$ 6 K) in the transition temperature is observed for Er-123 (Zn) sample. Figure 3.7 shows the temperature derivative of normalized resistivity ($d\rho_N/dT$) as a function of temperature for all the samples. The normalization was carried out with reference to room temperature resistivity for Er-123(pure). This figure reveals that the width of transition $(\Delta T)_R$ for the pure, Ni and Zn substituted samples is essentially similar and comparatively smaller than that for the Fe, Co and Ga substituted samples. The values of the transition widths for all the samples are listed in Table 3.2. The transition width has been calculated by taking the FWHM (Full width at half maximum) for all the samples from their derivative plots. As mentioned earlier, all the samples have been prepared under identical conditions, so that the difference in the values of $(\Delta T)_R$ for the two sets of samples can be attributed to the effect of the doping on the intrinsic properties of the superconducting phase.

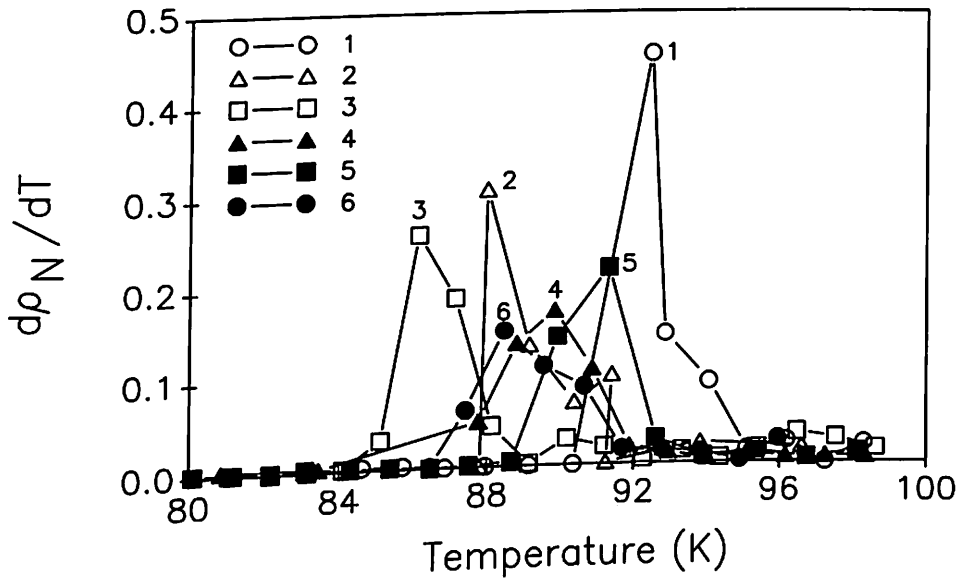

Figure 3.7: ($d\rho_N/dT$) vs T curves for (1) Er-123 (pure), (2) Er-123 (Ni), (3) Er-123 (Zn), (4) Er-123(Fe), (5) Er-123 (Co) and (6) Er-123 (Ga) [ρ_N is the normalized resistivity].

Table 3.2: Transition widths (FWHM) of all the samples

Sample	$(\Delta T)_{R,FWHM}$ (K)
Er-123(Pure)	1.63789
Er-123(Ni)	1.65094
Er-123(Zn)	2.29067
Er-123(Fe)	3.10010
Er-123(Co)	2.93041
Er-123(Ga)	3.58140

3.3.4 AC Susceptibility

Figure 3.8 shows the results of ac susceptibility ($\chi = \chi' - i\chi''$) measurements in the temperature range 77-130 K for all the six samples. From the χ' data, we find

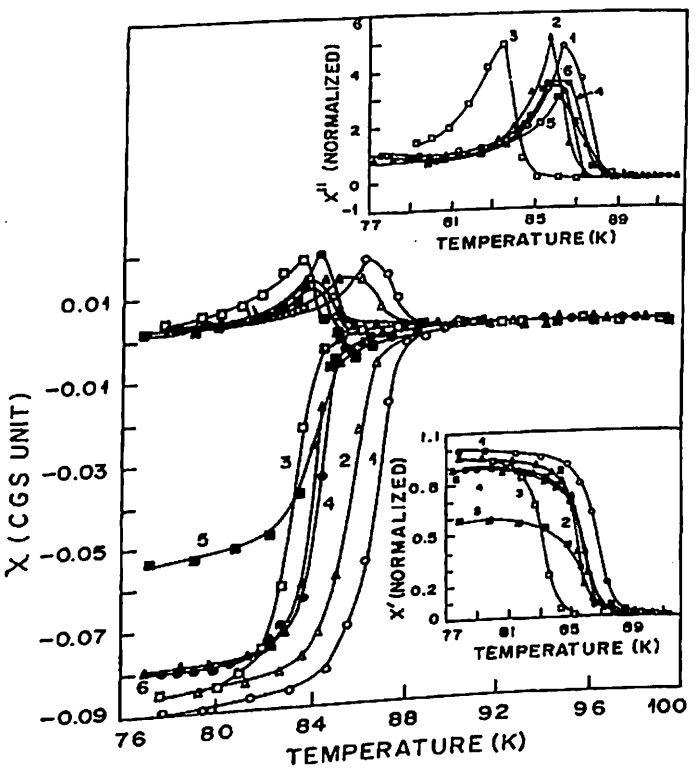

Figure 3.8: AC susceptibility ($\chi = \chi' - i\chi''$) vs Temperature (T) curves for (1) Er-123 (pure), (2) Er-123 (Ni), (3) Er-123 (Zn), (4) Er-123 (Fe), (5) Er-123 (Co) and (6) Er-123 (Ga). Lower inset: χ' (normalized) vs T curves; upper inset: χ'' (normalized) vs T curves.

that the flux exclusion onset temperature is 90.5 K, 89.5 K, 86 K, 90 K, 88.5 K and 89.6 K for the samples Er-123 (pure), Er-123 (Ni), Er-123 (Zn), Er-123 (Fe), Er-123 (Co) and Er-123 (Ga), respectively. As previously reported[105], the susceptibility and magnetization data are difficult to interpret in terms of the percentage of full diamagnetism. This is because in the field-cooled experiments Meissner fraction is dependent on factors such as external field, sample size and perfection and may bear little relation to the proportion of the superconducting phase present in the sample. Moreover, it may also be possible that the relative change in the diamagnetic signal could reflect an improvement in the superconductivity at the grain boundaries or a

better connection of superconducting paths in the sample. Furthermore, Hein[106] and Goldfrab[107] et al. have pointed out that ceramic samples must be pulverized, the intergranular coupling must be depressed, and/or the χ' value should be taken well below the intrinsic T_c, and even then the superconducting volume fraction is only a rough estimate. However, as the measurements were carried out under field-cooled and identical conditions on different samples, therefore the diamagnetic amplitude at a particular temperature can be compared in the first approximation. The lower inset of Fig. 3.8 shows the size of the χ' signals at 77 K for the different samples after normalization has been carried out with respect to the χ' value at 77 K for the pure sample. It is clear that the diamagnetic amplitude at 77 K for the samples Er-123 (Ni) and Er-123(Zn) is nearly the same and is comparable to the diamagnetic amplitude for the pure sample. However, for the samples Er-123 (Fe), Er-123(Co) and Er-123(Ga), it is significantly reduced.

The peak χ'' which is linked with the diamagnetic transition and is influenced by the Josephson-like coupling between the grains, is shown in the upper inset of Fig. 3.8 [normalized with reference to χ'' of Er-123 (pure)]. It may be mentioned here that both χ' and χ'' are very sensitive to intragranular and intergranular superconductivity. The behaviour of χ'' for all the substituted samples is essentially mutually analogous, and so there is no reason to believe that weak link effects are more dominating for any one set of substitutions.

All the samples were cut to the same dimension and have undergone the same sintering conditions (method of calcinations, oxygen flow, furnace temperatures, pressure exerted during the formation of the pellet etc.). Thus, it is assumed that the demagnetization factor for all the samples are similarly corrected. Therefore, one can compare the width of the superconducting transition as observed in χ' [$(\Delta T)_{\chi'}$] vs temperature plot of all the samples. Fig. 3.9 shows the $d\chi'/dT$ as a function temperature for all the samples. From this plot it is clear that like $(\Delta T)_R$, the width of the transition of the susceptibility plot $[(\Delta T)_{\chi'}]$ for Ni and Zn substituted samples is more or less the same as for the pure sample. However, it is comparatively large for the Fe, Co and Ga substituted samples.

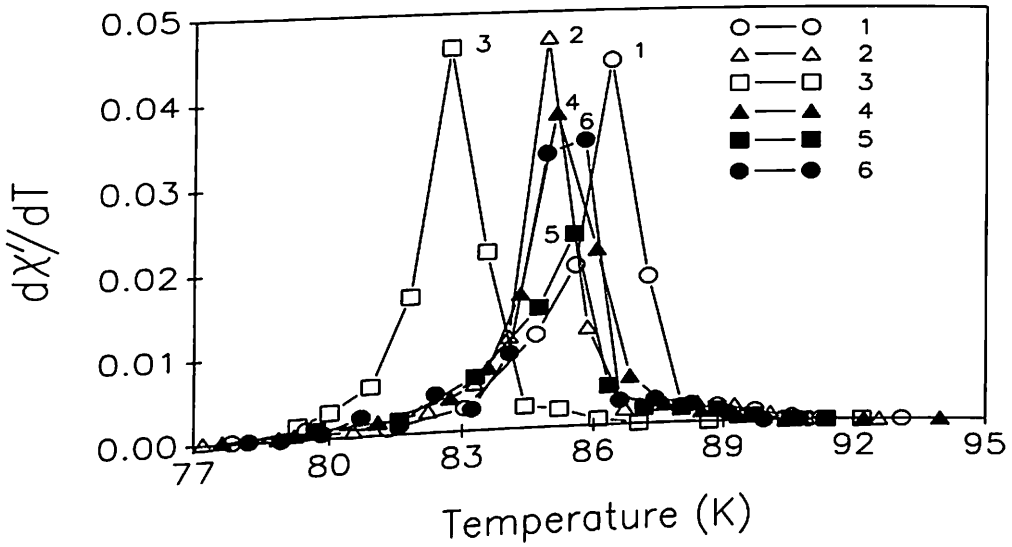

Figure 3.9: ($d\chi'/dT$) vs T curves for (1) Er-123 (pure), (2) Er-123 (Ni), (3) Er-123 (Zn), (4) Er-123 (Fe), (5) Er-123 (Co) and Er-123 (Ga).

3.3.5 Specific Heat

Figure 3.10 shows distinct and clear C_p anomalies at 90, 88, and 84 K respectively, for the samples Er-123 (Pure), Er-123 (Ni) and Er-123 (Zn). The inset of Fig. 3.10 shows the plot of C_p/T against temperature for the same samples. Fig. 3.11 shows the specific heat data of the samples Er-123 (Fe), Er-123 (Co) and Er-123 (Ga) and the inset depicts the plot of C_p/T as a function of temperature. The specific heat anomaly is also seen for these samples but it is relatively broad and smeared. The actual calculation of the specific heat jump has been done using the principle of 'equal area construction' at the mean field transition temperature T_c^{mf}. This principle is based on the fact that the entropy is conserved at the point of transition for the case of a second order phase transition. Superconducting to normal phase transition is infact, a second order phase transition. The specific heat jump calculation is shown in Fig. 3.12 for the zinc, iron and Gallium substituted samples. In this figure we have plotted C_p/T vs temperature for the samples and linearly extrapolated the data near and on both sides of the transition temperature towards that temperature (T_c^{mf}) where

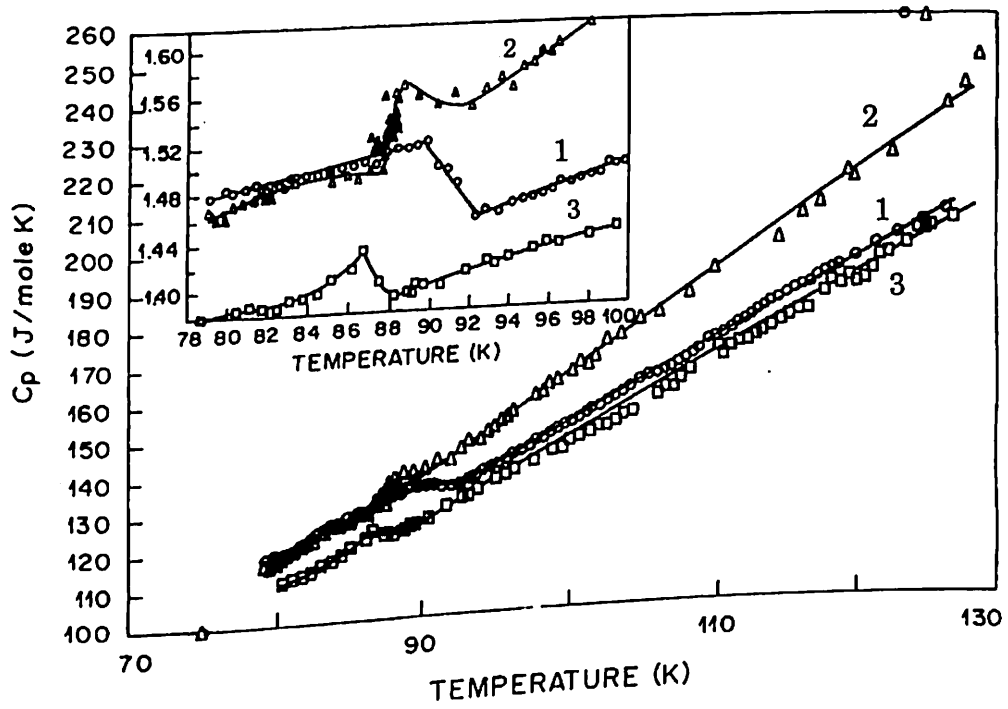

Figure 3.10: Molar specific heat (C_p) vs Temperature (T) curves for (1) Er-123 (pure), (2) Er-123 (Ni), and (3) Er-123 (Zn); the inset shows C_p/T vs T for these samples.

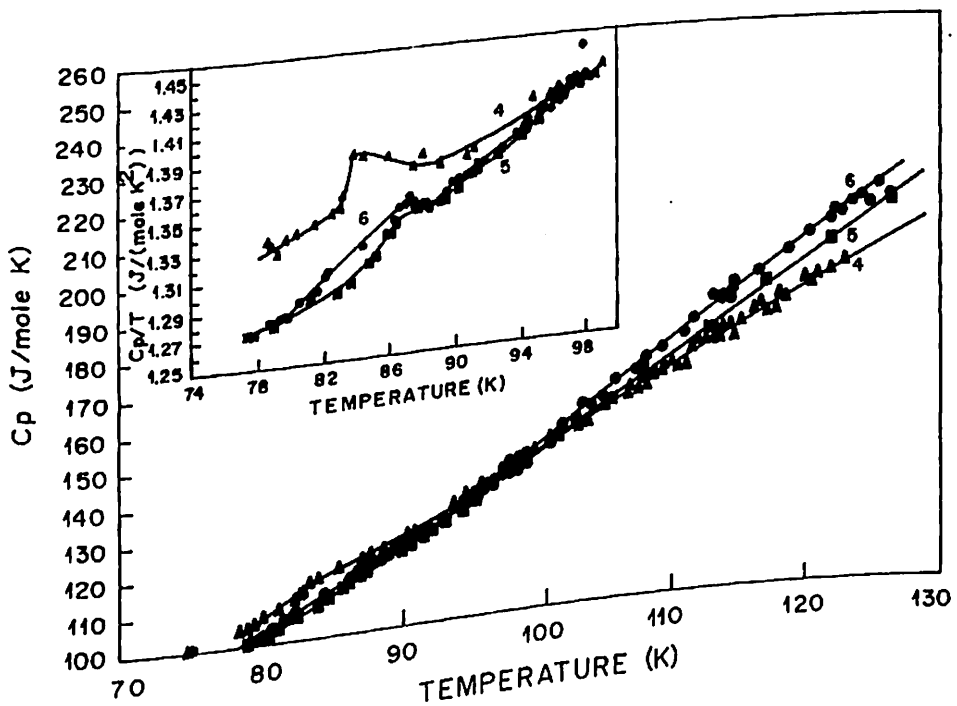

Figure 3.11: Molar specific heat (C_p) vs Temperature (T) curves for (4) Er-123 (Fe), (5) Er-123 (Co), and (6) Er-123 (Ga); the inset shows C_p/T vs T for these samples.

Table 3.3: T_c^{mf}, ΔC_p and $(\Delta C_p/T)_{T = T_c^{mf}}$ for all the samples

Sample	T_c^{mf} (K)	ΔC_p (J/mole K)	$(\Delta C_p/T)_{T = T_c^{mf}}$ (mJ/mole K^2)
Er-123(Pure)	91.05	6.92	76
Er-123(Ni)	89.37	4.11	46
Er-123(Zn)	87.47	3.76	43
Er-123(Fe)	85.05	2.81	33
Er-123(Co)	88.21	2.74	31
Er-123(Ga)	87.63	1.23	14

the two triangles (generated by the construction) become equal in area. The mean field transition temperatures thus calculated are listed in Table 3.3. The jump turns out to be within 4.5 J/mol K for the Ni and Zn substituted samples, while for the samples with Fe, Co and Ga substitution, it is less than 3 J/mol K. The estimated $\Delta C_p/T_c^{mf}$ for the substituted samples is between 20-48 mJ/mol K^2 . These parameters are in good agreement with the published data[43, 104, 108–110]. The pure sample shows a comparitively larger discontinity ($\Delta C_p/T_c \approx 76$ mJ/moleK^2) in the specific heat. Philips et al.[50] estimated that $\Delta C_p/T_c \approx 77$ mJ/moleK^2 for a fully superconducting 123 sample. Junod et al.[111] report a similar estimate for the 100% superconducting transition. Table 3.3 presents all these results. The characteristic parameters, of a solid like the Sommerfeld constant (γ) and the Debye temperature (θ_D), are difficult to estimate in these oxide superconductors because it is very difficult to separate out the electronic and phononic contributions to the specific heat in the case of these superconductors. Infact one method could be to apply a magnetic field greater than the critical value and measure the specific heat of the superconductor in its normal state down to liquid helium temperatures. In that case from the known approximations of the phononic contribution ($\approx f(\theta_D)T^3$) of a normal solid at very low temperatures and the linear electronic contribution (γT), we should be able to evaluate the Sommerfeld constant and the Debye temperature easily. This is the method employed for the determination of γ and θ_D for conventional superconductors. The difficulty, however,

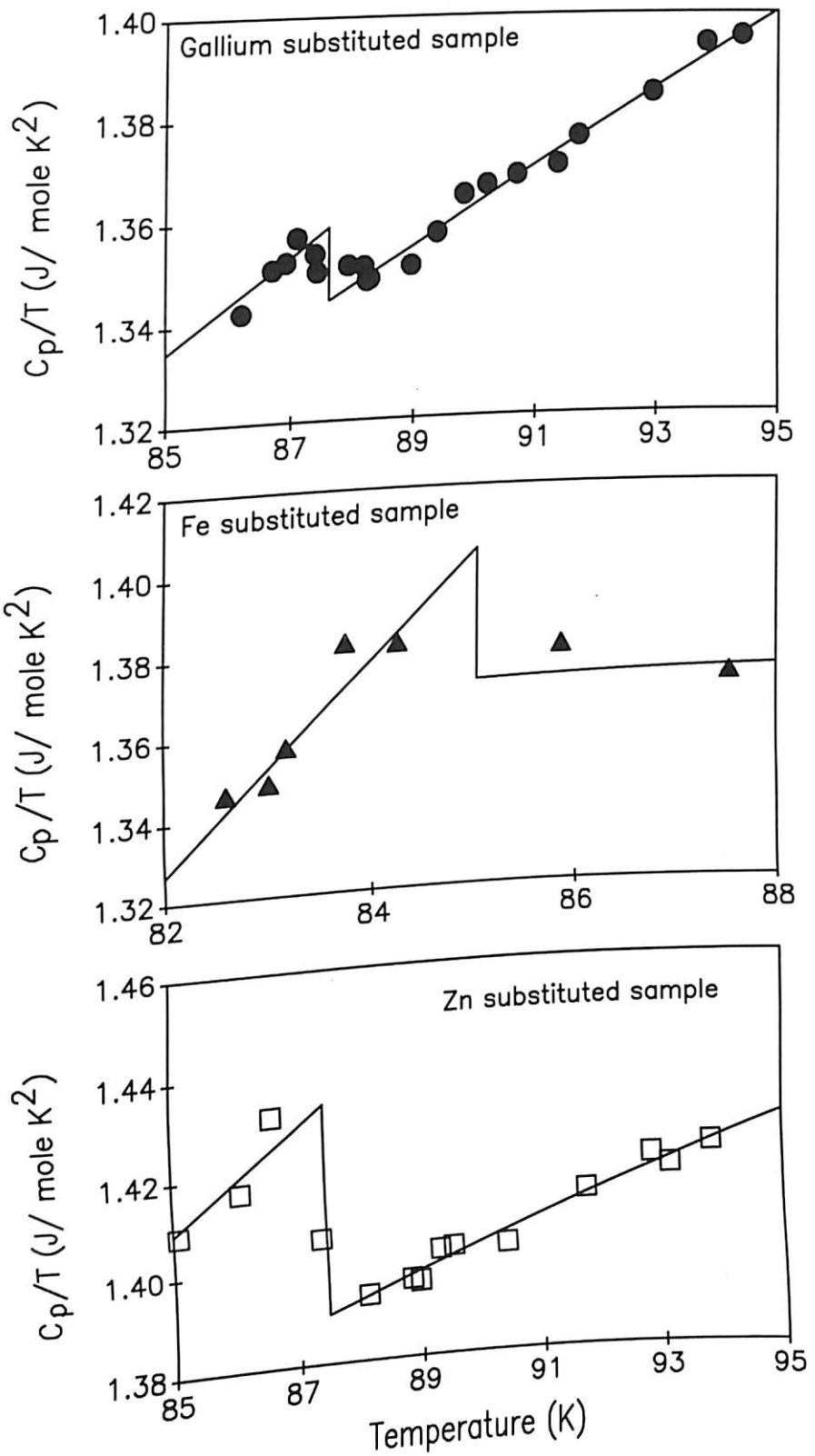

Figure 3.12: Equal area construction for the zinc, iron and gallium substituted samples

lies in the fact that the high T_c superconductors have a very high critical field at low temperatures (for the 123 superconductor the value of the critical field at liquid helium temperatures is around 100 T in a direction perpendicular to the CuO_2 planes and 300 T in a direction parallel to the planes) and therefore it is not possible to quench superconductivity down to liquid helium temperature range. Thus, to estimate the Sommerfeld constant and the Debye temperature in a high T_c superconductor some indirect method has to be applied. We have estimated the Sommerfeld constant (γ) from the normal state behaviour of the susceptibility. It is known that in the normal state a superconductor is paramagnetic in nature. A paramagnetic material obeys the Curie-Weiss law which is given below:

$$\chi = \chi_o + \frac{C}{T - \theta} \tag{3.1}$$

where χ_o is temperature independent (resulting from diamagnetic core contribution of different ions and Pauli paramagnetism), C is a constant and θ is the Curie-Weiss temperature. Thus, by plotting χ(T) vs $1/(T-\theta)$ and employing a straight line fit in the normal state the value of χ_o is obtained for all the samples. From this value the Pauli susceptibility is estimated by subtracting the contribution due to core diamagnetism of the different constituent ions. To obtain the core contribution for different samples the known diamagnetic contributions due to the different constituent ions are added. These values are given in Table 3.4. The diamagnetic susceptibilities associated with different samples are presented in Table 3.5. Having obtained the Pauli susceptibility, the Wilsons ratio is employed to obtain the Sommerfeld constant. This relation is given as

$$\frac{\gamma}{\chi_P} = \frac{1}{3}\left(\frac{\pi k_B}{\mu_B}\right)^2 \tag{3.2}$$

where χ_P is the Pauli susceptibility, k_B is the Boltzmann's constant and μ_B is the Bohr magneton. The value of the Sommerfeld constant obtained for the different samples is given in Table 3.5. The reported value of γ in these systems is in the range 20-50 mJ/mole K^2[104, 108, 112–116] and our rough values fall within this range.

Similarly, the calculation of Debye temperature is rather difficult in the case of the high temperature superconductors. Therefore, it is estimated from the actual

Table 3.4: Diamagnetic susceptibilities associated with different ions

Ion	Diamagnetic susceptibilities (X 10^{-10} m^3/mol)
Er^{3+}	−2.2629
Ba^{2+}	−4.0229
Cu^{2+}	−1.3826
Ni^{2+}	−1.5086
Zn^{2+}	−1.2571
Fe^{3+}	−1.2571
Co^{3+}	−1.2571
Ga3+	−1.0057
O^{2-}	−1.5086

Table 3.5: Diamagnetic susceptibility, Sommerfeld constant and Debye temperature of all the samples

Sample	Diamagnetic susceptibility (10^{-9} m^3/mol)	γ (mJ/mol K^2)	θ_D (K)
Er-123(Pure)	−2.5017	40	435
Er-123(Ni)	−2.5019	26	407
Er-123(Zn)	−2.5015	42	444
Er-123(Fe)	−2.5015	43	450
Er-123(Co)	−2.5015	28	450
Er-123(Ga)	−2.5011	25	446

experimental specific heat data by using the theoretical Debye function (Eq. 3.3) on the assumption that the three dimensional Debye model is valid in these systems. Since the electronic contribution to the specific heat in the normal state (γT) is known, therefore the lattice specific heat can be evaluated in the normal state by subtracting the electronic part from the experimental specific heat values. The calculated lattice specific heat values at different temperatures are used in the Debye equation (Eq. 3.3) where N′ denotes the number of atoms in a unit cell and the Debye temperature is treated as a variable.

$$C_p = 9N'R\left(\frac{T}{\theta_D}\right)^3 \int_0^{\frac{\theta_D}{T}} \frac{e^x\, x^4}{(e^x-1)^2} dx \qquad (3.3)$$

The obtained Debye temperatures are found to be temperature dependent, and the average value of the Debye temperature around the transition temperature has been calculated for all the samples and listed in Table 3.5. These values agree well with the reported values[104].

3.4 Discussion

The above mentioned results indicate two distinct types of behaviours :

(1) when divalent Ni and Zn are substituted,

(a) The transition width from the resistivity measurements as well as the susceptibility measurements both indicate that the substitution of Ni and Zn does not change the transition width significantly as compared to the pure sample.

(b) the relative size of the χ' signals at 77 K for the pure and the substituted samples are comparable.

(c) clear specific heat anomaly at the respective transition temperatures is seen for all the three samples; and

(2) when trivalent Fe, Co and Ga are substituted,

(a) both the $(\Delta T)_{R,FWHM}$ and the width from the susceptibility plot for the substituted samples are large as compared to the pure sample.

(b) the relative size of the χ' signals at 77 K for the substituted samples is lower as compared to the pure sample.

(c) the substituted samples show a broad specific-heat anomaly at the transition temperature in comparison to the pure and the nickel and zinc substituted samples.

It may be emphasized here that, as already mentioned, XRD and SEM studies for the above series of samples have given no indication of any macroscopic inhomogeneity in either the in-plane or out-of-plane substitutions. Thus, the above results may be ascribed primarily to the substitutions. In this context, it is interesting to mention that bulk Y-124 samples have shown the resistivity transition to be noticeably broadened for Fe, Co and Ga substitutions as compared to Ni and Zn substitution[117].

In order to understand the situation described above, we first analyze the resistivity data of all the samples in the mean field theory (MFT) to determine the excess conductivity due to fluctuations. The excess conductivity ($\Delta\sigma$) due to thermal fluctuations is defined as the deviation of the measured conductivity (σ_m) from the normal conductivity (σ_n). The normal conductivity is extracted from the background normal state resistivity (ρ_n) which is generally calculated using either the linear T dependent form[118]

$$\rho_n(T) = \rho_o + BT \tag{3.4}$$

or using the formula

$$\rho_n(T) = \rho_o' T + \frac{B'}{T} \tag{3.5}$$

suggested by Anderson-Zou[119]. In this study the experimentally obtained resistivity data have been fitted in the normal state with the linear resistivity formula of Eq. 3.4 for $T>2T_c^{mf}$ where T_c^{mf} is the mean field transition temperature as determined from the resistivity measurements. The resistivity curves of all the samples along with the linear background fits are shown in Figs. 3.13 and 3.14 for temperatures close to the transition temperatures. The values of ρ_o and B obtained from this fitting are listed in Table 3.6. The excess conductivity ($\Delta\sigma$) is given by

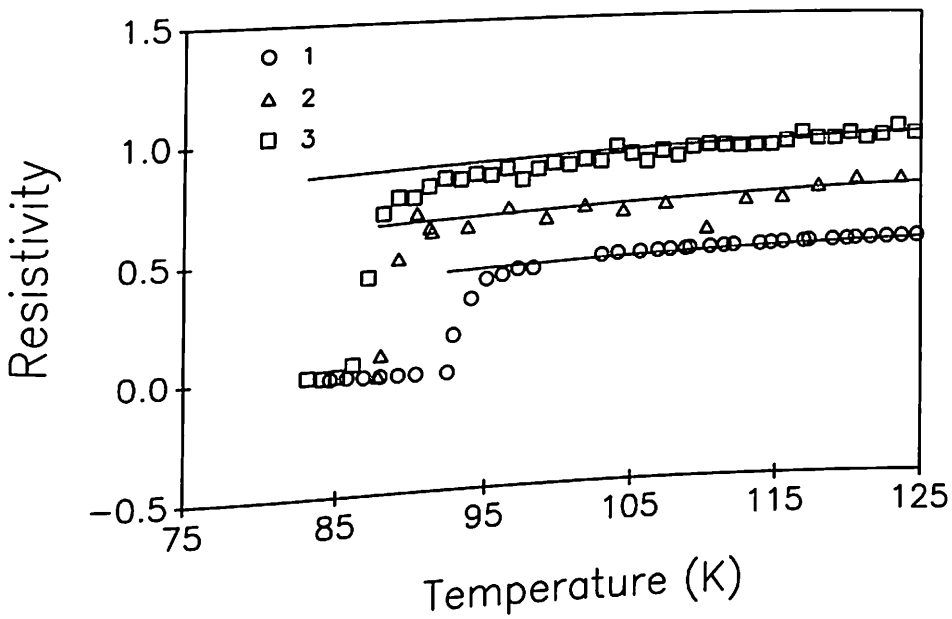

Figure 3.13: Resistivity vs Temperature for (1) Er-123 (pure),(2) Er-123 (Ni) and (3) Er-123 (Zn);solid line shows fitting of the data with $\rho_n(T) = \rho_o + B\,T$

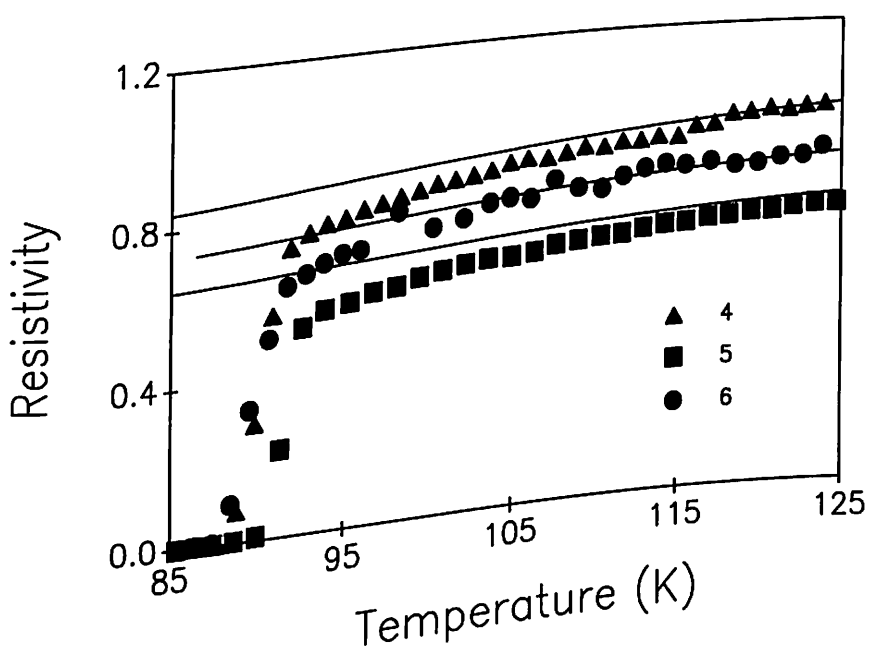

Figure 3.14: Resistivity vs Temperature for (4) Er-123 (Fe),(5) Er-123 (Co) and (6) Er-123 (Ga);solid line shows fitting of the data with $\rho_n(T) = \rho_o + B\,T$

Table 3.6: Parameters obtained from linear fitting of normal state resistivity

Sample	ρ (mΩ cm)	B (mΩ cm/K)
Er-123(Pure)	0.182	2.726
Er-123(Ni)	0.367	3.150
Er-123(Zn)	0.606	3.008
Er-123(Fe)	0.533	3.607
Er-123(Co)	0.344	2.974
Er-123(Ga)	0.466	3.102

$$\Delta\sigma = \frac{1}{\rho(T)} - \frac{1}{\rho_n(T)} \tag{3.6}$$

Above the critical temperature the fluctuation contribution to conductivity can be due to the Aslamazov-Larkin[120] and Maki-Thomson[121] terms. The Maki-Thomson contribution is considered to be negligible in cuprate superconductors because of their being in the dirty limit[94]. Aslamazov-Larkin model is used for analysis according to which

$$\Delta\sigma = \frac{e^2}{16\hbar t}(\epsilon)^{-1} \tag{3.7}$$

and

$$\Delta\sigma = \frac{e^2}{32\hbar\xi(0)}(\epsilon)^{-\frac{1}{2}} \tag{3.8}$$

for the case of 2-dimensional (2D) and 3-dimensional (3D) fluctuations respectively. In these equations $\epsilon = \frac{T-T_c^{mf}}{T_c^{mf}}$ is the reduced temperature, e is the electronic charge, t is the thickness of the superconducting layer, $\hbar$ is the reduced Planck's constant, T_c^{mf} is the mean-field critical temperature and $\xi(0)$ is the three-dimensional coherence length at T = 0 K. The mean field transition temperature can be determined in a number of ways. The two most commonly used methods are

(i) T_c^{mf} corresponds to temperature at which $\Delta\sigma^{-2} = 0$ in $\Delta\sigma^{-2}$ vs temperature plot.

(ii) Temperature corresponding to $d\rho/dT$ peak i.e. where $d^2\rho/dT^2 = 0$.

Using any one of the methods there is no change in the order parameter dimensionality of the systems in the mean-field-region. In the present study, however, the method is used in which T_c^{mf} is taken as the temperature corresponding to $d\rho/dT$ peak. The use of this method has been suggested by Upreti et al.[122, 123] for an unambiguous determination of T_c^{mf}. The Aslamazov Larkin model is valid only in the mean field region which is defined by $-3.5 \leq \ln\epsilon \leq -1.5$. The $\ln(\Delta\sigma)$ vs $\ln(\epsilon)$ plots for all the samples are shown in the Figs. 3.15 - 3.17. The linear fits carried out in the mean field region for the different samples are indicated in the same figures by solid lines. The slopes of the fitted lines are also indicated in the respective figures and from these the dimensionality of the fluctuations can be found out. If the slope is equal to or close to -1 then the fluctuations are 2-dimensional in nature, while a slope equal to or close to $-1/2$ indicates 3-dimensional fluctuations. For the case of the pure sample (Fig. 3.15) we do not find a single linear region which seems to indicate that there is no single power law dependence of the fluctuations. In fact the slopes of the two linear regions indicate a clear 3D-2D crossover of the order parameter dimensionality from a higher to a lower temperature. In the Zn, Fe, Co and Ga doped samples no such crossover is seen and the fluctuations in these samples behave as 2D in most part of the mean-field region. The data for the nickel substituted sample does not show any definite result as far dimensionality of the order parameter is concerned and so its plot has not been included. In pure YBCO Fontana et al.[124] have observed a crossover of the order parameter dimensionality from 2D-3D from higher to lower temperatures and a similar observation for the YBCO epitaxial thin films has been reported by Oh et al.[125]. Our observations on the bulk Er-123 (Pure) sample though in contradiction with the above mentioned studies, do match the findings of Ausloos et al.[126] who working on bulk YBCO samples reported a similar 3D-2D crossover from the high to the low temperature side. Upreti et al.[122] have studied the fluctuation effects in pure and 0.33% zinc doped epitaxial thin films of $YBa_2Cu_3O_{7-\delta}$ superconductor. They observe that zinc doped film shows a 2D behaviour in most part of the mean-field-region, a result similar to the zinc doped sample of the present study. In the undoped film however, they report a 2D-3D crossover on going from high to low temperature region.

Another effect associated with the fluctuations is the excess specific heat near the transition temperature. Therefore, the analysis of the specific heat data of all the samples has been carried out in the mean field region to determine the excess specific heat due to fluctuations. The linear fit of the background specific heat both above and below the transition temperature is carried out using the equation,

$$\frac{C_p^B}{T} = a_o + bT \tag{3.9}$$

The smooth background fitting is constructed both above and below T_c and this is shown in Fig. 3.18 and 3.19 for pure, Ni-doped, Zn-doped,Fe-doped and Co-doped samples. The excess specific heat (ΔC_p) is obtained from the equation

$$\Delta C_p = C_p - C_p^B \tag{3.10}$$

where C_p is the experimental specific heat data and C_p^B is the data of the background fit. The excess specific heat vs temperature plots for all the samples are shown in Fig. 3.20. This figure clearly shows the effect of fluctuations on the specific heat of all the samples.

Furthermore, it is seen that the observed C_p anomaly for Ni and Zn substituted samples is as distinct as for the pure sample. On the other hand, the C_p anomaly observed for Fe, Co and Ga substituted samples is significantly broadened, illustrating that the effect of fluctuations in these samples is comparatively much larger than in Ni and Zn substituted samples. This is indicative of more pronounced fluctuation effects occurring when Fe, Co and Ga are incorporated at the Cu(1) site. It must be mentioned here that the difference in the height of the specific heat anomaly for the samples, can be related partly to the difference in the volume fraction of the superconducting phase in the samples as well. Phillips et al.[50] have in fact suggested that the value of $\Delta C(T_c)$ for a sample provides a measure of the volume fraction of superconductivity. These findings, we suggest, are the direct manifestation of in-plane and out-of-plane disorder which the above substitutions create in the 123 structure. Zn and Ni, as they occupy CuO_2 planes, mainly contribute to a decrease in T_c while

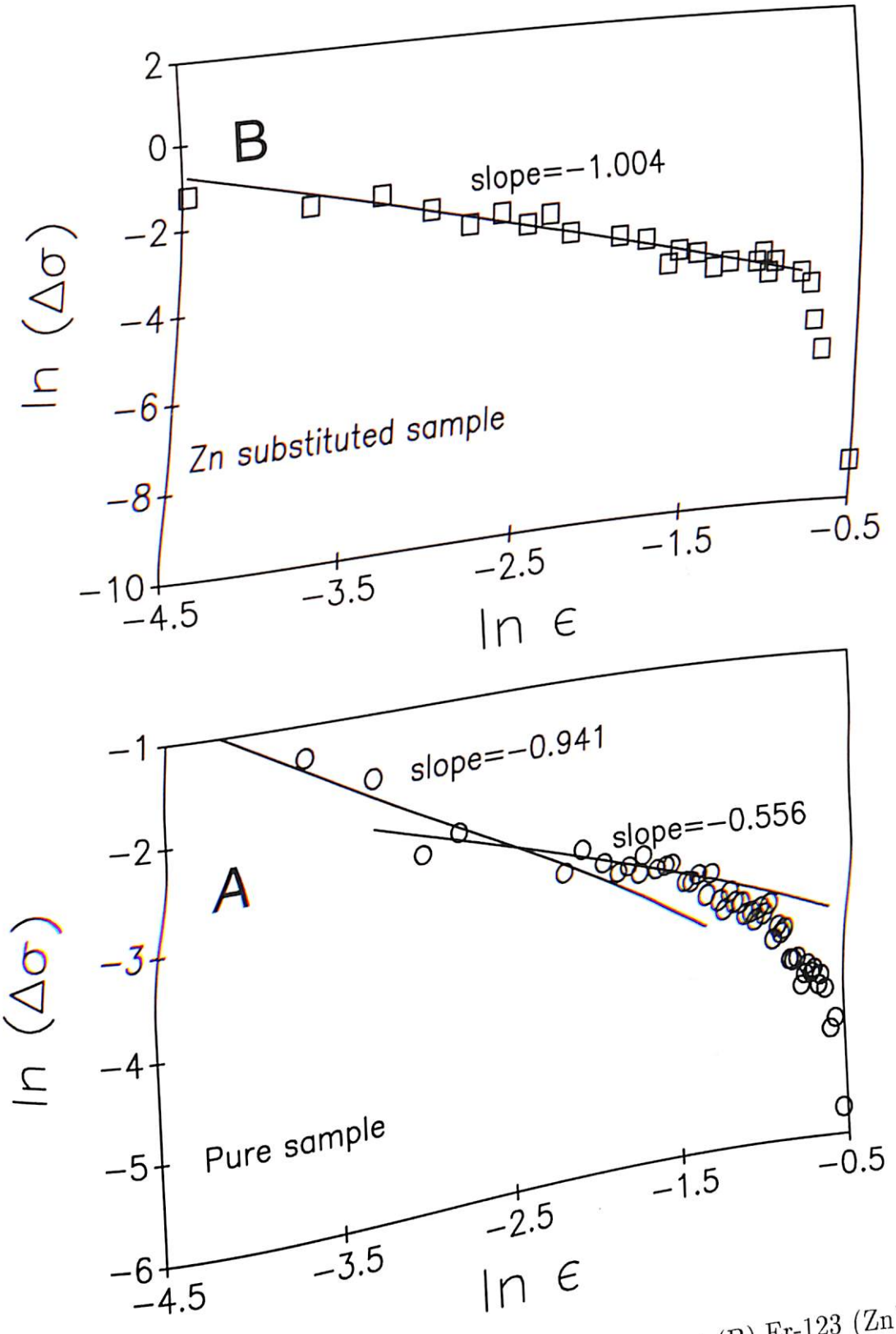

Figure 3.15: $\ln(\Delta\sigma)$ vs $\ln\epsilon$ for (A) Er-123 (Pure) and (B) Er-123 (Zn).

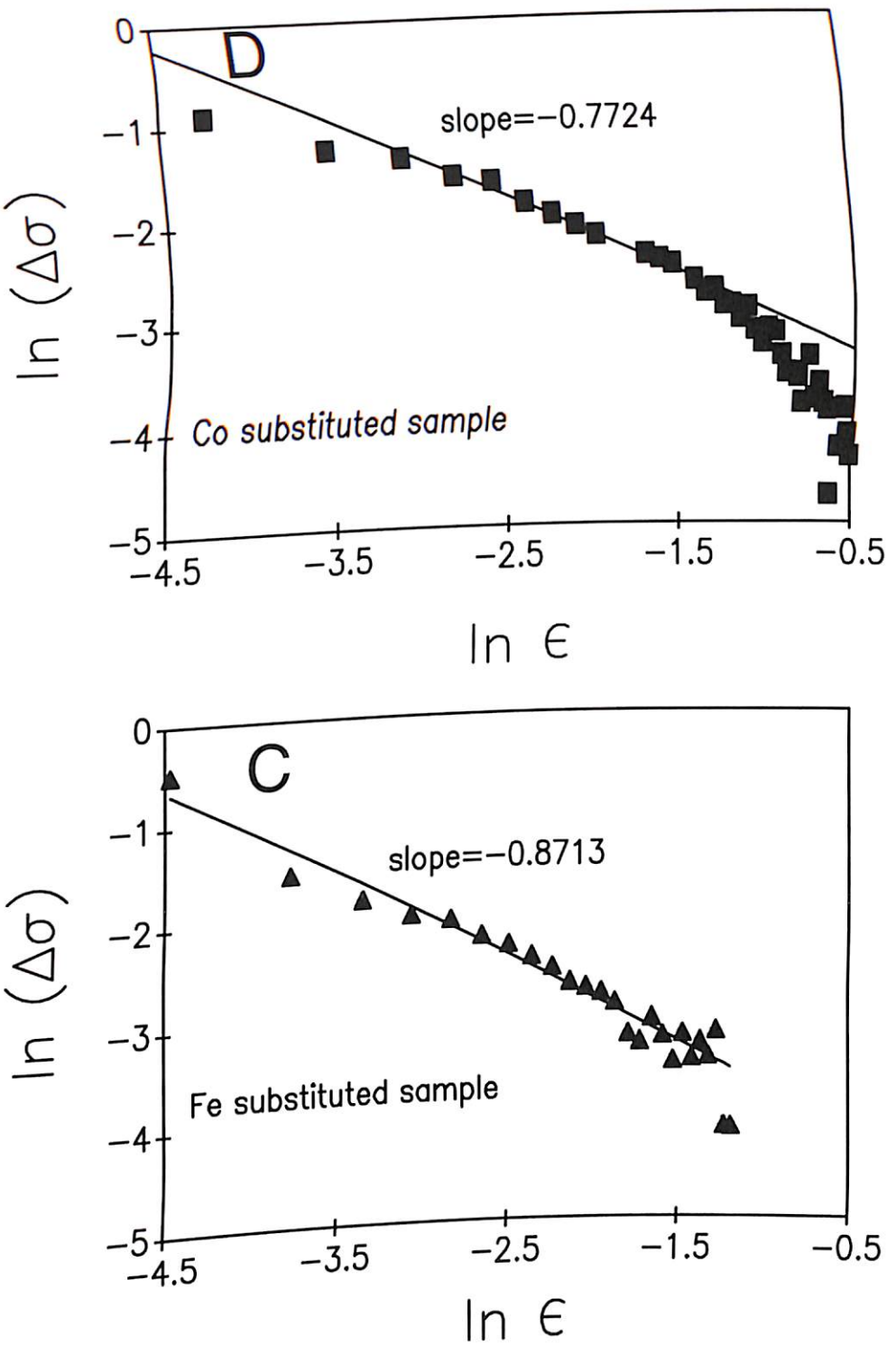

Figure 3.16: $\ln(\Delta\sigma)$ vs $\ln\epsilon$ for (C) Er-123 (Fe) and (D) Er-123 (Co).

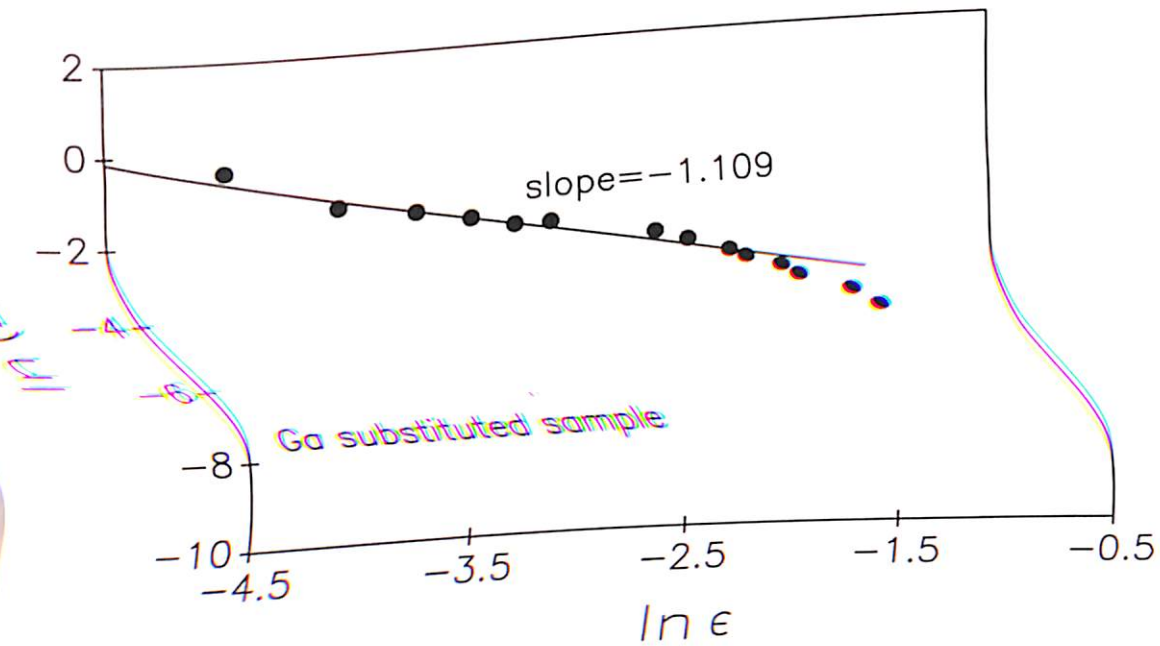

Figure 3.17: $\ln(\Delta\sigma)$ vs $\ln\epsilon$ for Er-123 (Ga).

they have little influence on the interlayer coupling between CuO_2 planes across the neighboring unit cells. On the other hand, Fe, Co and Ga substitute at the chain Cu(1) sites creating disorder between the CuO_2 layers of the adjoining unit cells and thereby weaken the coupling between them in the c-direction, where the range of coherence is already low. In effect this possibly results in transforming the system more towards two dimensions, leading to increased fluctuation effects, as observed in the resistivity, ac susceptibility and specific heat data of the present study.

3.5 Conclusions

In the present study resistivity, susceptibility and specific heat measurements have been carried out on some erbium based 123 superconductors both in the pure form and when Cu is partly (0.5%) replaced by divalent dopants Ni and Zn (in-plane disorder) and trivalent dopants Fe, Co and Ga (out-of-plane disorder). Excess conductivity and specific heat calculations have also been done for the samples.

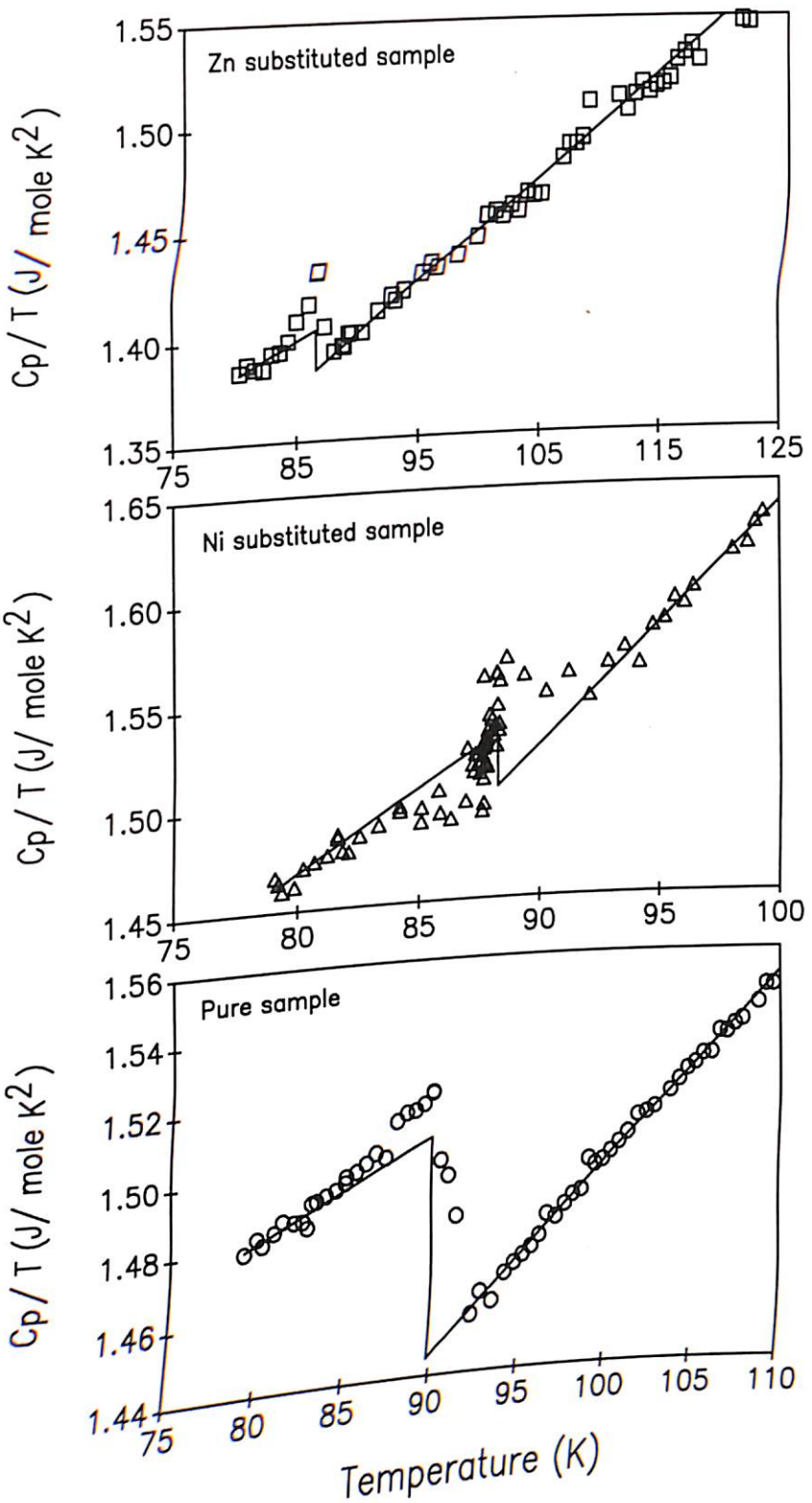

Figure 3.18: C_p/T vs Temperature plots for Pure, Ni-doped and Zn-doped samples. The continuous line shows the fitting of the data with $C_p^B/T = a_o + BT$ both above and below T_c.

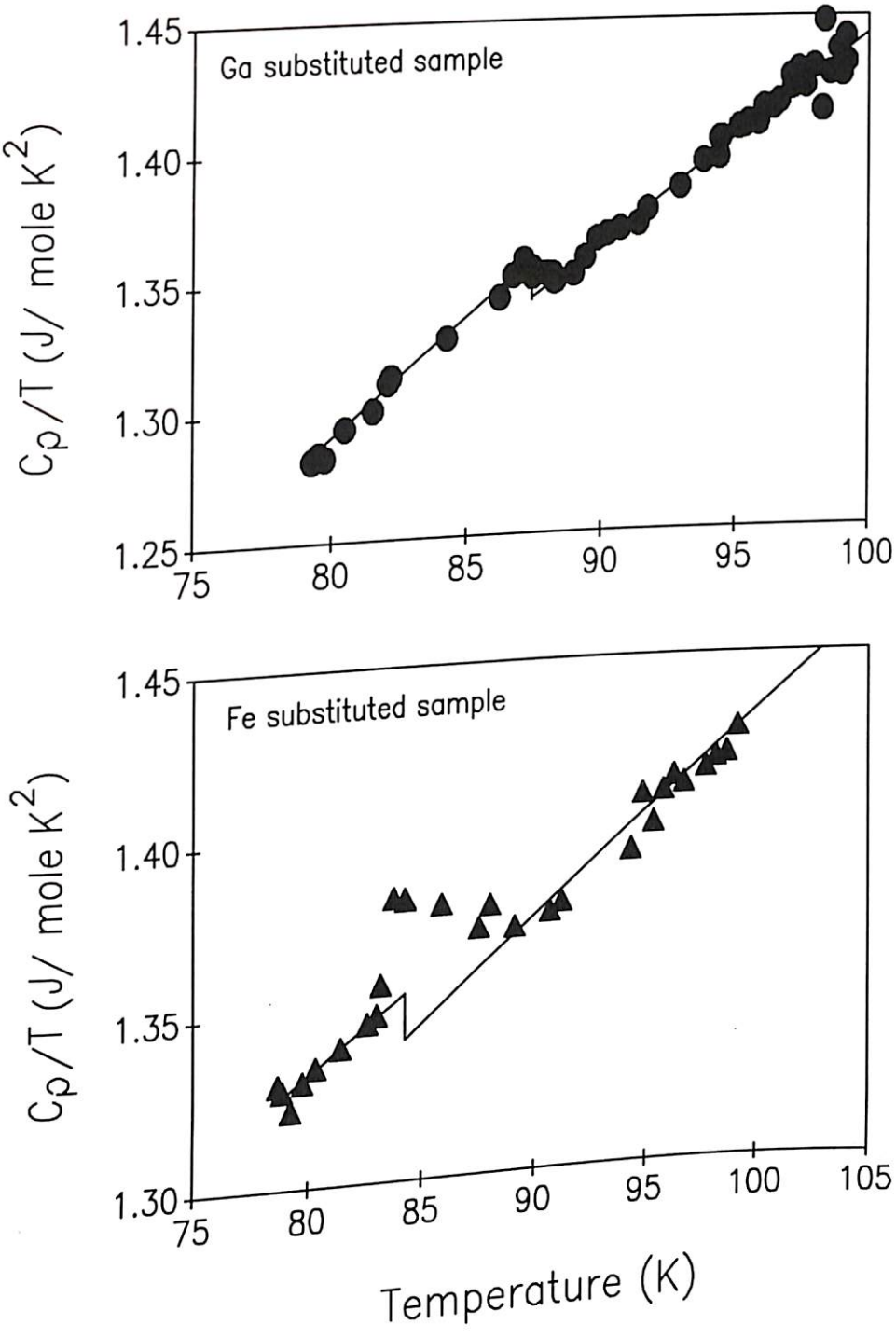

Figure 3.19: C_p/T vs Temperature plots for Fe-doped and Ga-doped samples. The solid line shows the fitting of the data with $C_p^B/T = a_o + BT$ both above and below T_c.

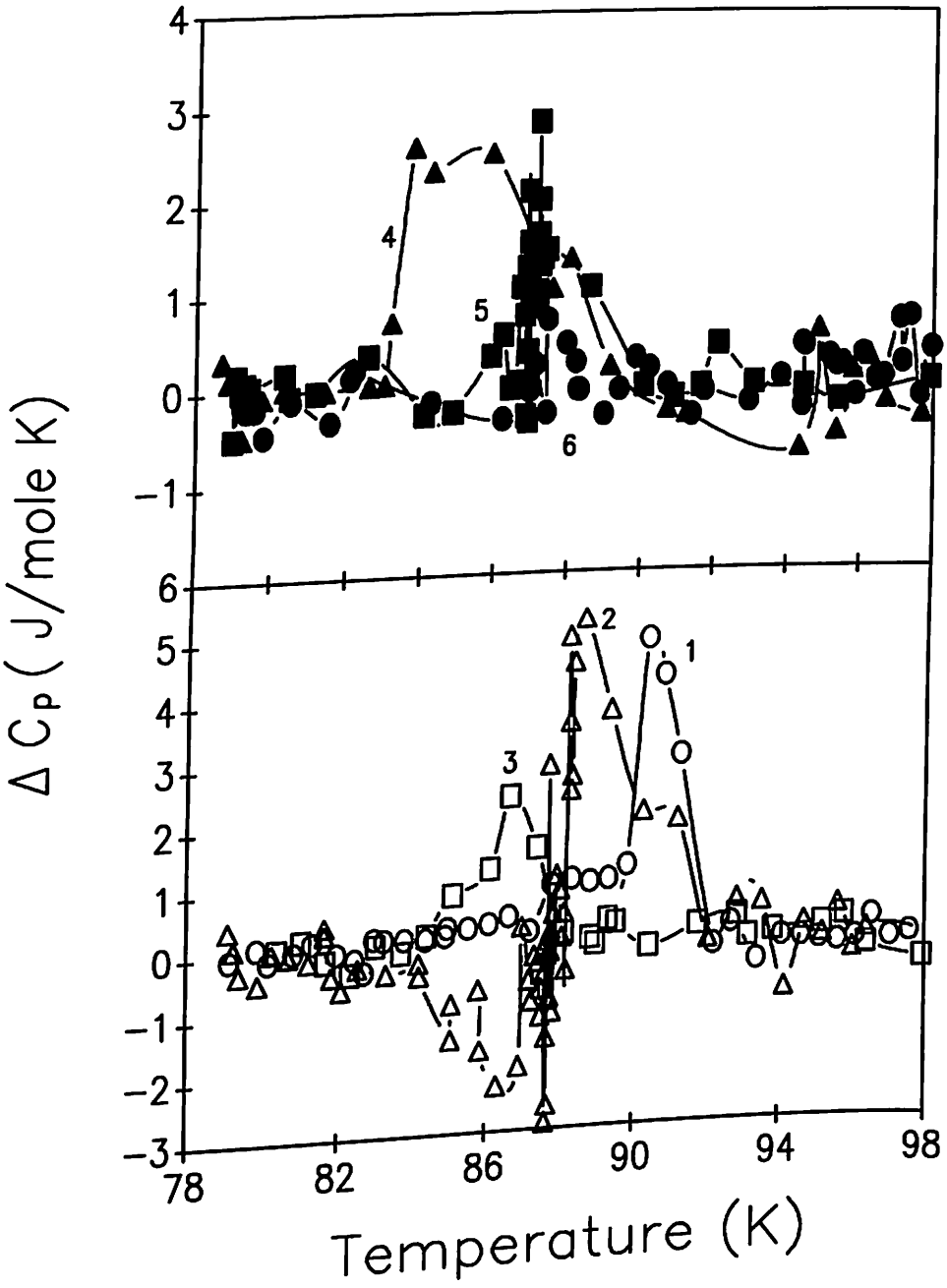

Figure 3.20: Excess specific heat (Δ C_p) vs Temperature for (1) Er-123 (Pure), (2) Er-123 (Ni), (3) Er-123 (Zn), (4) Er-123 (Fe) (5) Er-123 (Co) and (6) Er-123 (Ga).

The main result of this study is that out-of-plane disorder leads to an enhancement of fluctuation effects as compared to the in-plane disorder. This has been explained from the fact that out-of-plane disorder causes an enhanced decoupling of CuO_2 planes along the c-direction and thereby transforms the system more towards two-dimensions. This leads to an increase in the fluctuation effects. The in-plane-disorder, on the other hand, has a lesser influence on the interlayer coupling and hence the fluctuation effects are not as strong as in the case of out-of-plane disorder.

Chapter 4

Effect of lead substitution in the bismuth based cuprate system containing both low T_C and high T_C phases

4.1 Introduction

The discovery of superconductivity in La-Ba-Cu-O[127] and in Y-Ba-Cu-O systems[14] led to a intensive worldwide search for other superconducting oxides. The bismuth based superconducting oxide is one of the major discoveries of this time. Michel et al.[128] reported superconductivity at 20 K in the Bi-Sr-Cu-O system. Later, bulk superconductivity at 85 K and evidence of superconductivity at 110 K were found by several groups by adding Ca to this ternary system[21]. The Bi compounds form a homologous system $Bi_2Sr_2Ca_{n-1}Cu_nO_{2n+4+\delta}$ with transition temperatures of 20 K, 85 K and 110 K for n=1, 2 and 3 respectively[129]. The three superconductors are referred to by their cation ratios as 2201, 2212 and 2223 respectively. The Bi-2223 compound has an interesting behaviour. It shows a clear resistive transition at around 110 K, though due to a residual resistance T_c (R = 0) is observed only at a much lower temperature of around 75 - 85 K. This is due to the fact that Bi-2223 is usually formed as a multiphase compound, in which the volume fraction of high T_c (110 K phase) is reduced due to the presence of the low T_c 2212 (85 K) phase.

Since the discovery of high temperature superconductivity in Bi-Sr-Ca-Cu-O sys-

tem, a wide variety of methods for the synthesis have been explored to stabilize the 2223 phase[130]. Considering the difficulty in the formation of a pure 2223 phase from the stoichiometric composition, Sunshine et al.[23] first reported that partially replacing Bi by Pb in this system can increase the volume fraction of the 2223 phase and improve the bulk properties as well. This was confirmed by other groups also[131–133]. Although it is known that the mismatch of the valence state (Bi^{3+}/Pb^{2+}) produces a change in the electron density and thereby the superconducting properties, the role of Pb in the formation and stability of the high T_c phase needs a detailed study.

The chemical measurements show that Pb substitution is connected with the oxygen partial pressure[134]. While the high resolution STM/STS studies have revealed that Pb substitution at the Bi-site produces depletion of the excess oxygen, thereby improving the metallicity of the Bi-O layer[103]. It has been reported[132, 135–138] that the high T_c superconducting phase becomes stable and the superconducting transition becomes pronounced and reproducible [maximum $T_c(R=0)$] for the samples for which lead content is around 0.3-0.4 (15-20 at%). The specific heat measurements, show either a distinct anomaly or a broad hump in the vicinity of T_c for the Bi-based superconductors. Although this anomaly is comparatively weak, it is essentially analogous to what has been observed in rare earth based 1-2-3 superconductors[104, 139–141]. The broad hump which is characterized by a gradual change in the slope of the specific heat curve, has been attributed to intrinsic fluctuations which are present in the system[109, 142–144]. The Ginzburg-Landau coherence length in the high temperature superconductors is extremely low ($\approx$10 Å)[145, 146] . This leads to enhanced fluctuation effects in them as compared to the conventional superconductors. Therefore, the unusual shape of the specific heat anomaly may be due to inhomogeneous broadening caused by sample imperfections and the inherent fluctuations in the system. The sample inhomogeneities arise due to the intermixing of 2223 and 2122 phases in the multiphase Bi-system. Interestingly, a distinct anomaly in specific heat as well as a sharp transition in magnetic susceptibility has been observed in those samples where Pb content is around 0.4[139, 147]. Yu et al.[148] have shown that when the different phases are properly formed in the Bi-based system, a clear specific

heat jump at the transition temperature of each of the phases can be observed. A systematic investigation of formation and stabilization of the 2223 phase in the lead doped $(Bi)_{2-x}Pb_xSr_2Ca_2Cu_3O_{10+y}$ system has been carried out in the present study through XRD, STM, dc resistivity, ac susceptibility and specific heat measurements.

4.2 Experimental Details

The bulk polycrystalline samples of nominal composition $(Bi)_{2-x}Pb_xSr_2Ca_2Cu_3O_{10+y}$ (x = 0.0, 0.2, 0.3, 0.4, 0.5, 0.6 and 0.7) were prepared using the starting ingredients of purity 99.999% and following the procedure described in chapter 2. The different samples prepared are designated as BSCCO-P [Pure(x = 0)], BSCCO-X [where X = 2 to 7 (corresponding to x=0.2 to 0.7, respectively)].

The characterization of the samples for phase purity was carried out by X-ray diffraction using a Siemen's D-500 diffractometer with Cu Kα radiation. Electrical resistivity measurements were carried out from the room temperature to 77 K. In the ac susceptibility measurements the samples were cooled in a low field of 2.513 Oe [rms], and a frequency of 166.7 Hz superimposed with a dc field of 1 Oe through their transition temperatures [T_c] and χ' and χ'' were measured while warming up slowly. Suitable demagnetization factors for each sample taken from the instrument manual, were used to calculate the absolute values of susceptibilities. The specific heat of the samples was measured in the temperature range 77-120 K. The details of the measurement techniques are described in chapter 2.

4.3 Results

4.3.1 XRD

Fig. 4.1 shows the XRD pattern for the sample BSCCO-P. Fig. 4.2 depicts the XRD patterns for the samples BSCCO-2, BSCCO-3 and BSCCO-4 and Fig. 4.3 shows the same for the samples BSCCO-5, BSCCO-6 and BSCCO-7. Peaks corresponding to 2223 phase are represented by 'H', while those corresponding to 2122 phase are denoted by 'L'. The characteristic peaks of the high T_c phase at (002) [$2\theta \approx 4.9°$],

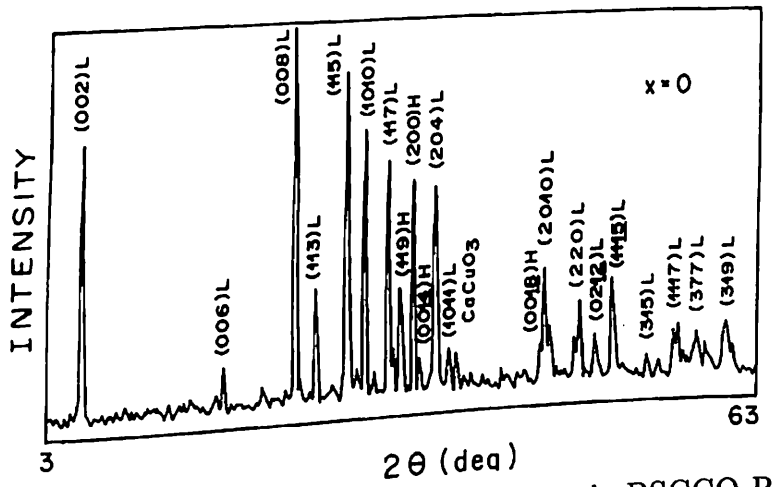

Figure 4.1: XRD pattern for the sample BSCCO-P

(0010) [$2\theta \approx 24°$], (0012) [$2\theta \approx 29°$] and (0014) [$2\theta \approx 33.9°$] etc. are observed in all the samples apart from the BSCCO-P and BSCCO-2 sample. The representative low T_c phase peak at (0020) [$2\theta \approx 56°$] is found to be present apart from (200) [$2\theta \approx 33.3°$] in all the samples. The characteristic peak of low T_c phase at (002) is found only in BSCCO-P sample. It may be pointed out that the peaks corresponding to the unreacted lead are not observed which means that lead is fully substituted in the parent lattice with the possible exception of a small percentage that may not have been detected by XRD. Furthermore, there are no lines corresponding to the double oxides such as $CaCu_2O_3$, Ca_2CuO_3 and Sr_2CuO_3. A few higher angle peaks [other than Pb] in the samples BSCCO-6 and BSCCO-7 appear which cannot be indexed. Therefore, except for BSCCO-P, both the phases are present in these samples and the predominant phase is the high T_c Bi-2223 phase. The BSCCO-P sample consists predominantly of the low T_c phase since it has only two peaks [(119) and (200)] corresponding to the high T_c phase. The lattice parameters have been calculated by taking all the important peaks for 2223 and 2122 phases considering the tetragonal Fnnn structure. Table 4.1 indicates the a,b and c parameters of the 2223 phase of all the samples. Table 4.2 shows the same for the 2212 phase of all the samples. Fig. 4.4 depicts the variation of the lattice parameter c of the 2223 phase with the doping level x of lead in the system. BSCCO-P data is not included as it is mostly dominated by the low T_c 2122 phase. Fig. 4.4 also shows the variation of the lattice parameter

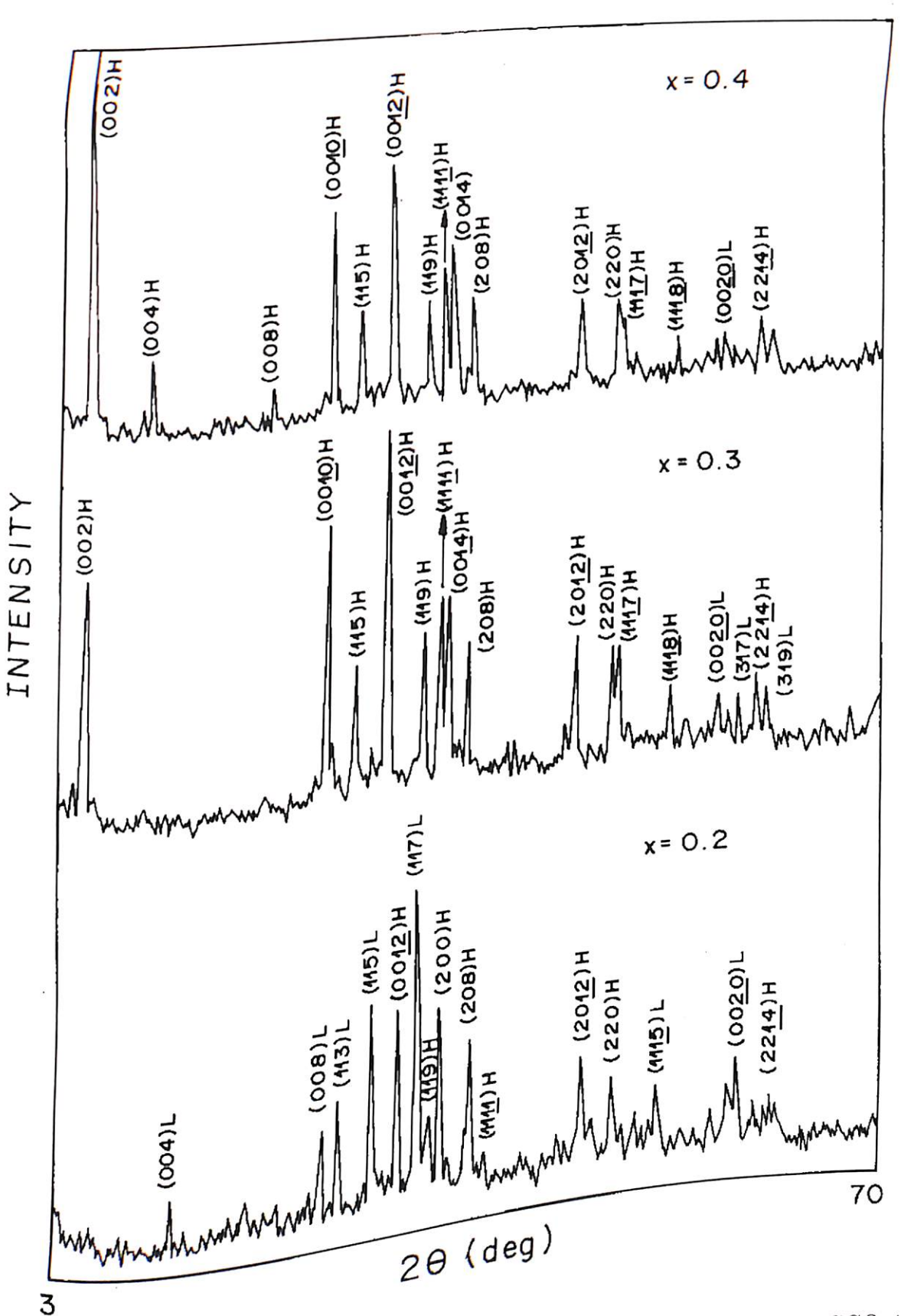

Figure 4.2: XRD patterns for the samples BSCCO-2, BSCCO-3 and BSCCO-4

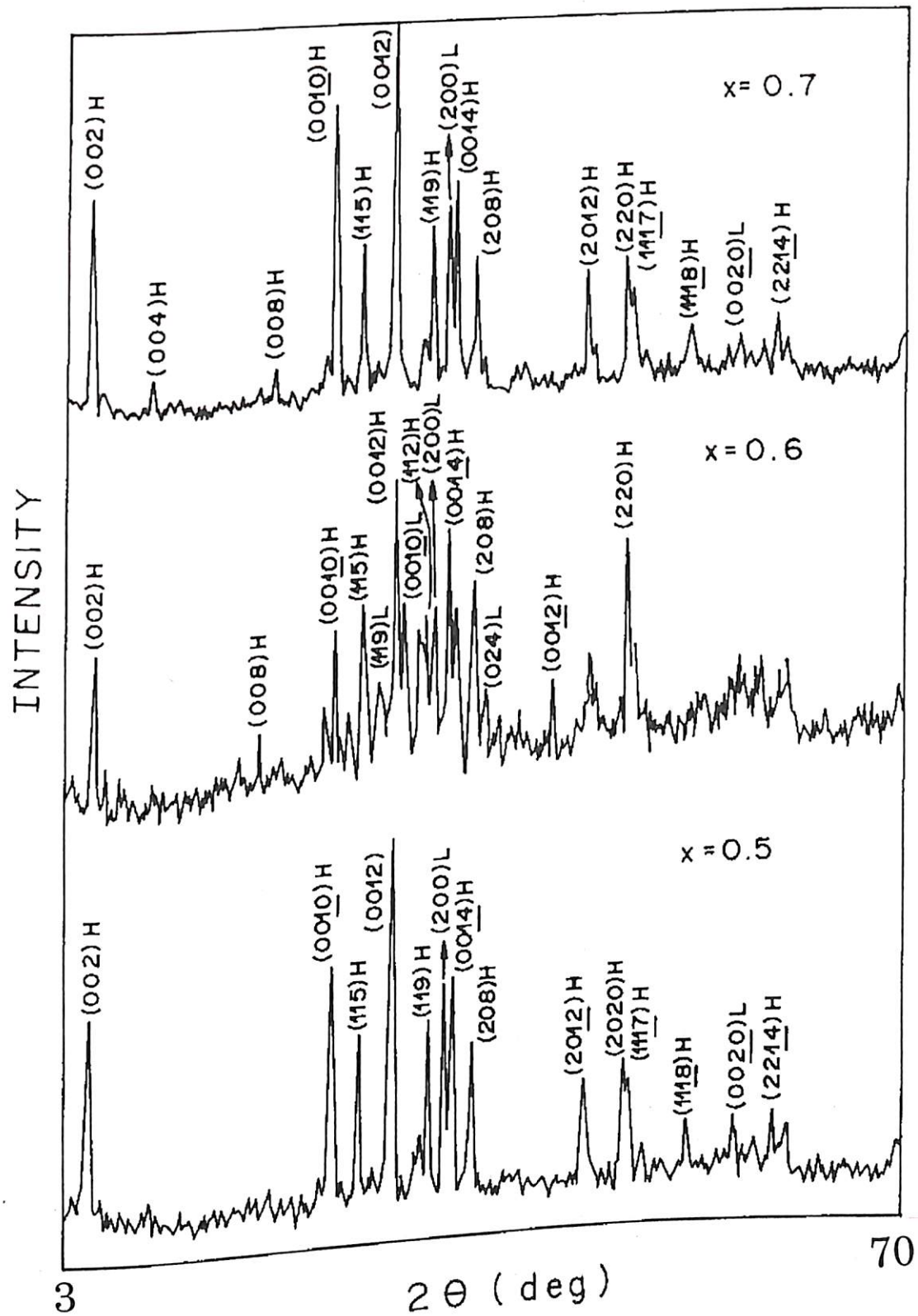

Figure 4.3: XRD patterns for the samples BSCCO-5, BSCCO-6 and BSCCO-7

Table 4.1: Lattice parameter variation of 2223 phase with different lead concentrations

Sample	Lattice parameters (Å)		
	a	b	c
BSCCO-2	5.34	5.34	36.20
BSCCO-3	5.32	5.32	36.66
BSCCO-4	5.44	5.44	37.12
BSCCO-5	5.46	5.46	37.17
BSCCO-6	5.46	5.46	37.23
BSCCO-7	5.46	5.46	37.23

Table 4.2: Lattice parameter variation of the 2212 phase with different lead concentrations

Sample	Lattice parameters (Å)		
	a	b	c
BSCCO-2	5.42	5.42	30.50
BSCCO-3	5.41	5.41	30.54
BSCCO-4	5.36	5.36	30.62
BSCCO-5	5.39	5.39	30.70
BSCCO-6	5.36	5.36	30.73
BSCCO-7	5.39	5.39	30.71

c of the 2122 phase with the doping level x. The same figure shows a comparison of our results with that of Rhee et al.[132]. It is clear that c parameter of 2223 phase increases with increase in x upto 0.4 and then almost saturates, which is in agreement with the results of Rhee et al.[132] and Jeremie et al.[138]. As far as As far as the c parameter of 2122 phase is concerned, Rhee et al.[132], Boekholt et al.[149] and our observations seem to indicate that it increases with the Pb substitution. However the decrease of c of 2122 phase with doping is also reported[136].

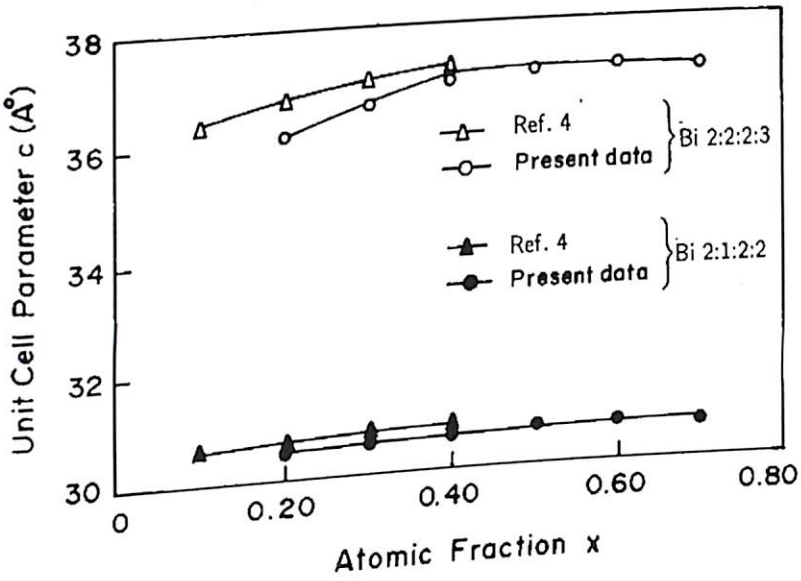

Figure 4.4: c parameter as a function of atomic fraction x

4.3.2 STM

The simultaneous existence of both low and high T_c phases in BSCCO-4 sample, can be seen in the high resolution STM image, obtained perpendicular to the c-direction of the unit cell, shown in Fig. 4.5. The clear molecular stacks of 2223 and 2122 phases with c-parameters 37.1 Å and 30.8 Å, respectively are seen in the figure. The micrograph shows the unit cells of these phases and their separation by a faulted region of Bi-O interface.

Figure 4.5: Intergrowth in BSCCO-4 showing a single unit cell of Bi-2223, a faulted region at the Bi-O interface, and two unit cells of Bi-2122; a top view scan 12 nm X 12 nm

4.3.3 Resistivity

The variation of the normalized resistance with temperature is shown for all the samples in Fig. 4.6. A systematic increase in both the T_c (onset) and T_c(R=0)

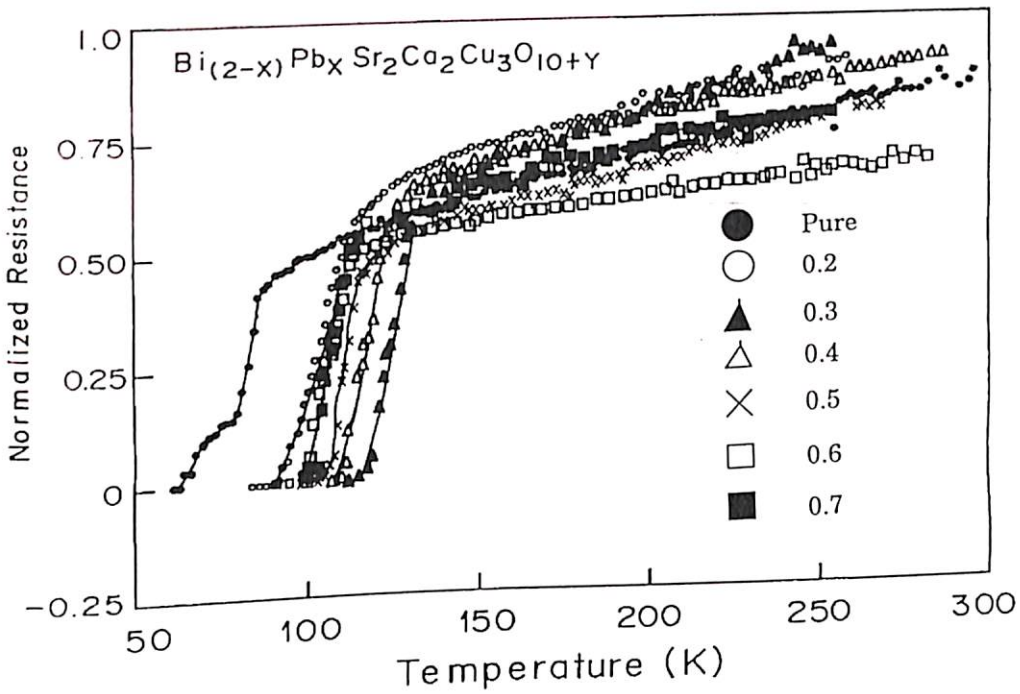

Figure 4.6: Normalized resistance vs temperature curves for BSCCO-P, BSCCO-2, BSCCO-3, BSCCO-4, BSCCO-5, BSCCO-6 and BSCCO-7

has been observed with the increase in lead content till the value of x is 0.3 and then although T_c(onset) remains in the vicinity of 115 K, T_c(R=0) starts decreasing with further increase in lead concentration. The highest T_c(R=0) is obtained for BSCCO-3 sample with a transition temperature of about 110 K and a resistive transition width of about 5 K. Thereafter, the zero resistance temperature decreases and the transition width slowly increases with a increase or decrease in the lead concentration from the optimum value of x = 0.3. From Fig. 4.6 it is evident that the pure sample shows an interesting behaviour. It is a multiphase sample where the transition starts at around 100 K, but due to a residual resistance the T_c (R=0) is achieved only at around 80 K. This kind of a behaviour for the lead free sample has been reported by Maeda et al.[21], though they used a slightly different composition for their sample. Fig. 4.7 shows the variation of T_c (R=0) for all the samples with the doping level x of lead

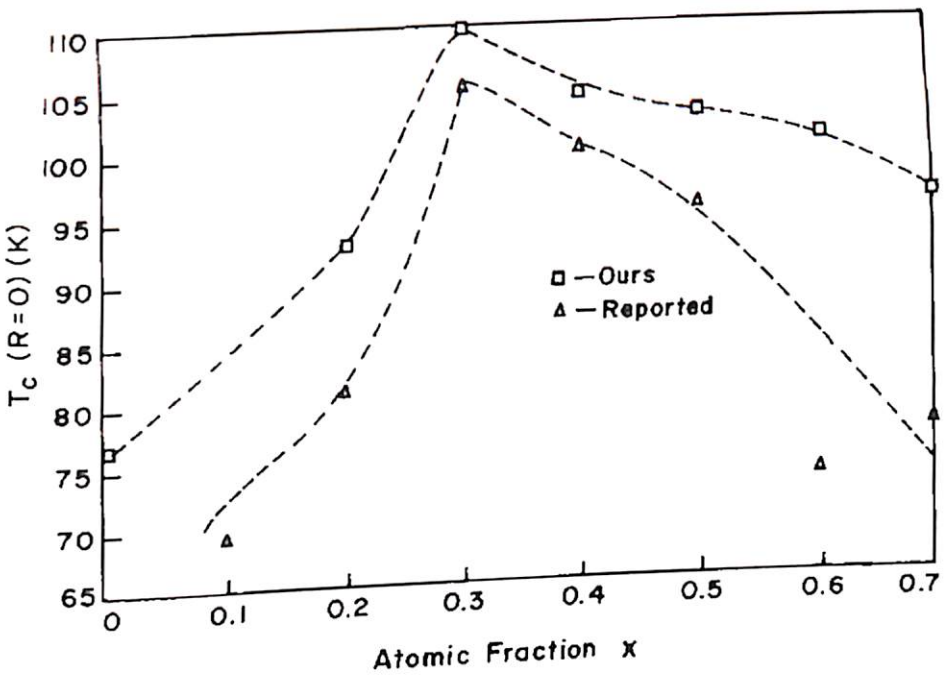

Figure 4.7: T_c(R=0) as a function of the atomic fraction (x) of Pb in Bi-2223 and compared with the reported data of Zhu et al. [Ref. 135]

in the system with a comparison of the reported T_c values of Ref. 135. A peak in T_c(R=0) at x=0.3 is observed in both the reports with a decrease in T_c(R=0) for a further increase or decrease in x.

4.3.4 AC Susceptibility

Fig. 4.8 shows the results of the ac susceptibility ($\chi = \chi' - i\chi''$) measurements in the temperature range 77-130 K for the samples BSCCO-3, BSCCO-4, BSCCO-5, BSCCO-6 and BSCCO-7. From the variation of χ' with temperature, it is seen that the flux expulsion starts at around 108 K for all the samples. However, for the samples BSCCO-3, BSCCO-4 and BSCCO-5, there is a second transition in χ' at a lower temperature of about 90 K and also for these three samples χ'' exhibits a peak just below this second transition temperature. In the samples BSCCO-6 and BSCCO-7, on the other hand, χ' shows only the transition at around 108 K. The second transition in χ' and the corresponding peak in χ'' are not observed down to the liquid nitrogen temperature (77 K). It is possible that χ'' peak of these samples as well as

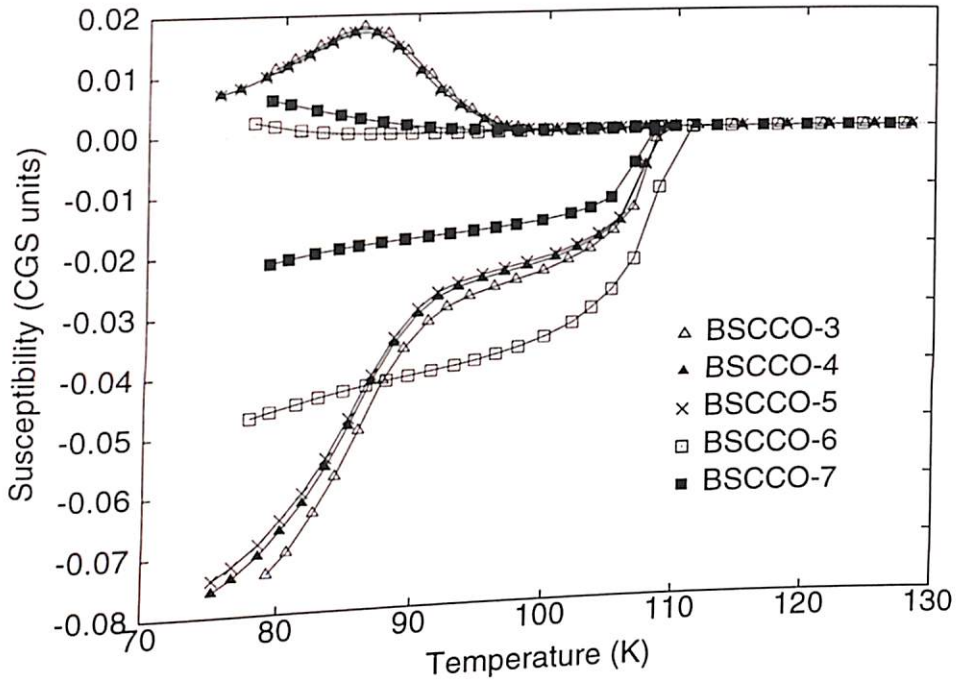

Figure 4.8: ac susceptibility vs temperature curves for BSCCO-3, BSCCO-4, BSCCO-5, BSCCO-6 and BSCCO-7

the second transition in χ' may occur below 77 K in these samples. The transition in χ' at around 108 K in the samples BSCCO-3, BSCCO-4, BSCCO-5, BSCCO-6 and BSCCO-7 confirms the presence of the high T_c 2223 phase in all these samples which is evident from their XRD patterns also. In the samples BSCCO-3, BSCCO-4 and BSCCO-5, the second transition in the χ' curves at about 90 K and the peak in the χ'' curves just below 90 K indicates the presence of the low T_c 2122 phase in these samples and also the occurrence of intergranular coupling in this phase. In the samples BSCCO-6 and BSCCO-7, there is no transition in χ' at 90 K and also no peak in the χ'' curves at this temperature. This suggests that increase in Pb content of the samples beyond around x=0.4-0.5, drastically affects the superconducting properties of the 2122 phase, whereas the 2223 phase seems to be relatively less affected.

As reported[105, 150–154], it is not proper to interpret the ac susceptibility data in field cooled conditions as an indicator of the percentage of the sample which is superconducting. The susceptibility value is dependent on factors such as external field, sample size and also sample perfection. It bears little relation to the proportion of the

superconductor present in the sample. Moreover, it is also possible that the relative change in the diamagnetic signal could reflect an improvement in the superconductivity at the grain boundaries or a better connection of superconducting paths in the sample. However, as the measurements were carried out under field cooled and identical conditions on different samples, the diamagnetic amplitude at a particular temperature, in the first approximation, can be considered as a qualitative measure of the relative amount of the superconducting phase present in the sample at that temperature. The approximate estimation of the relative volume fractions of the superconducting phases in the different samples can be carried out following the method in reference 155. The susceptibility data of the samples in Fig. 4.8 has been expressed in terms of relative susceptibility (for χ') and shown in Fig. 4.9. The values of χ' have been normalized

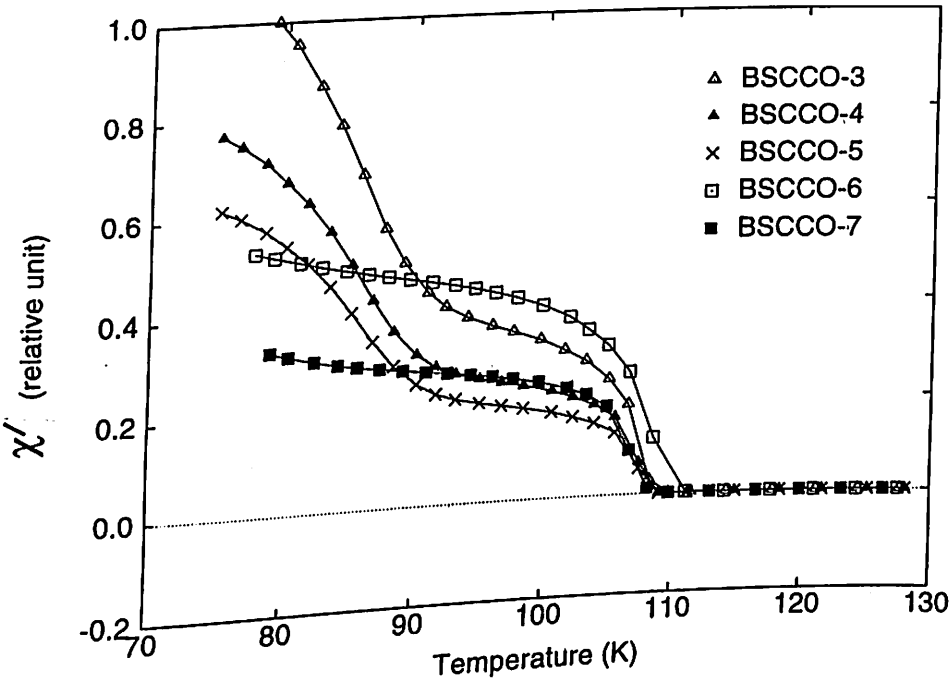

ure 4.9: Estimated χ'(relative) vs temperature for BSCCO-3, BSCCO-4, BSCCO-BSCCO-6 and BSCCO-7

h respect to the sample weight and with reference to χ' of BSCCO-3 at the liquid ogen temperature. From Fig. 4.9, it is seen that the diamagnetic amplitude of the ple above 90 K, that is above the transition temperature of the low T_c 2122 phase, reases as the Pb content of the sample is increased beyond x = 0.3, thereby im-

plying that the volume fraction above 90 K of the high T_c 2223 phase decreases in the samples containing lead concentration greater than around 0.3-0.4 .It is also observed from the values of χ' (Fig. 4.9) at 77 K, that the relative volume fractions [compared to that of sample BSCCO-3] of the total superconducting phase [2122 and 2223 phases combined] are 75%, 60%, 50% and 30% for the samples BSCCO-4, BSCCO-5 BSCCO-6 and BSCCO-7, respectively. This implies that if the total superconducting volume [2122+2223] of BSCCO-3 is 80% then it is 60% for BSCCO-4, 48% for BSCCO-5 and so on. It is therefore evident that with an increase in Pb content beyond 0.3, the total volume of the superconducting phase in the sample decreases. It may be mentioned here that in the case of BSCCO-6, the diamagnetic signal above 90 K is more than in the samples BSCCO-3, BSCCO-4 and BSCCO-5. This is because we were not able to estimate the sample volume and demagnetization correction factor for this sample. However, as is evident from the Figs.4.8 and 4.9, even for this sample the total superconducting volume at 77 K is less than that for the samples BSCCO-3, BSCCO-4 and BSCCO-5.

4.3.5 Specific Heat

Fig. 4.10 shows the variation of the molar specific heat (C_p) of the samples BSCCO-3, BSCCO-4 and BSCCO-5 with temperature (T). A distinct and clear specific heat anomaly can be seen at around 90 K for the BSCCO-3 and BSCCO-4 samples. The anomaly in these samples occurs at the transition temperature of the low T_c 2122 phase. In Fig. 4.11 is shown the molar specific heat data of the samples BSCCO-6 and BSCCO-7. A little fluctuation in the data is observed for these samples [BSCCO-6 and BSCCO-7] in the vicinity of the transition temperature of the low T_c phase, though no clear anomaly is seen. The specific heat anomaly can be more clearly seen in a plot of Cp/T versus the temperature. This has been shown for the samples BSCCO-3, BSCCO-4 and BSCCO-5 in Fig. 4.12 and for the samples BSCCO-6 and BSCCO-7 in Fig. 4.13. Fig. 4.12 shows that in the samples BSCCO-3, BSCCO-4 and BSCCO-5 the specific heat anomaly occurs at around 89 K, 92 K and 87 K respectively. The broadening of the anomaly due to intrinsic fluctuations in the system is also

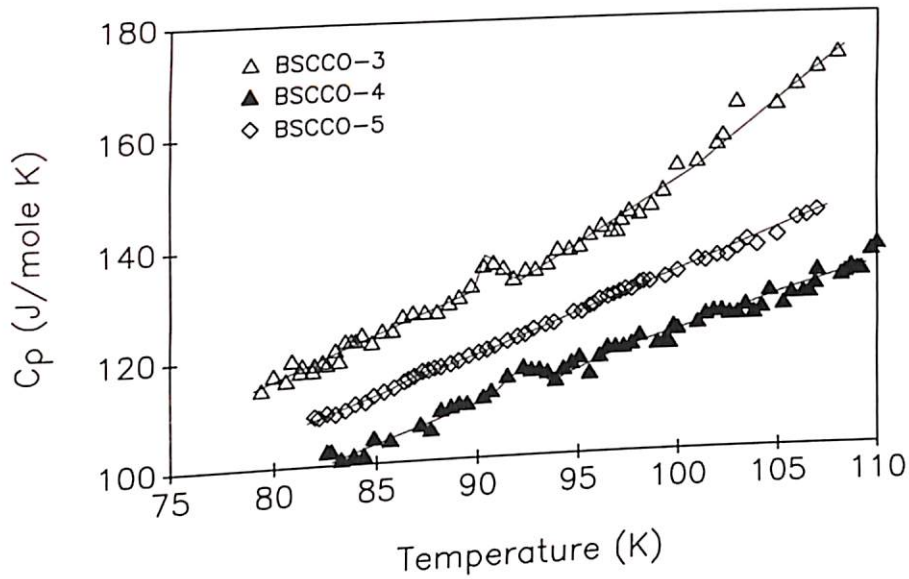

Figure 4.10: Molar specific heat (C_P) vs temperature (T) curves for BSCCO-3, BSCCO-4 and BSCCO-5

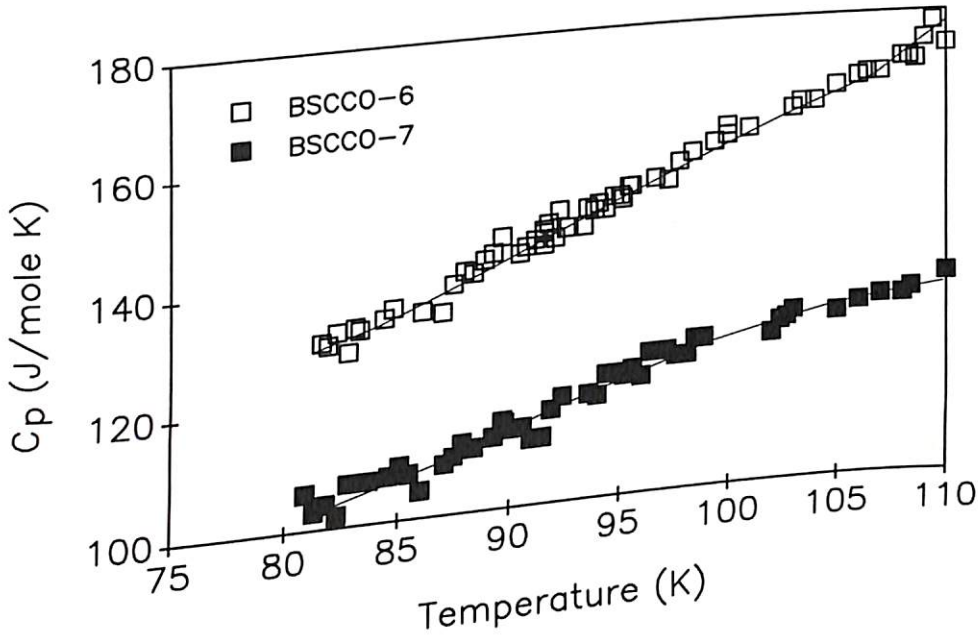

Figure 4.11: Molar specific heat (C_P) vs temperature (T) curves for BSCCO-6 and BSCCO-7

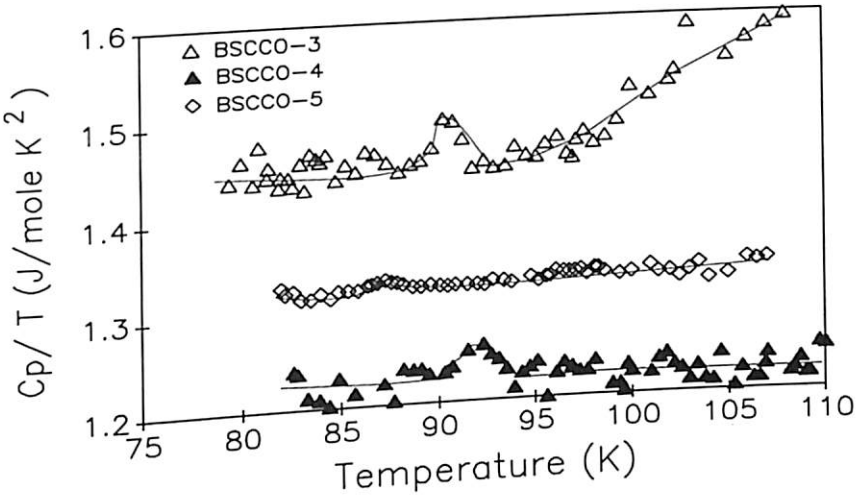

Figure 4.12: C_p/T vs T for the samples BSCCO-3, BSCCO-4 and BSCCO-5

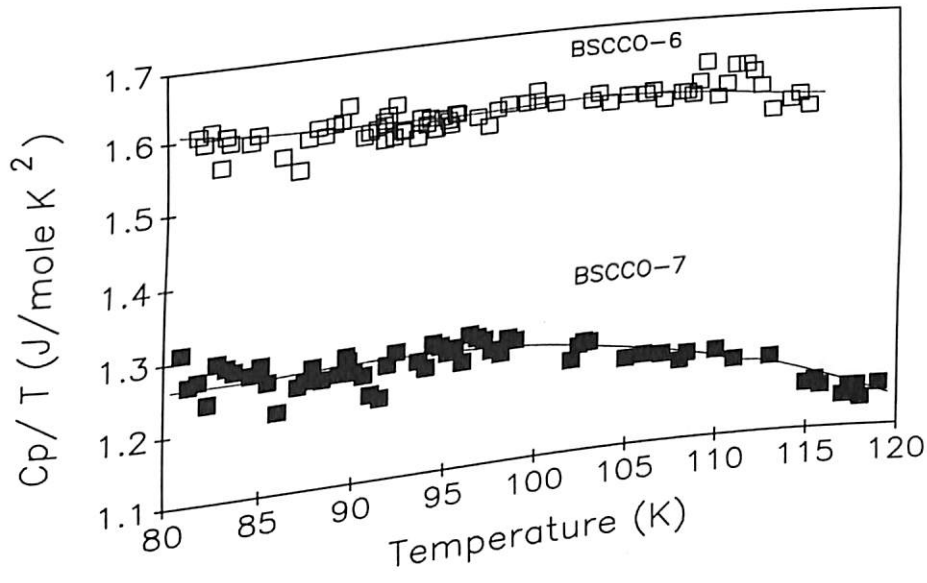

Figure 4.13: C_p/T vs T for the samples BSCCO-6 and BSCCO-7

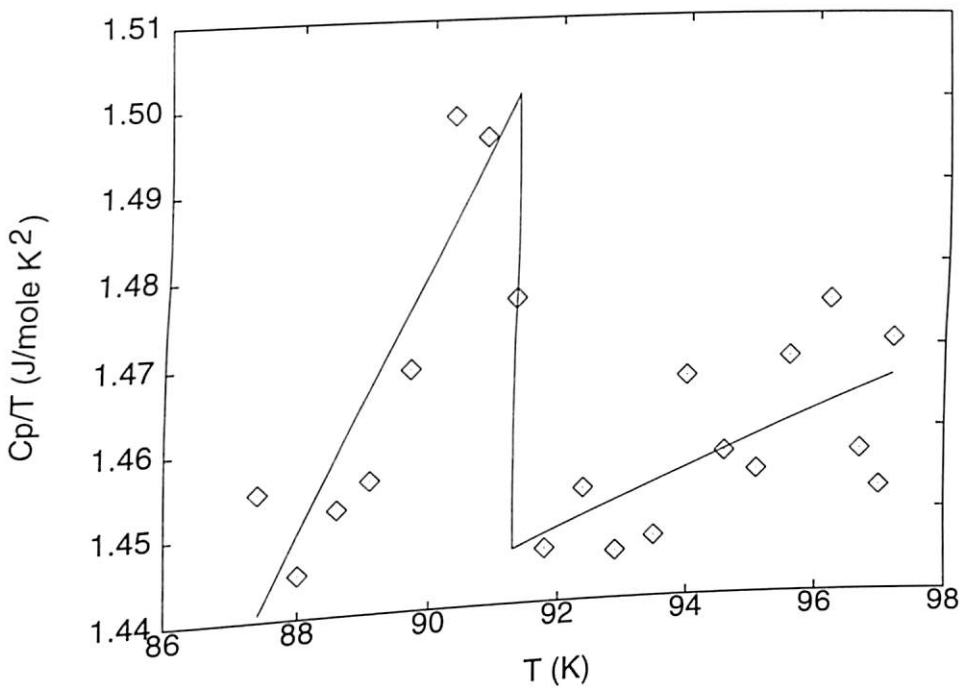

Figure 4.14: Equal area construction for the sample BSCCO-3

evident for the three samples. The specific heat jump which is associated with bulk superconducting properties, is calculated using the method of balance of entropy at the mean field transition temperature (T_c^{mf}). This method is based on the reasoning that since the superconducting transition is a second order phase transition, the first order derivative of the free energy or the entropy of the system should remain conserved at the transition point. For this purpose the usual method of equal area construction[45, 155, 156] around the mean field transition temperature is used in respect of samples BSCCO-3, BSCCO-4 and BSCCO-5. Figs. 4.14 and 4.15 show the entropy balance method as applied to the samples BSCCO-3 and BSCCO-5. The results of these calculations are shown in the Table 4.3. It may be mentioned that the jump in the specific heat thus calculated is rather critically dependent on the portion of the curve used for extrapolation from below and above the mean field transition temperature.

The characteristic parameters like the the Sommerfeld constant(γ) and the Debye temperature (θ_D) are difficult to estimate in these oxide superconductors, because the electronic contribution to the specific heat is very small in comparison to the phononic contribution near the transition temperature[157]. Thus the large back-

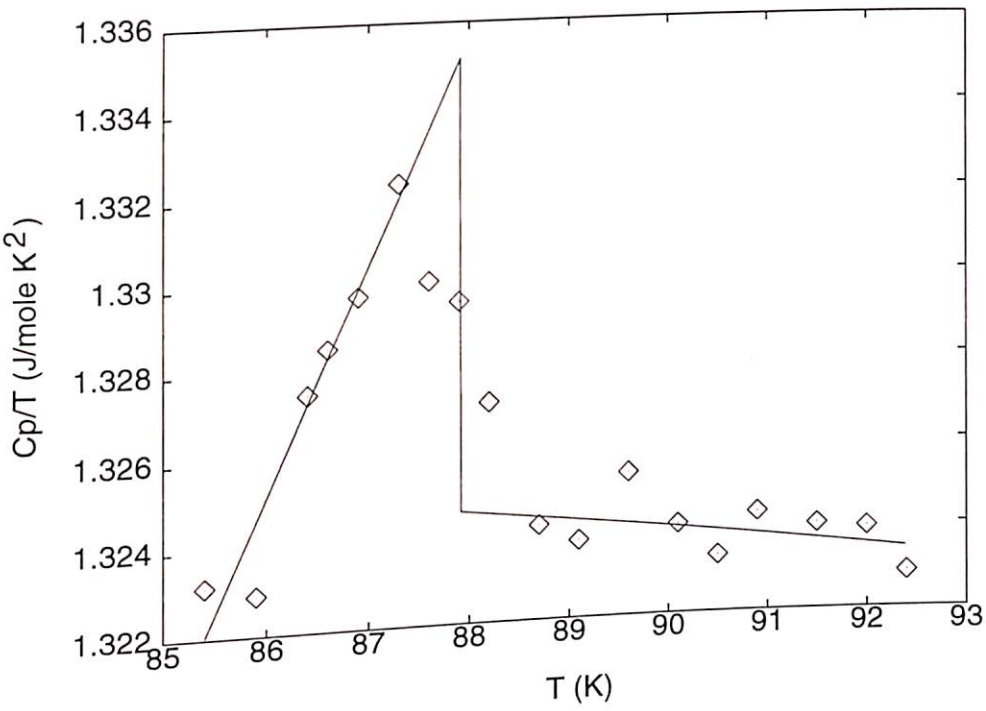

Figure 4.15: Equal area construction for the sample BSCCO-5

Table 4.3: Parameters calculated using the equal area construction

Sample	T_c^{mf} (K)	$\Delta C/T_c^{mf}$ (mJ/mol K^2)	$(\Delta C)_{T = T_c^{mf}}$ (J/mol K)
BSCCO-3	90.8	54	4.8
BSCCO-4	93.1	35	3.2
BSCCO-5	87.5	20	1.7

ground of phononic contribution masks the specific heat contribution due to the electrons. Hence, it is difficult to extract the parameters associated with the electronic specific heat at or above the transition temperature. The basic difficulty is that at this high temperature phononic contribution cannot be measured independently through suppression of superconductivity by using a high magnetic field or creating enormous disorder by irradiation. Moreover, the co-existence of multiple phases complicates the phonon density of states and the application of the mean field approximation is difficult. However, in order to indicate the possible trend in the nature of coupling, Sommerfeld constant [γ] was estimated in a first order approximation from the susceptibility experiment[158].

The molar susceptibility in its normal state can be fitted to the Curie-Weiss relation

$$\chi(T) = \chi_o + [C/(T + \theta)] \tag{4.1}$$

where χ_o is the temperature independent paramagnetic susceptibility, θ is the Curie-Weiss temperature and C is a constant. In the nearly-free-electron model γ is proportional to the Pauli susceptibility χ_P, and they are related by the Wilsons ratio

$$\frac{\gamma}{\chi_P} = \frac{1}{3}\left(\frac{\pi k_B}{\mu_B}\right)^2 \tag{4.2}$$

In the above equation k_B is the Boltzmann's constant and μ_B is the Bohr magneton. The core contribution to the diamagnetism is estimated by addition of the diamagnetic susceptibilities associated with the individual ions constituting the superconductor. The contributions corresponding to various ions which constitute the bismuth system are given in the Table 4.4. Using the Curie-Weiss relation for the sample BSCCO-3 the values $\chi_o = 1.75X10^{-4}$ emu/mol, C = 0.124 and θ = 210 K are obtained. After correcting the temperature independent susceptibility χ_o for the diamagnetic core contribution and neglecting the small Landau-Peierls diamagnetic term, the Pauli susceptibility is obtained and then using Eq. 4.2 the γ value for sample BSCCO-3 is found to be 48 mJ/mole K^2. The reported value of γ in these systems is in the range 10-50 mJ/mole K^2[158, 159] and our rough value falls within this region. The Debye temperature (θ_D) in the cuprate superconductors is calculated from the specific heat

Table 4.4: Diamagnetic susceptibility contribution of various ions

Ion	Diamagnetic susceptibility (X 10^{-10} m^3/mol)
Bi^{3+}	-3.14
Sr^{2+}	-1.89
Ca^{2+}	-1.00
Pb^{2+}	-3.52
Pb^{4+}	-3.27
Cu^{2+}	-1.38
O^{2-}	-1.51

data which is obtained experimentally at all temperatures using the theoretical Debye function

$$C = 9N'R(T/\theta_D)^3 \int_0^{\frac{\theta_D}{T}} \frac{e^x x^4}{(e^x - 1)^2} dx \qquad (4.3)$$

on the assumption that the three dimensional Debye model is valid in this system. In this equation N′ is the number of atoms in the unit cell of the superconductor and R is the molar gas constant. An iterative method has been developed to obtain the best fitted value. The obtained Debye temperatures are found to be temperature dependent and the average value of the Debye temperature around the transition temperature for the samples BSCCO-3 and BSCCO-4 is found to be 400 K and 350 K respectively.

4.4 Discussion

The results from these combination of experiments indicate two distinct types of behaviours,

(i) in the region of lead content $x \leq 0.4$ and

(ii) for $x > 0.4$.

$T_c(R=0)$ from the resistivity measurements, the flux exclusion onset temperature from ac susceptibility measurements and the anomaly observed in the specific heat measurements indicate a stabilization of the superconducting phase (2223+2122) in

the sample as the amount of lead x in the sample is increased from 0 to 0.4. However, when x is beyond 0.4, the absence of both the second transition in χ' and the specific heat anomaly at 90 K (x = 0.5 sample shows a small discontinuity) suggests that the overall proportion of the superconducting phase in the sample diminishes as a result of decrease of both the 2223 and 2122 phases in the system. The ionic radii of Bi^{3+} and Pb^{2+} are 1.03 Å and 1.19 Å respectively. Therefore, the substitution of Bi^{3+} with Pb^{2+} should result in a increase in the c parameter. This is substantiated through the XRD measurements, where in fact, an increase in the c parameter is observed with increasing lead content upto x = 0.4. But the saturation of the c parameter for the samples with lead content more than 0.4 suggests two possibilities, viz,

(i) When the lead content is increased beyond 0.4 then it does not substitute at the bismuth site but remains unreacted in the system.

(ii) When the lead content is increased beyond 0.4 it substitutes in the tetravalent state Pb^{4+} (ionic radius is 0.84 Å) at the Ca^{2+} (ionic radius is 0.99 Å) site

Since no peaks corresponding to unreacted lead have been observed in the XRD patterns, the first possibility can be ruled out. The second possibility seems to suggest that the c parameter should decrease when the value of x is increased beyond 0.4. From the XRD measurements however it has been found that the c parameter saturates beyond x = 0.4. Therefore, from the crystallographic point of view, it is conjectured that beyond the concentration of x =0.4 lead partially substitutes at the Bi^{3+} site in the Pb^{2+} state and partially at the Ca^{2+} site in the Pb^{4+} state. Since the substitution of lead at these two different sites has an opposite effect on the value of the c parameter, no overall significant change in its value on increasing the lead content beyond the value of 0.4 is observed. A similar possibility of lead getting substituted at the calcium site in the Bi-2223 samples has been discussed from the neutron diffraction experiments by Sastry et al.[160] and Miehe et al.[161]. As far as the change in c parameter of the 2122 phase is concerned, it seems to increase with substitution of lead, which agrees well with the findings of others as already pointed out. Thus at the initial level of substitution [Pb^{2+}/Bi^{3+}], the number of hole carriers increases resulting in

an increase in the conductivity in the Bi-O layer, which leads to an increase in the transition temperature on substitution of lead upto x = 0.4. However, when lead content is increased beyond 0.4, then, as mentioned earlier, it substitutes partially at both bismuth and calcium sites. The first process leads to an increase in the number of hole carriers. On the other hand, the second process, leads to a decrease in the number of hole carriers. This decrease is more rapid than the increase in the carriers caused by the first process. As a result a decrease in the transition temperature and an increase in the transition width has been observed in the resistivity measurements. The reduction in the number of hole carriers can also lead to a reduction in the superconducting volume fraction as has been observed in the susceptibility measurements. This may also smear off the specific heat anomaly on going beyond the lead content of 0.4.

From the specific-heat measurements the BCS coupling constant can be obtained from the expression $\Delta C/\gamma f T_c$, where f is the volume fraction of the superconducting phase. We know the value of the Sommerfeld constant, which is shown to be 48 mJ/mol K^2 and does not change appreciably for the two samples, BSCCO-3 and BSCCO-4. In the susceptibility measurement the volume fraction of the superconducting phase is shown to be roughly 80% and 60% at 77 K for the samples BSCCO-3 and BSCCO-4, respectively. The calculated values of $\Delta C/\gamma f T_c$ are obtained as 1.40 and 1.21 for BSCCO-3 and BSCCO-4, respectively, which are within the limit of the weak coupling BCS value of 1.43. On the other hand, tunneling experiments have shown that most of the high-T_c superconductors are strongly coupled, and consequently our present findings are in variance with such a contention. It needs to be pointed out that the point-contact tunneling experiments, especially when carried out on the cuprate superconductors, suffer from a general disadvantage due to the local presence of non-stoichiometric composition or of the oxide layer. The present results corroborate the weak-coupling nature of this material which is substantiated by various other methods mainly specific heat measurements[162].

Therefore, the specific heat and magnetic susceptibility measurements seem to indicate that properties like specific heat anomaly or flux expulsion due to the Meissner effect are observable only when the samples contain a substantial volume fraction of

the superconducting phase. However, as has been observed by others, we also find that a 2223 phase does not form a dense interpenetrating network; as a result it does not expel all the flux present in the sample and would allow the detection of the 2122 phase, while 2122 phase forms network easily, and this may result in the screening of the minority phase. Although the exact contribution of fluctuations of the order parameter has not been evaluated the clear specific heat anomaly shows that the nature of superconducting transition in BSCCO-3 and BSCCO-4 is similar to that of other observed systems.

4.5 Conclusions

In this study the results of resistivity, ac susceptibility and specific heat measurements carried out on the samples of $Bi_{2-x}Pb_xSr_2Ca_2Cu_3O_{10+y}(0 \leq x \leq 0.7)$ which were characterized by x-ray diffraction and high resolution scanning tunnelling microscopy have been presented. Using these results the role of lead in the formation and stabilization of the high T_c phase has been investigated.

The lattice parameter calculations from the XRD results show that the c parameter increases with the amount of Pb(x) substituted in the samples upto x = 0.4 and then it saturates. In the resistivity results a peak is observed in the $T_c(R = 0)$ for x = 0.3 and on increasing or decreasing lead from this optimal concentration the transition temperature reduces. Further, ac susceptibility results indicate that for all the samples flux exclusion onset temperature is around 108.5 K. However, for the samples with x = 0.3, 0.4 and 0.5 there is a second transition at a lower temperature of about 90 K and also a peak in the imaginary component of the susceptibility just below this temperature. Finally, the specific heat shows a discontinuity at around 90 K for the x = 0.3, 0.4 and 0.5 samples only. The samples with x = 0.6 and 0.7 show no discontinuity.

The main results of our analysis are that as lead is increased to 0.4 the total superconducting phase stabilizes. However, for x>0.4 there is decrease in the total superconducting phase. Another important conclusion of the study is that beyond

$x = 0.4$ lead substitutes partially at the bismuth site (as Pb^{2+}) and partially at the calcium site (as Pb^{4+}). This conjecture supports the observed experimental results of the different studies.

Chapter 5

Excess specific heat and conductivity studies in Bi-based cuprate systems -the effect of fluctuations in the high T_C phase

5.1 Introduction

Although the occurrence of the characteristic specific heat anomaly at the superconducting transition temperature T_c, has been confirmed[92, 93, 162] for a variety of high T_c compounds, little attention has been paid to the phenomenon of excess specific heat and conductivity associated with the fluctuations in the superconducting order parameter near the transition temperature. This is particularly true for the case of the high T_c phase (Bi-2223) of the Bi system especially when it constitutes one of the phases of the multiphase Bi system.

It is well established[92, 96, 97] that fluctuation effects are more pronounced in high T_c cuprates in comparison to the low T_c conventional systems. This is because of their anisotropic layer structures, lower carrier densities and high transition temperature values[163, 164]. These fluctuation effects are very important in high T_c oxides and could be be connected with 'spin gap' above T_c. Also due to fluctuations an excess conductivity is always observed in the high temperature superconductors[145]. The fluctuation study is significant in the high T_c superconductors because they are anisotropic in nature. Thus a careful examination of the dimensionality of transport is

of importance. In addition, the fluctuation analysis may give estimate of microscopic parameters like the coherence lengths and pair breaking time.

The presence of significant fluctuation effects around T_c cause the thermodynamic properties of HTSCs to be quite different from those of conventional superconductors. In particular the specific heat anomaly of the HTSCs deviate from the standard mean field behaviour i.e., the second order jump at T_c is modified due to superconducting fluctuations. In the rare earth based 123 systems the specific heat anomaly is a fairly large fraction (3-4%) of the total specific heat, whereas in bismuth and thallium based superconductors it is much less prominent. The deformation of the traditional shape of the anomaly due to fluctuations is relatively mild in rare earth based 123 and the lanthanum based 214 systems, while in the Bismuth and Thallium systems, the fluctuation contributions, however, dominate the anomaly at T_c.

A wide variety of experiments have earlier shown that the high T_c Bi-2223 phase in $Bi_{2-x}Pb_xSr_2Ca_2Cu_3O_{10+y}$ has the optimum stabilization for $x \approx 0.3$-0.4. When the lead content is either lower or higher than the optimal concentration then there occurs an intergrowth of low T_c Bi-2212 phase[83, 135] in the high T_c Bi-2223 phase. The occurrence of the intergrowth disorder in the Bi-2223 phase is expected to reduce the volume fraction of the high T_c phase in the system. By studying such a multiphase system, the ensuing contribution of fluctuation in both resistivity as well as in specific heat may be obtained which would essentially give an indication of the effect of superconducting fluctuations due to the intergrowth of low T_c phase in the high T_c matrix.

In the above background, a systematic study has been carried out in the Bi-2223 system $Bi_{1.7}Pb_{0.4}Sr_2Ca_2Cu_3O_{10+y}$ creating disorder first by increasing Cu content, and then replacing Sr partially by Ca, and finally by reducing the lead content with the effect that the lead stabilized high T_c 2223 phase gets adulterated due to the intergrowth of the low T_c phase. The formation of the mixed phase thereby influences the interlayer coupling between the successive stacks of CuO_2 planes of the neighbouring unit cells along the c-direction. The role of interlayer coupling in broadening the resistive transition of the Bi-2212 system has been elaborated by Samanta et al.[103]

on the basis of the scanning tunneling spectroscopic (STS) measurements. Therefore, a comparative study proposed in this investigation is expected to provide a useful insight into the possible role of fluctuations in conjunction with the presence of high T_c and low T_c phases in the intergrowth phenomenon.

5.2 Experimental Details

The bulk polycrystalline samples of nominal composition $Bi_{1.9}Pb_{0.1}Sr_2Ca_2Cu_3O_{10+y}$ (BPSCCO-1), $Bi_{1.8}Pb_{0.2}Sr_2Ca_2Cu_3O_{10+y}$ (BPSCCO-2), $Bi_{1.7}Pb_{0.4}Sr_2Ca_2$ $Cu_{3.6}O_{10+y}$ (BPSCCO-3) and $Bi_{1.7}Pb_{0.4}Sr_{1.6}Ca_{2.4}$ $Cu_{3.6}O_{10+y}$ (BPSCCO-4) were prepared using the starting ingredients of purity 99.999% and following the procedure described in chapter 2.

The characterization of the samples for phase purity was carried out by the X ray diffraction (XRD), using a Siemen's D-500 diffractometer with Cu-K_α radiation. The conventional four probe technique was used for studying the resistive transitions of the samples. The ac magnetic susceptibility was measured by a Lakeshore 7000 susceptometer. The samples were cooled in a low field of 2.513 Oe [rms] and frequency 166.7 Hz through their transition temperatures [T_c] and both χ' and χ'' were measured while warming up slowly. Suitable demagnetization factor for each sample taken from the instrument manual, was used to calculate the absolute value of susceptibility. The specific heat was measured by a fully automated quasi-adiabatic calorimeter. The details of the measurement techniques are described in chapter 2.

5.3 Results

5.3.1 XRD

Figure 5.1 shows the XRD patterns for all the samples. Peaks corresponding to 2223 phase are represented by 'H'(high), while those of 2212 phase are denoted by 'L'(low). The characteristic peaks of 'H' at (002) , (0010), (0012) and (0014) are present in the samples BPSCCO-2, BPSCCO-3 and BPSCCO-4. The characteristic peak of 'L' at (0020) is found to be present apart from (200) in all the three samples as well. In these

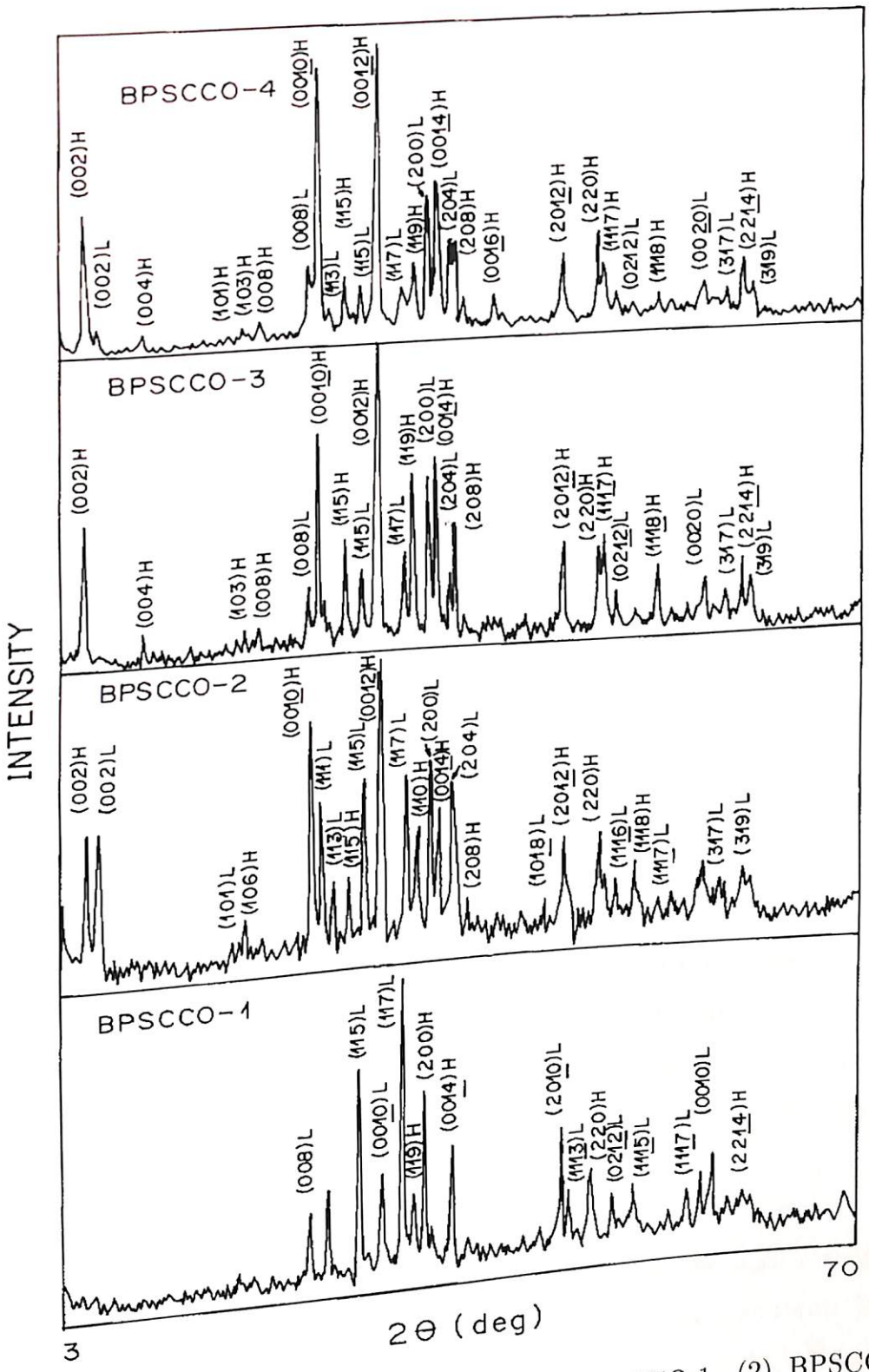

Figure 5.1: XRD patterns for the samples (1) BPSCCO-1, (2) BPSCCO-2, (3) BPSCCO-3 and (4) BPSCCO-4.

Table 5.1: Lattice parameters for the high T_c phase

Sample	a (Å)	b (Å)	c (Å)
BPSCCO-1	5.42	5.42	36.40
BPSCCO-2	5.40	5.40	36.90
BPSCCO-3	5.42	5.42	37.02
BPSCCO-4	5.42	5.42	36.50

Table 5.2: Lattice parameters for the low T_c phase

Sample	a (Å)	b (Å)	c (Å)
BPSCCO-1	5.40	5.40	30.65
BPSCCO-2	5.40	5.40	30.45
BPSCCO-3	5.38	5.38	30.50
BPSCCO-4	5.38	5.38	30.50

samples, although both the phases are present, the predominant phase is 'H'. On the other hand, in the case of sample BPSCCO-1 the low T_c phase seems to dominate. It may be pointed out that the peaks corresponding to the unreacted lead have not been observed in any of the samples. The lattice parameters for these samples are obtained by our optimization programme taking into account all of the peaks. The observed d values are compared with the calculated d values and the difference (d_{obs} - d_{cal}) is not more than 0.1%. The results of these calculations are shown in the Tables 5.1 and 5.2.

5.3.2 STM

The presence of 2223-phase in BPSCCO-3 can be seen in the high resolution STM image, obtained perpendicular to the c- direction of the unit cell, as shown in Fig. 5.2. The clear molecular stacks of three 2223 unit cells of c-parameter 37.1 Å are observed.

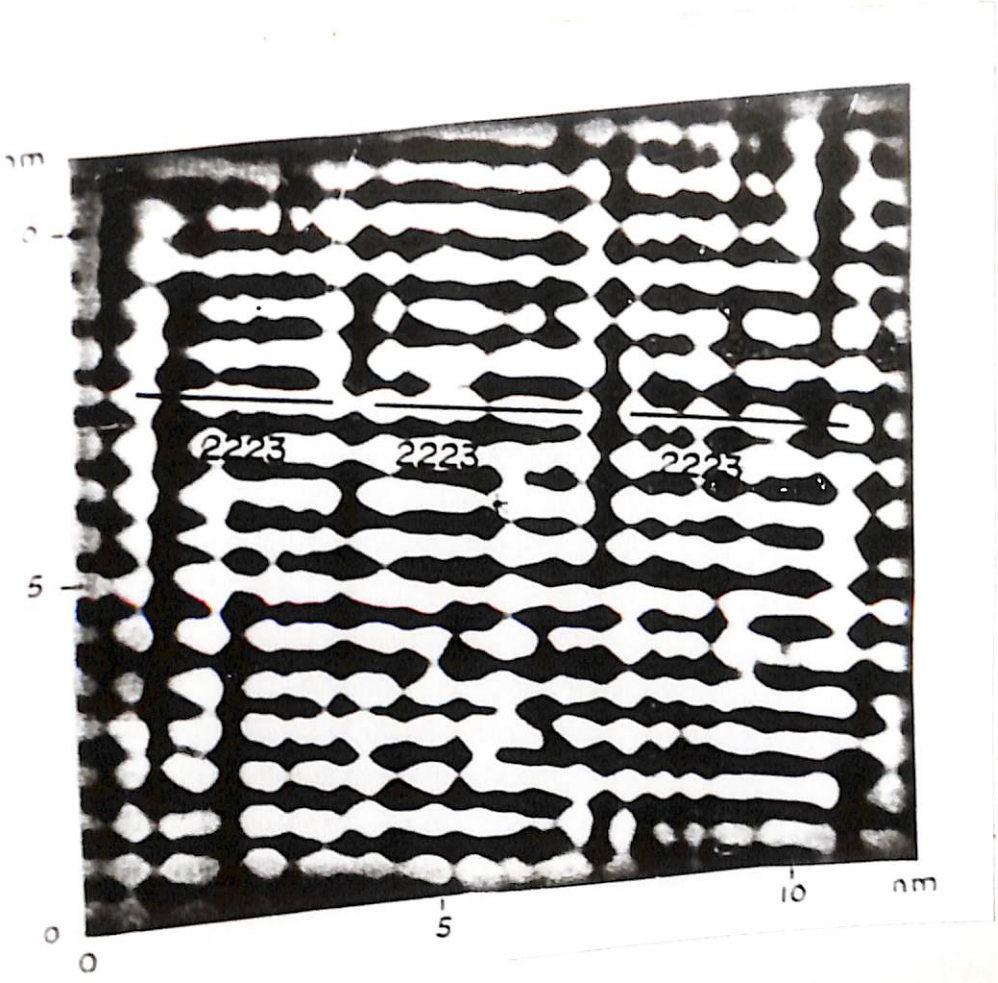

Figure 5.2: STM micrograph for the sample BPSCCO-3. Three single unit cells with c-parameter 37.1 Å have been indicated.

5.3.3 Resistivity

Figure 5.3 shows the variation of resistivity with temperature in the range 77 K - 300 K for all the four samples and the inset shows the same plot closer to the transition temperature. $T_c(R=0)$ is 82 K, 115 K, 106 K and 110 K for BPSCCO-1, BPSCCO-2, BPSCCO-3 and BPSCCO-4, respectively. For the samples BPSCCO-2, BPSCCO-

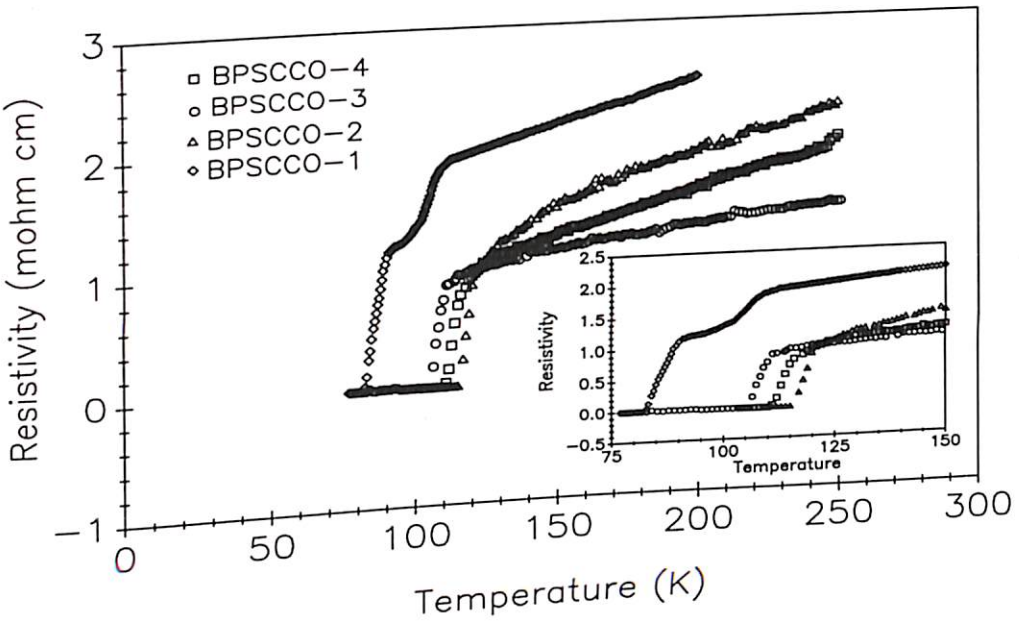

Figure 5.3: Resistivity (ρ) vs Temperature (T) curves for the four samples and the inset shows the ρ-T curves for all the samples close to T_c.

3 and BPSCCO-4, the behaviour of resistivity is made more clear in Fig. 5.4 by plotting ρ - ρ_o as a function of T-T_2. The parameters ρ_o and T_2 are defined later. The behaviour of the sample BPSCCO-1 is apparent from the resistivity plot itself. Thus, the resistivity of all the four samples shows the general behaviour sketched in Fig. 5.5. The temperatures T_1 and T_2 are the transition onset temperatures corresponding to the two different phases. In the case of BPSCCO-2, BPSCCO-3 and BPSCCO-4 samples these two phases correspond to the high-T_c Bi-2223 system, while for the BPSCCO-1 sample T_2 corresponds to the low-T_c Bi-2122 phase. The values of T_2 and T_1, and the crossover temperature T_o are presented in Table 5.3. It may be noted that the peculiar behaviour of resistivity shown in Figs. 5.4 and 5.5 has been observed

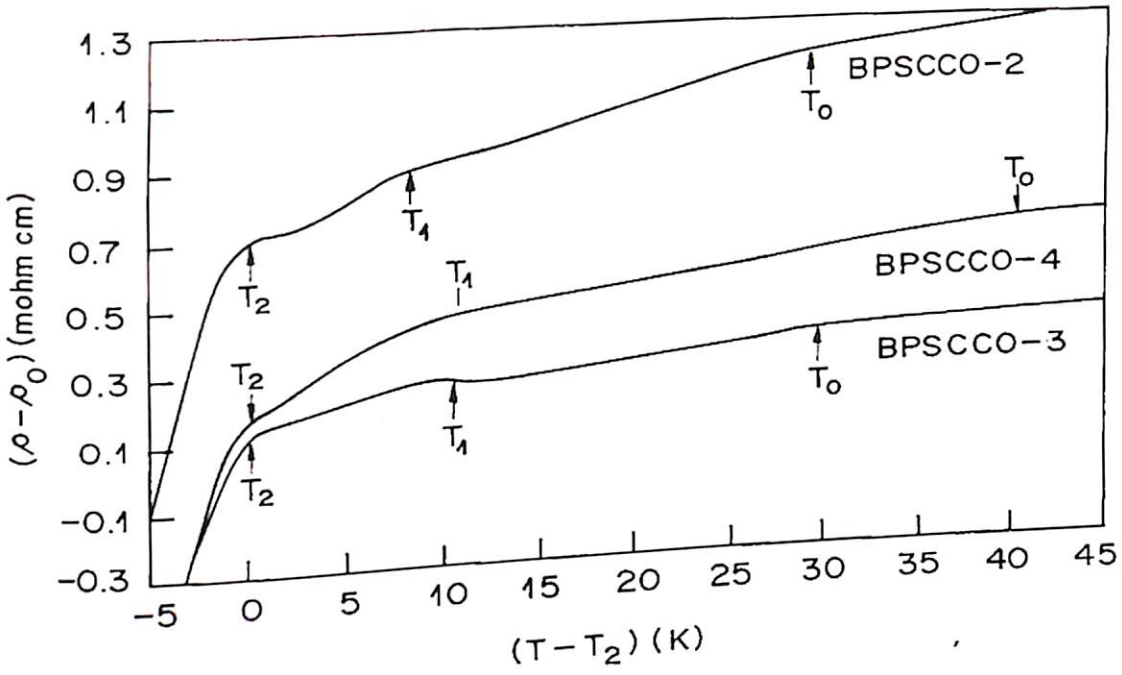

Figure 5.4: Typical behaviour of resistivity of the BPSCCO-2, BPSCCO-3 and BPSCCO-4 samples. $T_2(T_1)$ is the onset temperature for the low (high) temperature phase. T_o appears to show the crossover in resistivity due to spin gap.

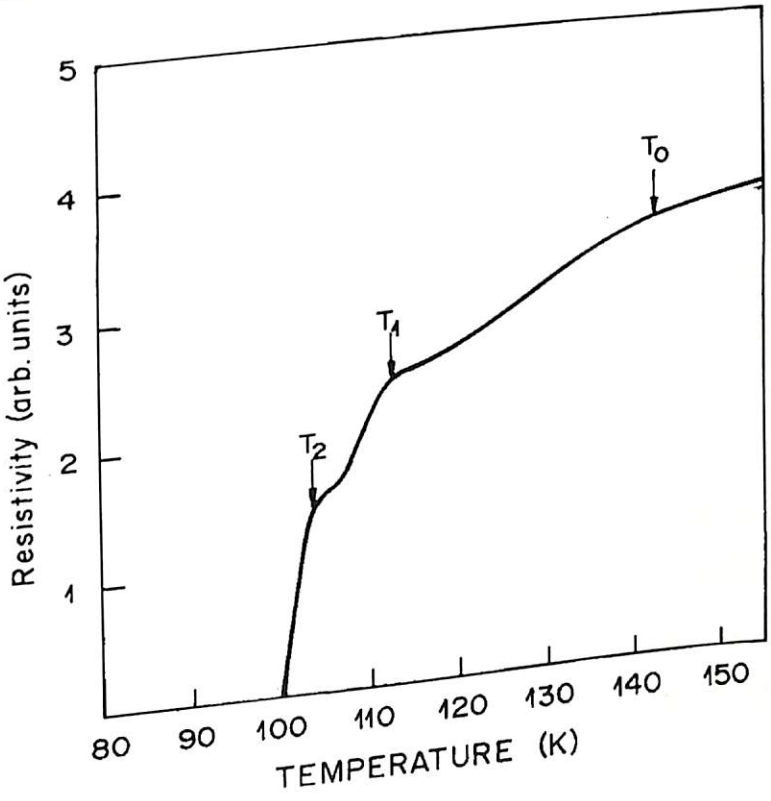

Figure 5.5: General resistivity behaviour of the samples

Table 5.3: Values of the parameters T_2, T_1, T_o, T_{ch}, ρ_o, ρ_1, a and J for the BPSCCO-1, BPSCCO-2, BPSCCO-3 and BPSCCO-4 samples

Sample	T_2 (K)	T_1 (K)	T_o (K)	T_{ch} (K)	ρ_o (mΩ cm)	ρ_1 (mΩ cm)	a	J
BPSCCO-1	91	112	170	104.2	1.11	0.72	1.00	0.0
BPSCCO-2	122	130	150	126.4	0.30	0.90	1.62	0.006
BPSCCO-3	111	122	140	116	0.72	0.26	1.45	0.02
BPSCCO-4	116	127	156	119.7	0.60	0.45	1.40	0.026

earlier also by several authors[135, 165]. In Ref. 166 the peculiar ρ-T behaviour arises in the Mn, Zn and Fe doped systems with the content of these impurities exceeding or near at about 13 at.%. The peculiar form of ρ vs T shown in Fig. 5.4 has not been observed by Nkum et al.[166] for the Bi-2223 system with the excess of Cu atoms. A weak signature of T_o and T_1 appears in the ρ - T curve observed by Samuel et al.[167]. Ciurchea et al.[168] found $\rho \propto$T in the Bi-2223 sample involving partial replacement of Sr by Ba. Gao et al.[158] also found $\rho \propto$T for Sb-disordered sample of Bi-2223.

5.3.4 AC Susceptibility

Figure 5.6 shows the results of susceptibility ($\chi = \chi'$-iχ'') measurements in the temperature range 77 - 130 K for the samples BPSCCO-2, BPSCCO-3 and BPSCCO-4, respectively. It can be seen from the χ' data that BPSCCO-2 and BPSCCO-3 have a single transition and the flux exclusion onset temperature is around 96K and 106K respectively for these samples. However, in BPSCCO-4, there is a double transition at 107 and 95 K, respectively. The susceptibility and magnetization data are difficult to interpret in terms of the percentage of full diamagnetism as the data of field-cooled experiments (Meissner fraction) depend on factors such as external field, sample size and perfection and may bear little relation to the proportion of the superconducting phase present in the sample. Moreover, it may also be possible that the relative change in the diamagnetic signal could also reflect an improvement in the superconductivity at the grain boundaries or a better connectivity of superconducting paths

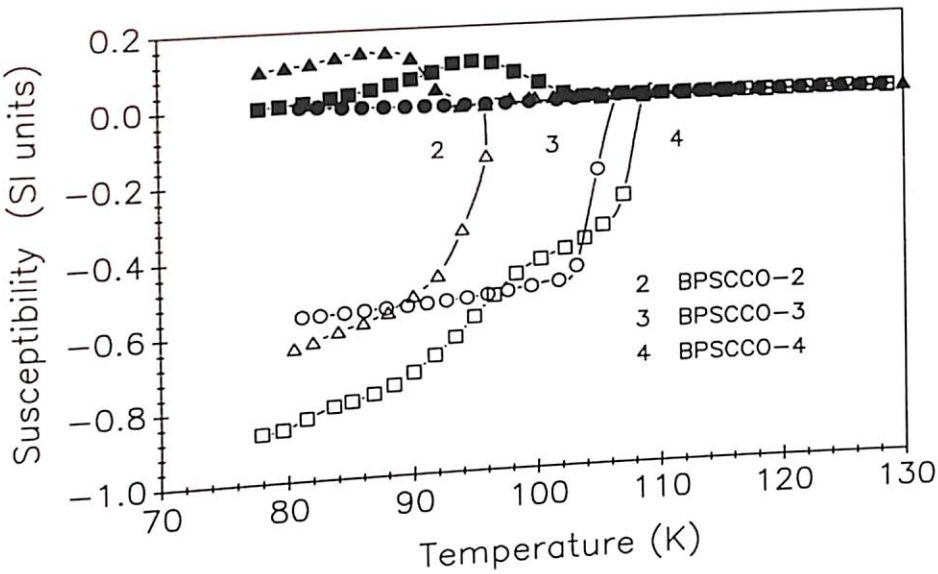

Figure 5.6: AC susceptibility vs temperature curves for BPSCCO-2, BPSCCO-3 and BPSCCO-4

in the sample. Furthermore, Hein[106] and Goldfrab[107] et al. have pointed out that ceramic samples must be pulverized and the intergranular coupling must be depressed and the χ' value should be taken well below the intrinsic T_c to estimate the volume fraction. However, the measurements were carried out under field-cooled and in identical conditions for different samples. Thus, the diamagnetic amplitude at a particular temperature can be compared in the first approximation. Fig. 5.7 shows the relative size of the χ' signals at 77K with reference to the sample BPSCCO-4. It is clear that the diamagnetic amplitude around 110 K for the sample BPSCCO-3 is comparatively larger than that of BPSCCO-4. Since the sample BPSCCO-2 has a lower T_c, it cannot be compared to the others at this temperature.

The peak χ'' is linked with the diamagnetic transition and is also influenced by the Josephson-like coupling between the grains. As discussed[83], both these χ' and χ'' are very sensitive to the intragranular and intergranular superconductivity. Since the behaviour of χ'' for all the substituted samples is essentially mutually analogous, there is no reason to believe that weak link effects are more dominating for one set of

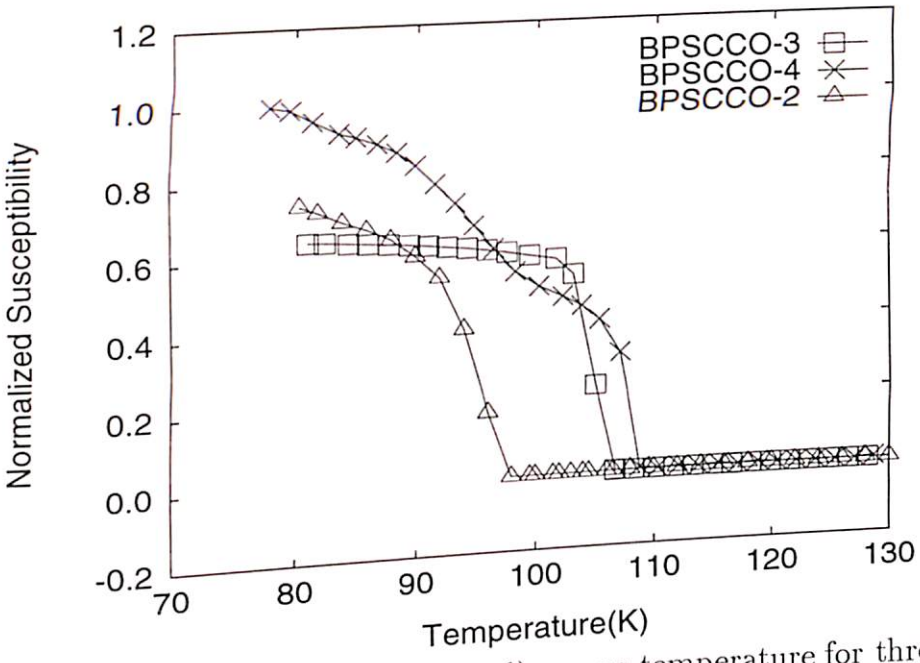

Figure 5.7: Estimated χ' (normalized) versus temperature for three samples

substitutions than the other.

Finally, all the samples were cut to the same dimension and were made to undergo the same sintering conditions in respect of furnace temperatures, pelletization pressure etc. Hence the demagnetization factor for each is similarly corrected. Therefore, one can compare the width of the superconducting transition as observed in χ' $[(\Delta T)'_\chi]$ in these samples. It is observed that the width of the transition of the sample BPSCCO-3 is comparatively lower than that of BPSCCO-2 and BPSCCO-4 samples.

5.3.5 Specific Heat

The specific heat data is shown in Fig. 5.8 for BPSCCO-2, BPSCCO-3 and BPSCCO-4 samples in the temperature range 75 to 125 K. A distinct and clear anomaly is observed at 95 K and 106 K respectively for the samples BPSCCO-2 and BPSCCO-3. However, in case of the sample BPSCCO-4 we find two anomalies at temperatures 110K and 85K respectively. The inset of Fig. 5.8 shows the plot of Cp/T against temperature for the samples BPSCCO-2, BPSCCO-3 and BPSCCO-4. The discontinuity in the specific heat at the above mentioned temperatures is seen more distinctly in this plot.

The jump in the specific heat at the transition temperature is obtained through the entropy conserving equal area construction method[45, 155, 156]. This has been

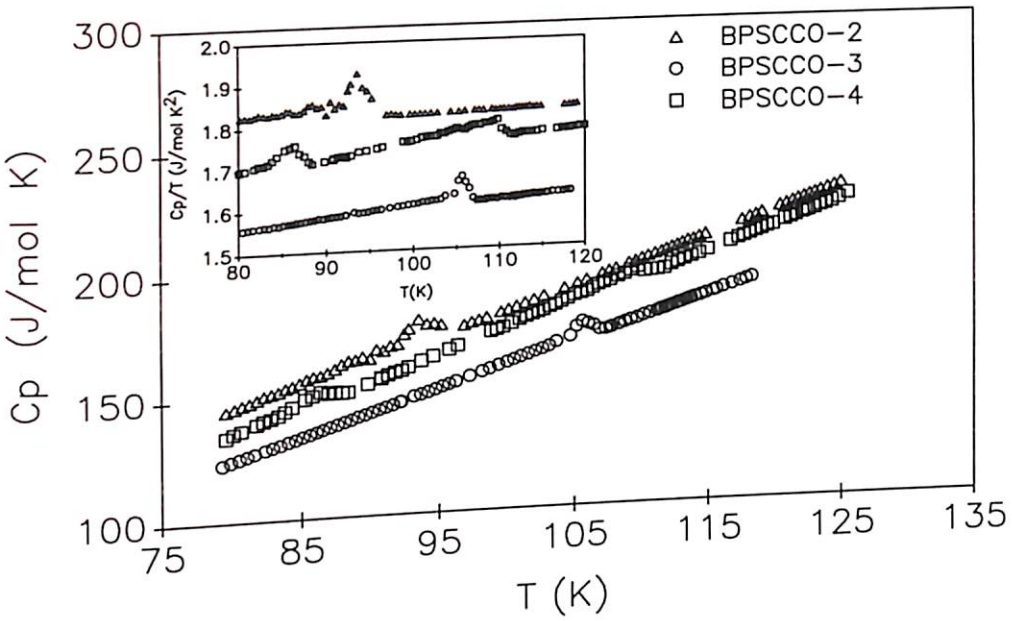

Figure 5.8: Molar specific heat (Cp) vs Temperature (T) curves for BPSCCO-2, BPSCCO-3 and BPSCCO-4 samples and the inset shows Cp/T vs T for these samples.

shown in the Fig. 5.9 for the sample BPSCCO-4. The results of these calculations are given in the Table 5.4 for all the samples. $\Delta Cp/T_c$ is 64 and 59 mJ/mol K^2 for BPSCCO-2 and BPSCCO-3 samples, and around 40 mJ/mol K^2 for the high T_c phase of BPSCCO-4 sample which agrees well with the published data[83, 84, 104, 143]. It may be mentioned in this regard that for the samples BPSCCO-2 and BPSCCO-3 the calculation of jump in the manner described above may have led to an over estimation of the jump to some extent. This is because the specific heat curve for these two

Table 5.4: Parameters calculated using the equal area construction

Sample	$\Delta C_p/T_c$ (mJ/mol K^2)	$(\Delta C_p)_{T_c}$ (J/mol K)
BPSCCO-2	64	6.18
BPSCCO-3	59	6.29
BPSCCO-4(L)	55	4.80
BPSCCO-4(H)	40	4.42

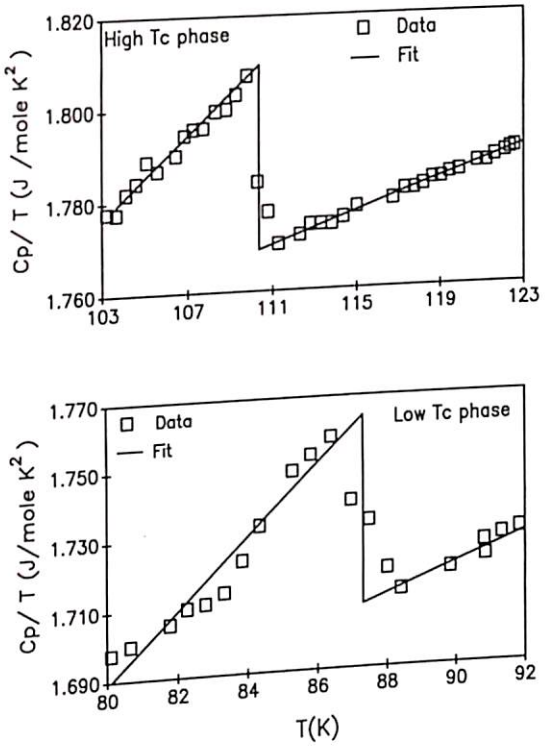

Figure 5.9: Equal area construction for the sample BPSCCO-4

samples has a rather distinct upward curvature just below the transition temperature. Hence, the accurate calculation of the jump is not possible.

5.4 Discussion

The results of these combination of experiments are summarized below:

1. There is a single and reasonably sharp specific heat anomaly and a single transition in χ' in the sample BPSCCO-3 where the domination of the stabilized high T_c Bi-2223 phase can be seen both in the XRD and STM micrographs.

2. A double transition is observed in susceptibility and two anomalies are seen in the specific heat measurement at around 106K and 95K, respectively in the BPSCCO-4 sample. In this sample Ca has been partially substituted at the Sr site. From the XRD, it is clear that in the BPSCCO-4 sample there is a deterioration of the lead stabilized Bi-2223 phase accompanied by the intergrowth of

2212 phase.

3. There is a single transition in susceptibility and a single specific heat anomaly at around 95K in the BPSCCO-2 sample. This may be considered as the intermediate T_c [T_c of 2223 phase is 110K and that of 2212 phase is 90K]. In this sample lead percentage has been reduced. Therefore, the reduction in Pb substitution increases the possibility of the intergrowth of the Bi-2122 phase and slowly transforms the system mainly to the low T_c phase.

4. Finally, in the sample BPSCCO-1, the resistivity curve is broad (T_1 - $T_2 \approx 21$K cf.Table 5.3) and gives rise to two superconducting transitions. The incomplete resistive transition at 110K, $T_c(R=0)$ at 82 K and absence of any specific heat anomaly may be attributed to the considerable deterioration of 2223 phase and the presence of the Bi-2212 phase and the faulted regions.

These observations are in agreement with the earlier reported observations on the multiphase Bi system containing both the 2223 and 2212 phases[84, 104, 143]. It may be mentioned that increase in T_c of the 2212 phase in BPSCCO-2 sample may be attributed to the proximity of the 2223 phase of a higher T_c. Such a proximity effect has earlier been observed both in the Bi and Tl based systems[143].

This study is essentially aimed to study the fluctuation effects due to the simultaneous presence of low T_c and high T_c phases. The present resistivity data (Fig. 5.3) is well defined in the normal state for the high T_c phase only. For the low T_c phase there is no way to work out the normal state resistivity. This difficulty is clarified in Figs. 5.4 and 5.5 where the typical behaviour of the resistivity of all the samples has been presented. In these figures T_1 (T_2) denote the onset temperature of the high (low) T_c phase respectively.

The manner in which T_2, T_1 and T_{ch} (mean field transition temperature) vary with disorder created in the system is now discussed. In BPSCCO-1 the lead content has been reduced as compared to the the optimal concentration required for max-

imum stabilization of the high T_c phase. In sample BPSCCO-2 lead content is more than that in BPSCCO-1 but it is still less than the optimal lead concentration. In BPSCCO-3 there a excess of copper and the sample BPSCCO-4 in addition to the excess Cu, has a calcium rich and a strontium deficient composition. In both BPSCCO-3 and BPSCCO-4 the lead content is around the concentration required to obtain the maximum stabilization of the high T_c phase. From Table 5.3 it can be seen that T_1 - T_2 ($\approx$8 K) is smallest for the BPSCCO-2 sample which is treated as the reference sample for the Pb, Cu and Sr/Ca disorder. A deficiency of Pb ions with respect to the BPSCCO-2 sample increases T_1-T_2 sharply (sample BPSCCO-1). When we move from the sample BPSCCO-2 to the samples BPSCCO-3 and BPSCCO-4 we expect T_{ch} to increase as now the Pb content is near the range of its optimum value. However from Table 5.3 it is found that T_{ch} decreases for the two samples. This means that Cu disorder decreases T_{ch} (This is opposite to the effect of excess of Cu atoms found in the $CeCu_{2.2}Si_2$ heavy electron system ([169]). Comparing the samples BPSCCO-3 and BPSCCO-4 it can be said that Sr/Ca disorder increases T_{ch}.

The temperature T_o corresponds to a crossover in the resistivity (or carrier-carrier scattering rate). Values of T_o, T_1 and T_2 are presented in Table 5.3. The typical variation of resistivity between T_1 and T_2 is present in all the four samples, although it is significant only in the BPSCCO-1 sample. This typical variation of resistivity of the BPSCCO samples between T_2 and T_1 shows the presence of two phases in all the samples. The temperature T_o is associated possibly with the spin gap[170] in the BPSCCO-2 , BPSCCO-3 and BPSCCO-4 samples. This viewpoint is based on the observation that T_o = 150, 140, 156K (for the samples BPSCCO-2, BPSCCO-3 and BPSCCO-4 respectively) is of the same order as in other high T_c materials involving the spin-gap[170, 171]. The other argument in the favour of the presence of a spin-gap in the resistivity lies in the fact that the resistivity slope is less above T_o than that below T_o[171]. In the BPSCCO-1 sample T_o does not appear to be due to spin gap because T_o is not clearly defined in this sample (cf.Fig.5.3). In fact away from T_c resistivity of BPSCCO-1 sample is similar to that of Zn doped $YBa_2Cu_3O_{7-\delta}$[172].

With the above complications in the behaviour of resistivity it is difficult to obtain the resistivity behaviour for normal state of the low T_c phase. We therefore limit ourselves to the analysis of the fluctuation conductivity of the high T_c phase only. For the high T_c phase the mean field transition temperature T_{ch} is taken as the mean of the temperatures T_2 and T_1. In literature there is no unique way for estimating the mean-field transition temperature[173]. Out of the various existing ways the one where this temperature is defined as the midpoint of the resistive transition is chosen. The values of T_{ch} obtained in this way are presented in Table 5.3.

We now turn to the specification of the normal state resistivity for the high T_c phase. As the resistivity shows a crossover at T_o, and is complicated beyond T_o its value upto T_o only is taken into consideration. It is seen from Fig. 5.4 that for the BPSCCO-2, BPSCCO-3 and BPSCCO-4 samples ρ is not linear between T_1 and T_o. This is not unexpected for the disordered polycrystalline samples of the high T_c materials. In fact, it may be noted that except for the pure single crystals corresponding to only a limited range of the carrier hole density the behaviour of resistivity for the high T_c materials is in general non linear[172, 174–176]. The reason of such a behaviour of resistivity is not yet understood properly[176]. The resistivity of the present samples, between T_1 and T_o, is therefore, considered to be given by

$$\rho_N = \rho_o + \rho_1 \left(\frac{T}{T_{ch}}\right)^a \tag{5.1}$$

Eq. 5.1 and Table 5.3 enable us to specify the normal state resistivity of all the samples. The values of the parameters ρ_o, ρ_1, a and T_{ch} are presented in Table 5.3 for all the samples.

After specifying the normal state resistivity of all the samples the fluctuation conductivity (corresponding to the high T_c phase) is defined by

$$\Delta\sigma = \left(\frac{1}{\rho_{obs}}\right) - \left(\frac{1}{\rho_N}\right) \tag{5.2}$$

In this equation ρ_{obs} is the observed resistivity. In order to analyze the fluctuation conductivity a suitable model is required. In this connection it is noticed that in the Bi-2223 system the adjacent CuO_2 layers lie at an average distance of about 10Å.

Because of this the Bi-2223 system will be highly anisotropic and thus can be treated as an array of two dimensional planes coupled by Josephson coupling[173]. Under such circumstances most appropriate model for describing the fluctuation conductivity is the one due to Lawrence and Doniach[177]. According to this model the excess conductivity is given by

$$\Delta\sigma_{LD} = \left(\frac{C}{\epsilon}\right)\left(1 + \frac{4J}{\epsilon}\right)^{-1/2} \tag{5.3}$$

In the said equation

$$C = \frac{e^2}{16\hbar\, d} \tag{5.4}$$

$$\epsilon = \frac{(T - T_{ch})}{T_{ch}} \tag{5.5}$$

$$J = \left[\frac{\xi_c(0)}{d}\right]^2 \tag{5.6}$$

In the above equations e is the electronic charge, $\hbar$ is the reduced Planck's constant, d is the average distance between the CuO_2 planes, and $\xi_c(0)$ is the zero temperature coherence length along the c-axis. In Eq. 5.3 the physically interesting parameter is the Josephson coupling parameter J. It is estimated using the following form of Eq. 5.3[122]

$$\frac{1}{\epsilon(\Delta\sigma)^2} = \left(\frac{1}{C^2}\right)\epsilon + \frac{4J}{C^2} \tag{5.7}$$

Using this equation we plot $1/\epsilon(\Delta\sigma)^2$ vs ϵ, and employ a straight line fit in the mean-field region. The mean field region in high T_c superconductors is believed to start from about T_{ch}+1.5K[178]. However, according to a recent estimate[145] the mean field region may start from about 10K above T_{ch}. A recent study on specific heat of HTSC by Braun et al.[143] and Regan et al.[179] pedicts a mean-field region in the temperature range of about 6K above T_{ch}. In view of these studies on an average the mean-field region may be considered to start from about 4-5K above the mean-field transition temperature T_{ch}. In this sense Eq. 5.7 is used to fit the observed data from $\epsilon > 0.03$. From the intercept $(4J/C^2)$ and slope $(1/C^2)$ of the straight line obtained in this way the value of J is found for the different samples. These values are presented in Table 5.3. It is clear from these values that fluctuations in the BPSCCO-1 are most

Table 5.5: The values of the parameters T_{ch}^{sh}, critical region width and $\xi_{GL}(0)$ for the samples

Sample	T_{ch}^{sh} (K)	Critical region width(K) below T_{ch}^{sh}	above T_{ch}^{sh}	$\xi_{GL}(0)$ (A)
BPSCCO-2	94.0	0.016	0.018	16.696
BPSCCO-3	105.8	0.022	0.021	19.029
BPSCCO-4	110.0	0.017	0.025	18.848

The first term in the above equation represents the electronic contribution, while the second term represents the phononic contribution to the specific heat. The fitting of the specific heat data by this equation both above and below the temperature where the anomaly occurs is shown in the Fig. 5.10 for the three samples BPSCCO-2, BPSCCO-3 and BPSCCO-4. The fluctuation or the excess specific heat is obtained using the equation

$$\Delta C_{fl} = C_p - C_{fit} \tag{5.9}$$

In this equation C_p is the observed specific heat and C_{fit} is obtained as described above.

The fluctuation specific heat is fitted by the two and the three dimensional formula

$$\Delta C_{fl\pm}^{(2)} = C_{\pm}^{(2)} t^{-1} \tag{5.10}$$

$$\Delta C_{fl\pm}^{(3)} = C_{\pm}^{(3)} t^{-1/2} \tag{5.11}$$

where $\pm$ indicates above(below) the transition and $t = (T - T_{ch}^{sh}/T_{ch}^{sh}))$. T_{ch}^{sh} is the high-T_c phase transition temperature obtained from the specific heat data. The variation of excess specific heat with temperature and its fitting with the above mentioned two and three dimensional formulae are shown in Figs. 5.11 and 5.12. The values of T_{ch}^{sh} are shown in Table 5.5. It may be noted that T_{ch}^{sh} is different from T_{ch} (Tables 5.3 and 5.5). This is not expected to create any problem as the samples under study are polycrystalline and multiphase samples. It may be mentioned that in the case of sample BPSCCO-2 the value of T_{ch}^{sh} is smaller than T_{ch}. This may be due to the fact

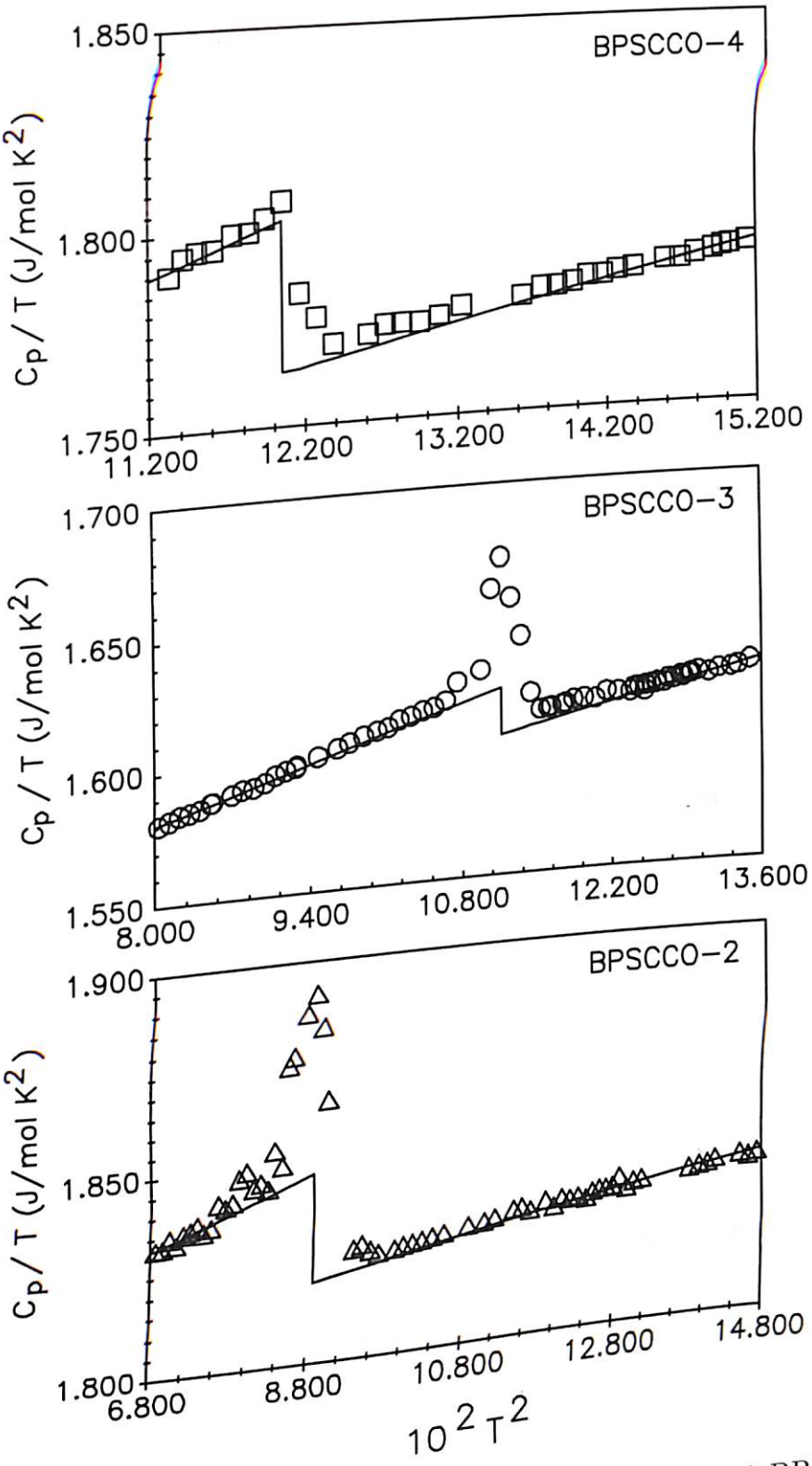

Figure 5.10: Cp/T - T^2 fitting for BPSCCO-2, BPSCCO-3 and BPSCCO-4 ; the continuous line shows the fitting of the data with $Cp^B/T = a_o + b\ T^2$ both above and below T_c.

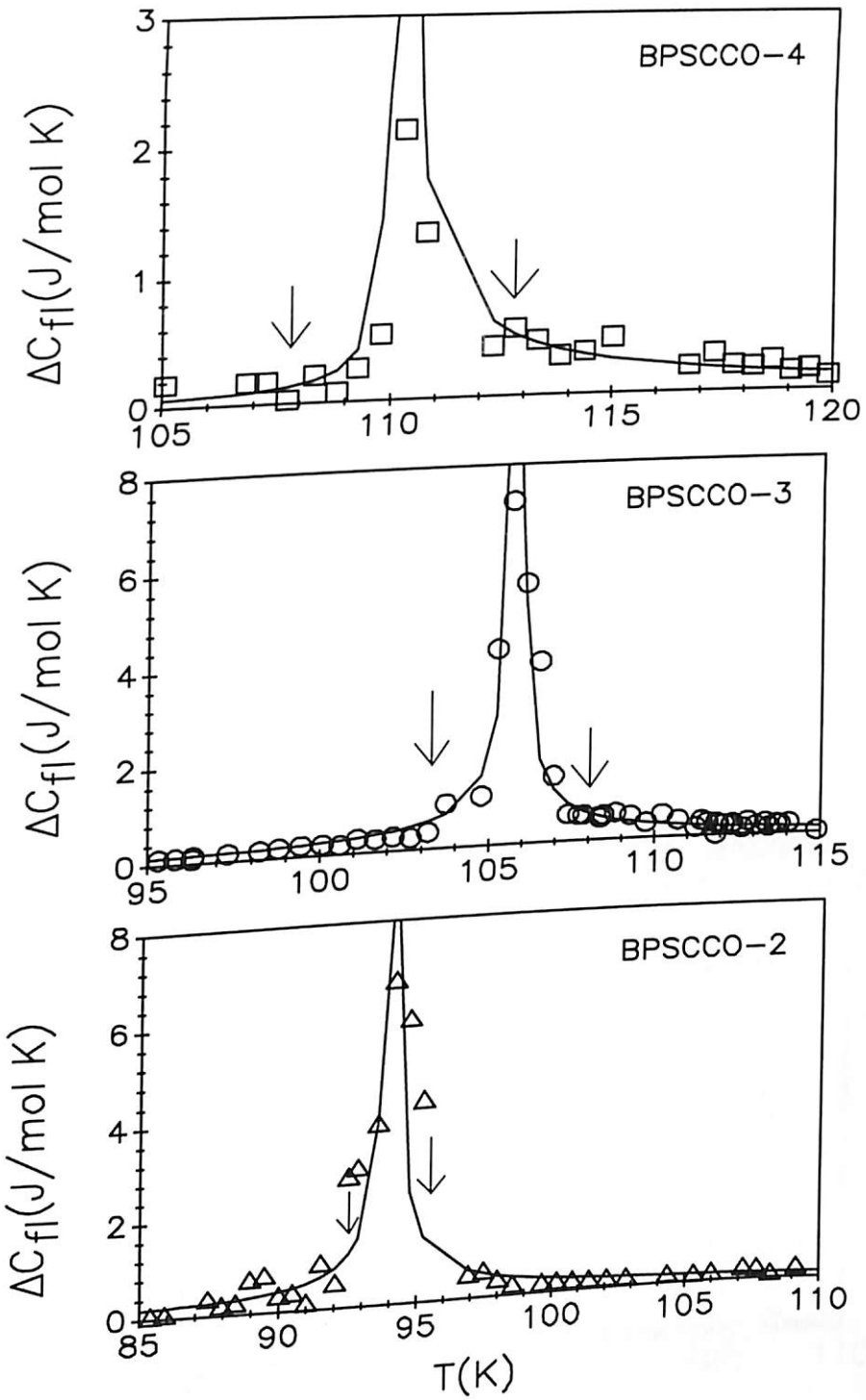

Figure 5.11: The excess specific heat, ΔC_{fl} versus temperature for the samples (1) BPSCCO-2, (2) BPSCCO-3 and (3) BPSCCO-4. The solid line shows the two-dimensional fit to the observed ΔC_{fl}. The vertical arrows show the temperatures from where two-dimensional fit to ΔC_{fl} appears to deviate from the observed values.

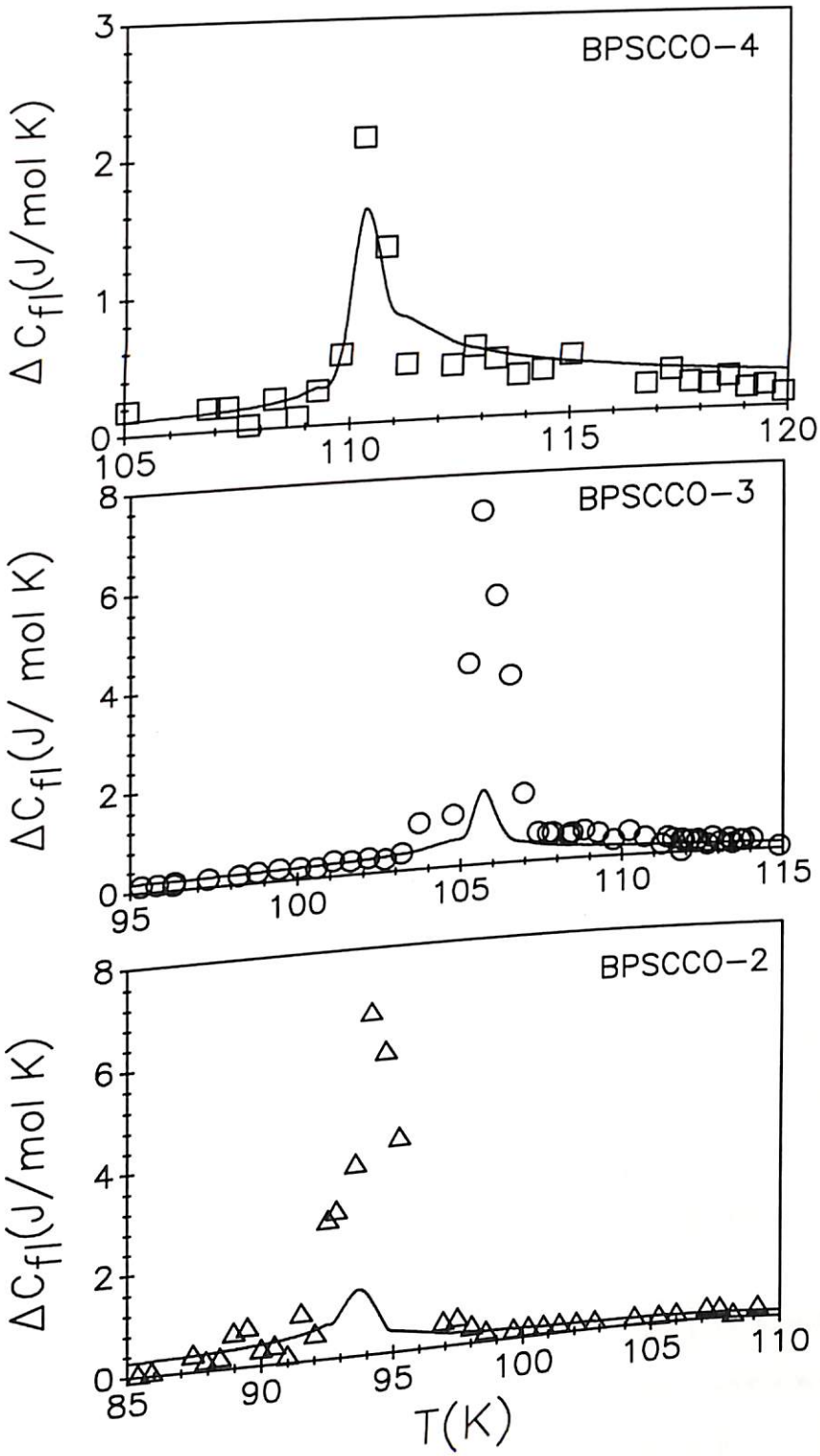

Figure 5.12: The excess specific heat, ΔC_{fl} versus temperature for the samples (1) BPSCCO-2, (2) BPSCCO-3 and (3) BPSCCO-4. The solid line shows the three-dimensional fit to the observed ΔC_{fl}.

that the volume fraction of the Bi-2223 phase is so less that there is no diamagnetic signal or a specific heat jump corresponding to the high T_c phase. As is clear from Figs. 5.11 and 5.12 two-dimensional (2D) fit is more appropriate for all the samples in the normal as well as the superconducting region. From the 2D fit of Fig.5.11 the relative magnitudes of the critical region have been estimated. In Fig. 5.11 the onset of the critical region for $T > T_{ch}^{sh}$ as well as $T < T_{ch}^{sh}$ is indicated by arrows. The onset of the critical region is specified as the temperature where the 2D fit to the fluctuation specific heat ΔC_{fl} starts to show increasing deviation from the excess specific heat data. The values of the critical region determined in this manner $[T - T_{ch}^{sh}/T_{ch}^{sh}]$ are shown in Table 5.5. From these values it is clear that the effect of 2D fluctuation in the specific heat remains closest to T_{ch}^{sh} in the case of the BPSCCO-2 sample. This agrees well with the result obtained on the basis of the fluctuation conductivity. It is also clear from the Table 5.5 that in this sense sample BPSCCO-4 will be more 2D than sample BPSCCO-3 for $T < T_{ch}^{sh}$, while sample BPSCCO-3 will be more 2D than sample BPSCCO-4 for $T > T_{ch}^{sh}$. It is, therefore, difficult to say with certainty which of these samples is more two-dimensional. It is worth noticing that the resistivity analysis shows sample BPSCCO-3 having only a little higher degree of 2D behaviour than sample BPSCCO-4. Thus, the results of specific heat are not in clear contradiction of the resistivity results.

On the basis of the above analysis of the fluctuation conductivity and fluctuation specific heat, it is clear that the disorder due to the presence of extra Cu atoms ($x'' = 0.6$) makes the system less two-dimensional. The presence of disorder in the SrO and Ca planes (due to partial replacement of Sr by Ca) appears to enhance the effect of disorder due to Cu.

Employing the coefficients $C\pm$ (involved in the specific heat) the Ginzburg-Landau (GL) coherence length at zero temperature, $\xi_{GL}(0)$ has also been estimated. For calculating these values, the relation indicated below, is employed:

$$\xi_{GL}(0) = (k_B \ V_m \ / \ 8\pi C_+)^{\frac{1}{3}} \qquad (5.12)$$

In this equation k_B is the Boltzmann's constant and V_m is the molar volume of the sample. The calculated values of $\xi_{GL}(0)$ are presented in Table 5.5. Since $\xi_{GL}(0)$ is a three-dimensional quantity, no inference can be drawn about the system on the basis of this quantity.

5.5 Conclusions

In this study the results of our measurements on the resistivity and specific heat of the Bi-2223 based cuprate systems have been presented. While it is relatively clearer to identify the superconducting phase transition in the case of specific heat, the identification of the point where superconducting phase transition takes place is difficult from the resistivity data. The presence of the Bi-2122 phase affects the resistivity of the considered samples, although the extent of this effect varies from sample to sample. The temperature difference T_1 - T_2 characterizes this variation. It is clear that in the case of the BPSCCO-2, BPSCCO-3 and BPSCCO-4 samples the effect of the Bi-2122 phase is indirect as it divides the high T_c phase in two parts with onset temperatures T_1 and T_2 differing by 8-11 K. In the case of the BPSCCO-1 sample, where there is no disorder due to extra Cu, the Bi-2122 phase shows its effect directly with T_1-T_2 = 21 K which is almost double than that for the BPSCCO-2, BPSCCO-3 and BPSCCO-4 samples.

It is seen that the mean-field superconducting transition temperatures obtained from the resistivity data, T_{ch} and from the specific heat jumps, T_{ch}^{sh} differ remarkably. This shows that the effect of the Bi-2212 phase appears differently on the electric and thermodynamic behaviour of the present system.

The resistivity and specific heat has been analyzed in terms of fluctuations near the mean-field transition temperature. The main result of our analysis is that Cu disorder makes the BPSCCO system less two-dimensional and the disorder in the SrO and Ca planes due to partial replacement of Sr by Ca (in the BPSCCO-4 sample) seems to further enhance the effect of Cu disorder. This may be explained from the fact that when there is a intergrowth of the low T_c Bi-2212 phase in the high T_c Bi-2223 phase

the resultant lattice defects at the interface of the two phases can lead to a decrease in the anisotropy of the multiphase system as compared to the pure high T_c Bi-2223 phase. This has been reflected in the present result where the BPSCCO-4 sample shows a less degree of two- dimensionality as compared to BPSCCO-3 sample in the conductivity studies and also in the specific heat studies (for $T > T_{ch}^{sh}$).

Chapter 6

Conclusions

The present study investigates in detail different properties of several high temperature superconductors. A major part of the work is devoted to the understanding of the thermal properties of the studied superconductors as manifest in their specific heat data.

For acquiring the specific heat data a calorimeter has been developed based on isoperibolic technique. The calorimeter is designed to take care of problems which occur in case of samples with low thermal conductivity, low emissivity coefficient and specific heat strongly varying with temperature. For these conditions a more elaborate and better procedure for evaluation of post-heating curves has been used. The post-heating driftline is fitted with a second order polynomial function instead of the usual linear fitting. This allows a study of any type of sample with less than 1% absolute error in the specific heat data.

The first set of samples studied comprised of Er-based 123 superconductors. A comprehensive study was carried out on the pure phase and also on the substituted samples in which Cu was partly (0.5%) replaced by the metallic dopants Ni, Zn, Fe, Co and Ga. The transition width as seen in the dc resistivity and ac susceptibility measurements seems to be broadened in the case of the out-of-plane (Fe^{3+}, Co^{3+}, Ga^{3+}) substitutions as compared to the pure sample. On the other hand in-plane-substitutions (Ni^{2+} and Zn^{2+}) seem to have a relatively lesser effect on the transition widths. Similarly for out-of-plane substitutions the specific heat anomaly is broad and smeared as compared to the pure and in-plane-substitution samples. Thus out-of-plane substi-

tutions exhibit a domination of the fluctuation effects on account of their decoupling the CuO_2 planes along the c direction where the range of coherence is quite low. This transforms the system more towards 2 dimensional and consequently a enhancement in fluctuation effects takes place.

A systematic study was carried out on the bismuth based superconductors to investigate the role of lead in the stabilization of the high T_c (Bi-2223) phase in the multiphase bismuth system. It was found that the lead content of around 15-20 at% is critical for maximum stabilization of the Bi-2223 phase. The transition temperature is highest for this particular sample and it decreases on both the higher and lower side of the critical lead concentration. Also the volume fraction and consequently the discontinuity in the specific heat is maximum for the sample with critical lead concentration. The results have been explained on the basis of the assumption that upto a concentration of 20 at% lead substitutes at the bismuth site in the valence state 2+ and beyond 20 at% it substitutes partly at the bismuth site (valence state 2+) and partly at the calcium site in the valence state 4+. Thus upto 20 at% lead, the concentration of holes in the system keeps on increasing. On increasing the lead content beyond 20 at %, the partial substitution of lead at the bismuth and calcium sites in the different valence states takes place. The hole concentration increases due to substitution at bismuth site, while it decreases due to substitution at the calcium site. The overall effect is that the hole concentration decreases in the system and this can explain the observed results of resistivity, susceptibility and specific heat measurements.

In addition a examination of another set of mixed phase bismuth based samples was carried out. The aim was to study the role of disorder in the stabilized high T_c (Bi-2223) phase from the low T_c (Bi-2122) phase in conjunction with the fluctuation effects. Excess conductivity studies were carried out in the framework of the Lawrence-Doniach model while the excess specific heat was analyzed using the 2D and 3D Gaussian formulae. The results show that Cu disorder makes the bismuth system less two dimensional and the disorder in the SrO and Ca planes due to partial replacement of Sr by Ca seems to further enhance this effect of Cu disorder.

References

[1] H. K. Onnes, Leiden Comm. 124 C(1911).

[2] W. Meissner and R. Ochsenfeld, Naturwissenschaften **21**, 787(1933).

[3] *Superconductivity and its Applications*, ed. J. E. C. Williams, Pion. Ltd., London, 5(1970).

[4] *Applied Superconductivity*, ed. Vernon L. Newhouse, John Wiley and sons Inc., New York, 35(1964).

[5] A. A. Abrikosov, Sov. Phys. JETP **5**, 1174(1957).

[6] K. Mendelssohn, Rev. Mod. Phys. **36**, 7(1964).

[7] F. London and H. London, Proc. Royal Society (London) **A149**, 72(1935).

[8] F. London and H. London, Physica **2**, 341(1935).

[9] V. L. Ginzburg and L. D. Landau, Sov. Phys. JETP **20**, 1064(1950).

[10] J. Bardeen, L. N. Cooper and J. R. Schrieffer, Phys. Rev. **108**, 1175(1957).

[11] J. G. Bednorz and K. A. Muller, Z. Phys. B **64**, 189(1986).

[12] H. Takagi, S. Vchida, K. Kitawaza, S. Tanaka, Jpn. J. Appl. Phys. **26**, L123(1987).

[13] R. J. Cava, R. B. van Dover, B. Batlogg and A. Rietmann, Phys. Rev. Lett. **58**, 408(1987); C. W. Chu, P. H. Hor, R. L. Meng, L. Gao, Z. J. Huang and Y. O. Wang, Phys. Rev. Lett. **58**, 405(1987).

[14] M. K. Wu, J. R. Ashburn, C. J. Torng, P. H. Hor, R. L. Meng, L. Gao, Z. L. Huang, Y. Q. Wang and C. W. Chu, Phys. Rev. Lett. **58**, 908(1987).

[15] T. Siegrist, S. Sunshine, D. W. Murphy, R. J. Cava and S. M. Zahurak, Phys. Rev. B **35**, 7137(1987).

[16] Z. X. Zhao, Int. J. Mod. Phys. B1 (187), Lecture held at the spring Meeting of the American Phys. Soc. in New York, March 1987.

[17] Z. Fisk, J. D. Thompson, E. Zirngiebe, J. L. Smith and S. W. Cheong, Solid State Communications **62**, 743(1987).

[18] P. H. Hor, R. L. Meng, Y. Q. Wang, L. Gao, Z. J. Huang, J. Bechtold, K. Forster and C. W. Chu, Phys. Rev. Lett. **58**, 1891(1987).

[19] L. Soderholm, K. Zhang, D. G. Hinks, M. A. Beno, J. D. Jorgensen, C. U. Segre and I. K. Schuller, Nature **328**, 604(1987).

[20] J. K. Liang, X. T. Xu, S. S. Xie, G. H. Rao, X. Y. Shao and Z. G. Duan, Z. Phys. B **69**, 137(1987).

[21] Hiroshi Maeda, Yoshiaka Tanaka, Masao Fukutomi and Toshihisa Asano, Jpn. J. Appl. Phys. **27**, L209(1988).

[22] A. M. Hermann and Z. Z. Sheng, Nature **332**, 138(1988).

[23] S. A. Sunshine, T. Siegrist, L. F. Schneemeyer, D. W. Murphy, R. J. Cava, B. Batlogg, R. B. vanDover, R. M. Fleming, S. H. Glarum, S. Nakahara, R. Farrow, J. J. Krajewski, S. M. Zahurak, J. V Waszczak, J. H. Marshall, P. Marsh, L. W. Rupp Jr. and W. F. Peck, Phys. Rev. B **38**, 893(1988).

[24] R. M. Hazen, L. W. Finger, R. J. Angel, C. T. Prewitt, N. L. Ross, C. G. Hadidiacos, P. J. Heaney, D. R. Voblen, Z. Z. Sheng, A. Elali and A. M. Hermann, Phys. Rev. Lett. **60**, 1657(1988).

[25] A. Schilling, M. Cantoni, J. D. Guo and H. R. Ott, Nature **363**, 56(1993).

[26] L. Gao, Z. J. Huang, R. L. Meng, J. G. Lin, F. Chen, I. Beauvais, Y. Y. Sun, Y. Y. Xue and C. W. Chu, Physica C **213**, 261(1993).

[27] S. W. Tozer, A. W. Kleinsaasser, T. Penney, D. Kaiser and F. Holtzberg, Phys. Rev. Lett. **59**, 1768(1987).

[28] T. Ito, H. Takagi, S. Ishibashi, T. Ido and S. Uchida, Nature **350**, 596(1991).

[29] S. Martin, A. T. Fiory, R. M. Fleming, G. P. Espinosa and A. S. Cooper, Appl. Phys. Lett. **54**, 72(1989).

[30] X. D. Xiang, W. A. Vareka, A. Zettl, J. L. Corkill, M. L. Cohen, N. Kijima and R. Gronsky, Phys. Rev. Lett. **68**, 520(1992).

[31] *Anisotropy Effects in Superconductors*, ed. H. W. Weber, (Plenum, Oxford 1977).

[32] M. B. Ruhemann, *Low Temperature Physics*, Cambridge University Press, London, 1937.

[33] E. S. R. Gopal, *Specific Heat at Low Temperatures*, Plenum Press, New York, 1966.

[34] P.L. Dulong and A. T. Petit, Ann. Chim. Phys. **10**, 395(1819).

[35] L. Boltzmann, Adad. Wissen. Wien., Sitzungsber. **63**, 679(1871).

[36] H. F. Weber, Phil. Mag. **49**, 161(1875).

[37] W. Nernst, Akad. Wiss. Berlin, Sitzber. **52**, 933(1906).

[38] A. Einstein, Ann. Physik **22**, 180(1907).

[39] W. Nernst and F. A. Lindemann, Z. Elektrochem **17**, 817(1911).

[40] P. Debye, Ann. Physik **39**, 789(1912).

[41] A. J. Rutgers, Physica **3**, 999(1936).

[42] R. Srinivasan and V. Sankaranarayanan, Rev. Solid State Sci. **2**, 277(1988).

[43] A. Junod, A. Bezinge, D. Eckert, T. Graf and J. Muller, Physica C **152**, 495(1988).

[44] N. E. Phillips, R. A. Fisher, R. Caspary, A. Amato, H. B. Radousky, J. L. Peng, L. Zhang and R. N. Shelton, Phys. Rev. B **43**, 11488(1991).

[45] B. F. Woodfield, R. A. Fisher, N. E. Phillips, R. Caspary, P. Hellman, F. Steglich and T. Wolf, Physica C **234**, 380(1994).

[46] A. Junod, D. Eckert, T. Graf, E. Kaldis, J. Karpinski, S. Rusiecki, D. Sanchez, G. Triscone and J. Muller, Physica C **168**, 47(1990).

[47] A. Chakraborty, A. J. Epstein, D. L. Cox, E. M. McCarron and W. E. Farneth, Phys. Rev. B **39**, 12267(1989).

[48] J. S. Urbach, D. B. Mitzi, A. Kapitulnik, J. Y. T. Wei and D. E. Morris, Phys. Rev. B **39**, 12391(1989).

[49] S. A. Collacot and R. Driver, Physica C **167**, 598(1990).

[50] N. E. Phillips, R. A. Fisher, J. E. Gordon, S. Kim, A. M. Stacy, M. K. Crawford and E. M. McCarron III, Phys. Rev. Lett. **65**, 357(1990).

[51] A. P. Ramirez, R. J. Cava, G. P. Espinosa, J. P. Remeika, B. Batlogg, S. Zahurak and E. A. Rietman, Mater. Res. Soc. Symp. Proc. **99**, 459(1987); D. Eckert, A. Junod, T. Graf and J. Muller, Physica C **153-155**, 1038(1988).

[52] A. Amato, R. A. Fisher, N. E. Phillips and J. B. Torrance, Physica B **165-166**, 1337(1990).

[53] D. J. Thouless, Ann. Phys. **10**, 553(1960).

[54] L. G. Aslamazov and A. I. Larkin, Sov. Phys. Solid State, **10**, 875(1968).

[55] L. N. Bulaevskii, V. L. Ginzburg and A. A. Sobyanin, Physica C **152**, 378(1988).

[56] L. N. Bulaevskii, Int. J. Mod. Phys. B **4**, 1849(1990).

[57] W. Nernst, Chem. Abstr. **4**, 2397(1910).

[58] Gaede, Phys. Zeits. **4**, 805(1902).

[59] E. H. Griffiths and E. Griffiths, Phil. Trans. A 213(1913);Proc. Roy. Soc. A **89**, 561(1914).

[60] Nernst and Lindemann, Journal de Physique **4**, 9(1910); Lindemann, Ann. d. Physik **36**, 395(1911).

[61] J. C. Southard and D. H. Andrews, J. Franklin Inst. **209**, 349(1930).

[62] E. S. Watson, M. J. O' Neill, J. Justin and N. Brenner, Anal. Chem **36**, 1233(1964).

[63] A. V. Narlikar, S. K. Agarwal and C. V. N. Rao, *Studies of High Temperature Superconductors*, vol. 1, ed. A. V. Narlikar, Nova Sci. Pub., New York, 341(1989).

[64] S. K. Agarwal and A. V. Narlikar, *Progress Crystal Growth and Characterization*, vol.28, 219(1994).

[65] *Chemistry of High Temperature Superconductors*, ed. C.N.R. Rao, World Scientific Publications (1991).

[66] C.N.R. Rao, Phil. Trans. R. Soc. A **336**, 595(1991).

[67] T. Uzumaki, K. Yamanaka, N. Kamehara and K. Niwa, Jap. J. Appl. Phys. **28**, L75(1989).

[68] *New Directions in Solid State Chemistry*, ed. C.N.R Rao and J. Gopalakrishnan, Cambridge University Press (1989).

[69] M. Marezio, Acta. Cryst. A **47**, 640(1991).

[70] Shigeki Kobayashi, Yasuyoshi Saito and Shigetaka Wada, Jap. J. Appl. Phys. **28**, L772(1989).

[71] A. Oota, K. Ohba, A. Ishida, H. Noji, A. Kirihigashi, K. Iwaski and H. Kuwajima, Jap. J. Appl. Phys. **29**, 1262 (1990).

[72] Barry E. Jones, *Instrumentation, Measurement and Feedback*, Tata McGraw Hill, TMH ed. 1978.

[73] E.F. Westrum Jr., G. T. Furukawa and M. C. McCullough, *Experimental Thermodynamics*, vol I, ed. J. P. McCullough and D. W. Scott (London: Butterworth), *133 (1968)*.

[74] E. Gmelin, Thermochemica Acta **29**, *1(1979)*.

[75] T. Matsuo, Thermochemica Acta **163**, 57(1990).

[76] E. Gmelin, Thermochemica Acta **110**, 183(1987).

[77] H. Preston-Thomas, Metrologia **27**, 3(1990).

[78] W. H. Keesom and J. A. Kok, Proc. Acad. Sci. Amsterdam **35**, 294(1932).

[79] J. S. Kouvel, Journal of Applied Physics **27**, 639(1956).

[80] T. D. Cheung, W. K. Chan, and *J. S. Kouvel, Rev. Sci. Instrum.* **53**, *820(1982)*.

[81] S. B. Ota and E. Gmelin, Meas. Sci. Technol., **3** 1047(1992).

[82] A. K. Bandyopadhyay, P. Maruthikumar, G. L. Bhalla, S. K. Agarwal and A. V. Narlikar, Physica C **165**, 29(1990).

[83] A. K. Bandyopadhyay, E. Gmelin, B. V. Kumaraswamy, V. P. S. Awana, Deepak Varandani, Nirupa Sen and A. V. Narlikar, Phys. Rev. B **48**, 6470(1993).

[84] A. K. Bandyopadhyay, Deepak Varandani, E. Gmelin and A. V. Narlikar, Phys. Rev. B **50**, 462(1994).

[85] Deepak Varandani, A.K. Bandyopadhyay, V. S. Yadav, E. Gmelin and A. V. Narlikar, Meas. Sci. Technol. **7**, 511(1996).

[86] *CRC Handbook of Chemistry and Physics*, ed. R. C. Weast, 57th Edition (Cleveland, OH: CRC, 1976-77) ; *CRS Handbook of Chemistry and Physics*, ed. D.R. Lide, 74th ed. (Cleveland, OH: CRC, 1993-94).

[87] G. V. Williams and J. L. Tallon, Physica C **258**, 41(1996).

[88] J. M. Tarascon, P. Barboux, P. F. Miceli, L. H. Greene, G. W. Hull, M. Eibschutz and S. A. Sunshine, Phys. Rev. B **37**, 7458(1988).

[89] Y. Maeno, T. Tomita, M. Kyogoku, S. Awaji, Y. Aoki, K. Hoshino, A. Minami and T. Fujita, Nature **328**, 512(1987).

[90] E. Takayama-Muromachi, Y. Uchida, and K. Kato, Jpn. J. Appl. Phys. **26**, L2087(1987).

[91] A. V. Narlikar, S.K. Agarwal and C. V. N. Rao, *Studies of High Temperature Superconductors* vol. 1, Nova Science Publishers, New York, edited by A. V. Narlikar, 341(1989).

[92] Y. Iye, *Studies of High Temperature Superconductors*, vol. 1 , ed. A. V. Narlikar, Nova Sci. Pub., New York, 166 (1989).

[93] M. Akinaga, *Studies of High Temperature Superconductors*, vol. 8, ed. A.V. Narlikar, Nova Sci. Pub., New York, 297(1989).

[94] W.J. Skocpol and M. Tinkham, Rep. Prog. Phys. **38**, 1049(1975).

[95] S.B. Ogale, R.D. Vispule and S.M. Kanetkar, Ind. J. Pure and Appl. Phys. **30**, 666 (1992).

[96] S. E. Inderhees, M. B. Salamon, N. Goldenfeld, J. P. Rice, B. G. Pazol, D.M. Ginsberg, J. Z. Liu and G. W. Crabtree, Phys. Rev. Lett. **60**, 1178 (1988).

[97] D. Sanchez, A. Junod, J.-Y. Genoud, T. Graf and J. Muller, Physica C **200**, 1(1992).

[98] C. Y. Yang, A. R. Moodenbaugh, Y. L. Wang, Y. W. Xu, S. M. Heald, D. O. Welch, M. Suenaga, D. A. Fisher and J. E. Pennerhahn, Phys. Rev. B **42**, 2231(1990).

[99] R. Dupree, A. Gencten and D. McK. Paul, Physica C **193**, 81(1992); A. Gencten, R. Dupree and D. McK. Paul, ibid. **216**, 491(1993).

[100] H. Alloul, T. Ohno, H. Casalta, J. F. Marucco, P. Mendels, J. Arabski, G. Collin and M. Mehbod, Physica C **171**, 419(1990); P. Mendels, H. Alloul, J. F. Marucco, J. Arabski and G. Collin, ibid. **171**, 429(1990).

[101] X. Zhang, K. WW. Yip, and C. K. Ong, Physica C **234**, 99(1994).

[102] R. Liang, T. Nakamura, H. Kawaji, M. Itoh and T. Nakamura, Physica C **170**, 307(1990).

[103] S. B. Samanta, P. K. Dutta, V. P. S. Awana, E. Gmelin and A. V. Narlikar, Physica C **178**, 171(1991).

[104] D. R. Harshman and A. P. Mills, Jr., Phys. Rev. B **45**, 10684(1992).

[105] A. Sumiyama, H. Endo, J. Tsuchiya, N. Kijima. M. Mizuno and Y. Oguri, Jpn. J. Appl. Phys. **28**, L373(1989).

[106] R. A. Hein, Phys. Rev. B **33**, 7539(1986).

[107] R. B. Goldfarb, M. Lelental and C. A. Thompson, *Magnetic Susceptibility of Superconductors and Other Spin Systems*, Plenum, New York, 49(1991).

[108] J. C. Van Miltenburg and A. Schuijff, K. Kadowaki, M. Van Sprang, J. Q. A. Koster, Y. K. Huang and A. A. Menovsky, Physica C **146B**, 319(1987).

[109] W. Schnelle, P. Ernst and D. Wohlleben, Ann. Physik **2**, 109(1993).

[110] V. Breit, P. Schweiss, R. Hauff, H. Wuhl, H. Claus, H. Rietschel, A. Erb and G. Muller-Vogt, Phys. Rev. B **52**, R15727(1995).

[111] A. Junod, *Physical Properties of High Temperature Superconductors*, vol. II, ed. D. M. Ginsberg, World Scientific Publications, 13(1990).

[112] A. Junod, A. Bezinge and J. Muller, Physica C **152**, 50(1988).

[113] W. C. Lee, R. A. Klemm and D. C. Johnston, Phys. Rev. Lett. **63**, 1012(1990); W. C. Lee and D. C. Johnston, Phys. Rev. B **41**, 1904(1990).

[114] V. N. Naumov, Phys. Rev. B **49**, 13247(1994).

[115] V. G. Bessergenev, Yu. A. Kovalevskaya, V. N. Naumov and G. I. Frolova, *Physica C* **245**, 36(1995).

[116] V. N. Naumov, G. I. Frolova, E. B. Amitin, V. E. Fedorov, P. P. Samoilov, Physica C **262**, 143(1996).

[117] S. P. Pandey, M. S. Hegde, B. V. Kumaraswamy and A. V. Narlikar, Physica C **206**, 207(1993).

[118] J. Viera and F. Vidal, Physica C **159**, 468(1989).

[119] P. W. Anderson and Z. Zou, Phys. Rev. Lett. **60**, 132(1988).

[120] L. G. Aslamazov and A. I. Larkin, Phys. Lett. A **26**, 235(1968).

[121] K. Maki and R. S. Thomson, Phys. Rev. B **39**, 2767(1989).

[122] U. C. Upreti, R. Lal, S. K. Agarwal, A. V. Narlikar and S. B. Ogale, Ind. J. Pure and Appl. Phys. **34**, 951(1996).

[123] U. C. Upreti and A. V. Narlikar, Solid State Communications **100**, 615(1996).

[124] M. Fontana, Solid State Communications **69**, 621(1989).

[125] B. Oh, K. Char and A. D. Kent, Phys. Rev. B **37**, 7861(1988).

[126] M. Ausloos and C. H. Laurent, Phys. Rev. B **37**, 611(1988).

[127] J. G. Bednorz and K. A. Muller, Z. Phys. B **64**, 189(1986).

[128] C. Michel, M. Hervieu, M. M. Borel, A. Gradin, F. Deslandes, J. Provost and B. Raveau, Z. Phys. B **68**, 421(1987).

[129] J. M. Tarascon, W. R. McKinnon, P. Baraboux, D. M. Hwang, B. G. Bagley, L. H. Greene, G. W. Hull, Y. LePage, N. Stoffel and M. Giroud, Phys. Rev. B **38**, 8885(1988).

[130] J. M. Tarascon, Y. LePage, P. Baraboux, B. G. Bagley, L. H. Greene, W. R. McKinnon, G. W. Hull, M. Giroud and D. M. Hwang, Phys. Rev. B **37**, 9382(1988).

[131] S. M. Green, C. Jiang, Yu Mei, H. L. Luo and C. Politis, Phys. Rev. B **38**, 5016(1988).

[132] C. K. Rhee, C. J. Kim, H. G. Lee, I. H. Kuk, J. M. Lee, I. S. Chang, C. S. Rim, P. S Han, S. I. Pyun and D. Y. Won, Jpn. J. Appl. Phys. **28**, L1137(1989).

[133] J. L. Tallon, R. G. Buckley, M. R. Prestland, P. W. Gilberd, I. W. M. Brown, M. Bowden and R. Goguel, Phase Transitions **19**, 171(1989).

[134] H. K. Lee, K. Park and D. H. Ha, J. Appl. Phys. **70**, 2764(1991).

[135] B. Zhu, L. Lei, S. L. Yuan, S. B. Tang, W. Wang, G. G. Zheng, W. Y. Guan and J. Q. Zheng, Physica C **157**, 370(1989).

[136] H. K. Liu, S. X. Dou, N. Savvides, J. P. Zhou, N. X. Tan, A. J. Bourdillon, M. Kviz and C. C. Sorrell, Physica C **157**, 93(1989).

[137] Huanbo Zhang and Hiroshi Sato, Physica C **214**, 265(1993).

[138] A. Jeremie, K Alami-Yadri, J-C Grivel and R. Flukiger, Supercond. Sci. Technol. **6**, 730(1993).

[139] Jin Rong-Ying, Shi Fan, Qi-Ze Ran, Shi-Ni-Cheng, Shi Zhen-Hua, and Zhou Shou-Zeng, Physica C, **158**, 255(1989).

[140] A. Schilling, H. R. Ott and P. Hulliger, Physica C 161, 628(1989).

[141] R. A. Fisher, S. Kim, Y. Wu, N. E. Phillips, H. M. Ledbetter and K. Togano, Physica C **162-164**, 502(1989).

[142] W. Schnelle, E. Braun, H. Broicher, H. Weiss, H. Geus, S. Ruppel, M. Galffy, W. Braunisch, A. Waldorf, F. Seidler, and D.Wohlleben, Physica C **161** 123(1989).

[143] E. Braun, W. Schnelle, J. Harnischmacher, D. Wohlleben, C. Allgeier, W. Reith, J. S. Schilling, J. Bock, E. Preisler, G. J. Vogt, Z. Phys. B: Cond. Matt. **84**, 333(1991).

[144] W. Schnelle, N. Knauf, J. Bock, E. Preisler and J. Hudepohl, Physica C **209**, 456(1993).

[145] D. S. Fisher, M. P. A. Fisher and D. A. Huse, Phys. Rev. B **43**, 130(1991).

[146] O. Jeandupeux, A. Schilling and H. R. Ott, Phys. Rev. B. **53**, 12475(1996).

[147] W. C. Lee, J. H. Cho and D. C. Johnston, Phys. Rev. B **43**, 457(1991).

[148] M. K. Yu, J. P. Franck, M. A. K. Mohammed, W. A. Miner, J. Jung and S. Gygax, Physica C **162**, 468(1989).

[149] M. Boekholt, D. Gotz, H. Idnik, M. Fleuster, T. Hahn, E. Woermann and G. Guntherodt, Physica C **185-189**, 789(1991).

[150] H. Mazaki, T. Ishida and T. Sakuma, Jap. J. Appl. Phys. **27**, L811(1989).

[151] K. Kitazawa, Y. Tomioka, T. Hasegawa, K. Kishnio, M. Naito, T. Matsushita, I. Tanaka and H. Kojima, Supercond. Sci. Technol. 4, 535(1991).

V. Kartsovnik, G. Yu. Logvenov and K. Ya. Soifer, Cryogenics **30**, 647(1990).

[139] Jin Rong-Ying, Shi Fan, Qi-Ze Ran, Shi-Ni-Cheng, Shi Zhen-Hua, and Zhou Shou-Zeng, Physica C, **158**, 255(1989).

[140] A. Schilling, H. R. Ott and F. Hulliger, Physica C **161**, 626(1989).

[141] R. A. Fisher, S. Kim, Y. Wu, N. E. Phillips, H. M. Ledbetter and K. Togano, Physica C **162-164**, 502(1989).

[142] W. Schnelle, E. Braun, H. Broicher, H. Weiss, H. Geus, S. Ruppel, M. Galffy, W. Braunisch, A. Waldorf, F. Seidler, and D.Wohlleben, Physica C **161** 123(1989).

[143] E. Braun, W. Schnelle, J. Harnischmacher, D. Wohlleben, C. Allgeier, W. Reith, J. S. Schilling, J. Bock, E. Preisler, G. J. Vogt, Z. Phys. B: Cond. Matt. **84**, 333(1991).

[144] W. Schnelle, N. Knauf, J. Bock, E. Preisler and J. Hudepohl, Physica C **209**, 456(1993).

[145] D. S. Fisher, M. P. A. Fisher and D. A. Huse, Phys. Rev. B **43**, 130(1991).

[146] O. Jeandupeux, A. Schilling and H. R. Ott, Phys. Rev. B. **53**, 12475(1996).

[147] W. C. Lee, J. H. Cho and D. C. Johnston, Phys. Rev. B **43**, 457(1991).

[148] M. K. Yu, J. P. Franck, M. A. K. Mohammed, W. A. Miner, J. Jung and S. Gygax, Physica C **162**, 468(1989).

[149] M. Boekholt, D. Gotz, H. Idnik, M. Fleuster, T. Hahn, E. Woermann and G. Guntherodt, Physica C **185-189**, 789(1991).

[150] H. Mazaki, T. Ishida and T. Sakuma, Jap. J. Appl. Phys. **27**, L811(1989).

[151] K. Kitazawa, Y. Tomioka, T. Hasegawa, K. Kishnio, M. Naito, T. Matsushita, I. Tanaka and H. Kojima, Supercond. Sci. Technol. **4**, 535(1991).

[152] M. V. Kartsovnik, G. Yu. Logvenov and K. Ya. Soifer, Cryogenics **30**, 647(1990).

[153] B. P. Singh, S. P. Pandey, R. K. Nayar, B. V. Kumaraswamy and A. V. Narlikar, Phys. Rev. B **46**, 3573(1992).

[154] A. M. Campbell, F. J. Blunt, J. D. Johnson and P. A. Freeman, Cryogenics **31**, 732(1991).

[155] C. Meingast, R. Ahrens, R. Blank, H. Burkle, B. Rudolf and H. Wuhl, Physica C **173**, 309(1991).

[156] J. E. Gordon, R. A. Fisher and N. E. Phillips, Phil. Mag. B **65**, 1389(1992).

[157] E. Gmelin, *Studies of High-Temperature Superconductors*, Vol. 2. ed. A. V. Narlikar, Nova Sci. Pub., New York, 95(1989).

[158] Y. Gao, E. Crow, G. H. Myer, P. Schlottmann, J. Schwegler and N. D. Spencer, Physica C **165**, 340(1990).

[159] Z. Chen, H. Liu, Z. Mao, K. Wang, X. Zhan and Y. Zhang, Physica C **156**, 834(1988).

[160] P. V. P. S. S. Sastry, J. V. Yakhmi and R. M. Iyer, Solid State Physics Symposium, Varanasi, 1991, ed., A. Sequera.

[161] G. Miehe, T. Vogt, H. Fuess and M. Wilhelm, Physica C **171**, 339(1990).

[162] D. Wohlleben, E. Braun, W. Schnelle, J. Harnischmacher, S. Ruppel and R. Domel, *International Conference on Superconductivity*, ICSC, Bangalore, ed. S. K. Joshi, C. N. R. Rao and S. V. Subramanyam, World Scientific, Singapore, 194(1990).

[163] G. Deutscher, Physica C **15**, 153(1988).

[164] C. J. Lobb, Phys. Rev. B **36**, 1930(1987).

[165] R. K. Nkum, A. Punnett and W. R. Datars, Physica C **202**, 371(1992).

[166] R. K. Nkum and W. R. Datars, Physica C **192**, 215(1992).

[167] E. Isaac Samuel, S. Ravi and V. Seshu Bai, Solid State Communications **96**, 441(1995).

[168] D. Ciurchea, A. V. Pop, O. Cozar, Gh Ilonca, V. I. Geru, V. Pop and L. A. Konopko, Supercond. Sci. Technol. **9**, 88(1996).

[169] U. Rauchschwalbe, Physica B+C **147**, 1(1987).

[170] J.M. Tranquada, P.M. Gehring, G. Shirane, S. Shamoto and M. Sato, Phys. Rev. B **46**, 5561 (1992); G.V.M Williams, J.L. Tallon, R.Meinhold and A. Janossy, Phys. Rev. B **51**, 16503 (1995).

[171] N. F. Mott, Phil. Mag. Lett. **68**, 245 (1993).

[172] G. Ilonca, M. Mehbod, A. Lanchbeen, and R. Deltour, Phys. Rev. B **47**, 15265 (1993).

[173] S. H. Han and O. Rapp, Solid State Communications **94**, 661 (1995).

[174] H. Takagi, B. Batlogg, H. L. Kao, J. Kwo, R. J. Cava, J. J. Krajewski and W. F. Peck Jr., Phys. Rev. Lett. **69**, 2975 (1992).

[175] B. Wuyts, V.V. Moshchalkov and Y. Bruynseraede, Phys. Rev. B **51**, 6115 (1995).

[176] E. Dagotto, Rev. Mod. Phys. **66**, 763 (1994).

[177] W. E. Lawrence and S. Doniach, in *Proceedings 12th International Conference Low Temperature Physics* Kyoto 1979, ed. E. Kanda, Keigaku, Tokyo, 361(1970).

[178] C. Totton, A. Diaz, A. Pomar, J. A. Veira and F. Vidal, Phys. Rev. B **49**, 13143 (1994).

[179] S. Regan, A. J. Lowe and M. A. Howson, J. Phys. Cond. Matter **3**, 9245 (1991).

List of Publications

1. Effect of Ni Mev ion irradiation on the resistivity of $Bi_{1.7}Pb_{0.35}Sr_2Ca_2Cu_3O_{10+x}$ at low ion fluence.

   Nirupa Sen, A.K.Bandyopadhyay, P.Sen, Umesh Tiwari, **Deepak Varandani**, V.P.S. Awana and A.V. Narlikar.

   Solid State Communications 82, 555(1992).

2. Effect of lead substitution in bismuth-based cuprate systems containing both low-Tc and high-Tc phases.

   A.K.Bandyopadhyay, E.Gmelin, B.V.Kumaraswamy, V.P.S.Awana, **Deepak Varandani** and A.V.Narlikar.

   Physical Review B 48, 6470(1993).

3. Resistivity, magnetic susceptibility and specific heat studies of the substituted ErBa2(Cu1-xMx)3O7-y [(M: Ni,Zn,Fe,Co,Ga) and x=.005], - the effect of site dependent substitutional disorder.

   A.K.Bandyopadhyay, **Deepak Varandani**, E.Gmelin and A.V.Narli kar.

   Physical Review B, 50, 462(1994).

4. Effect of Fe substitution on the magnetism and superconduc tivity of YBa2Cu3O7-y system with variable oxygen con tent.

   V.P.S. Awana, R.Lal, **Deepak Varandani**, A.V.Narlikar and S.K. Malik.

   Supercond. Sci. Technol. 8, 745(1995).

5. A simple, versatile and high precision quasi-adiabatic calorimeter for the specific-heat measurement in the temperature range 77-300K.

   Deepak Varandani, A.K. Bandyopadhyay, V.S. Yadav, E. Gmelin and A.V. Narlikar.

   Measurement Science and Technology 7, 511(1996).

6. Low temperature specific heat and related studies on pure and substituted phases of high Tc cuprates.

   Deepak Varandani, A.K. Bandyopadhyay and A.V. Narlikar.

   Book chapter: Superconductivity, Theoritical and Experimental effects, Editor K.N. Srivastava.

7. Excess specific heat and conductivity studies in the Bi-based cuprate systems-the effect of fluctuations in the high Tc phase.

   Deepak Varandani, A.K. Bandyopadhyay, E. Gmelin, R. Lal and A.V. Narlikar.

   Submitted to Physical Review B.

8. A quasi-adiabatic calorimeter for specific-heat measurements of samples with low thermal conductivity in the temperature range 77-300 K.

   Deepak Varandani, A. K. Bandyopadhyay and A. V. Narlikar.

   Proceedings of the International Conference on Instrumentation , Aug. 8-10, 1996, Banglore, India, Ed. B. S. Ramprasad, S. Asokan, K. Rajanna, N. C. Shivaprakash , Vol. 26, 467(1996).

9. Specific heat measurements of the lead substituted Bi-systems.

   Deepak Varandani, A. K. Bandyopadhyay and A. V. Narlikar.

   Presented at the Fifteenth National Symposium On Cryogenics , Sept. 12-14, 1996, New Delhi.

10. Specific heat measurements of the substituted RE-123 systems.

    Deepak Varandani, A. K. Bandyopadhyay and A. V. Narlikar.

    Presented at the Fifteenth National Symposium On Cryogenics , Sept. 12-14, 1996, New Delhi.

Appendix

Solid State Communications, Vol. 82, No. 7, pp. 555–558, 1992.
Printed in Great Britain.

0038-1098/92 $5.00 + .00
Pergamon Press Ltd

EFFECT OF ^{58}Ni MeV ION IRRADIATION ON THE RESISTIVITY OF $Bi_{1.7}Pb_{0.35}Sr_2Ca_2Cu_3O_{10+x}$ AT LOW ION FLUENCE

Nirupa Sen, A.K. Bandyopadhyay, P. Sen,† Umesh Tiwari,† Deepak Varandani, V.P.S. Awana and A.V. Narlikar

National Physical Laboratory, New Delhi 110012, India
†School of Physical Sciences, J.N.U., New Delhi 110067, India

(*Received* 1 *January* 1992 *by C.N.R. Rao*)

Heavy ion ^{58}Ni MeV ion irradiation at room temperature of high T_c $Bi_{1.7}Pb_{0.35}Sr_2Ca_2Cu_3O_{10+x}$ is reported. We show through *in-situ* resistivity measurements that at low fluence, formation of stable Frenkel pairs takes place together with possible defect annealing. The changes in T_c at low fluence is not appreciable. This is possibly a result of chemical substitution of Cu by Ni, a technique suitable to engineer new materials for potential applications.

1. INTRODUCTION

ION IMPLANTATION usually creates disorder in any material depending upon the energy, type of bombarding particles and quality of the sample. As a result of disorder, a host of physical properties are found to change, in particular, for high T_c superconducting materials, the superconducting transition temperature (T_c), critical current (J_c) etc. [1, 2]. Therefore, controlled ion implantation for production of localised defects in a material, and thereby a specific change in its properties would lead to the search for new approaches in the fabrication and processing of high T_c materials into devices. A large number of reports on the effect of different types of radiation on high T_c materials have already been reported in literature, which were carried out by γ-ray [3–5], electron [6, 7], neutron [8, 9] and ion irradiation.

In this paper, we report a preliminary investigation of the creation of controlled defects using ion beams with a view to engineer defects for potential applications. Low beam currents in the order of 0.2–0.4 pnA (particle nano ampere) were used to irradiate a sample of $Bi_{1.7}Pb_{0.35}Sr_2Ca_2Cu_3O_{10+x}$ using ^{58}Ni ions at 75 MeV. *In-situ* resistivity measurements as a function of fluence showed that the resistivity of the sample increases monotonically, showing saturation beyond a fluence of 500×10^{11} ions cm^{-2}. While the off-line measurements, mainly resistivity and magnetic susceptibility, of the irradiated sample show that T_c does not change appreciably. R–T measurements are in conformity with the formation of vacancy interstitial Frenkel pairs and the saturation is explained as due to the recombination of such defects.

2. EXPERIMENTAL

The synthesis of Pb substituted multiphase high quality polycrystalline $Bi_{1.7}Pb_{0.35}Ca_2Sr_2Cu_3O_{10+x}$ in the bulk form was prepared by solid state reaction using all the ingredients whose purity was better than 4 N. The starting mixture, thoroughly ground, was calcined three times for 12 h each at 820, 830 and 840°C in succession and finally quenched to room temperature. After regrinding, the sample was pressed at 6 Kbar and a final heat treatment carried out on the pellets at 865°C for 48 h and furnace cooled to room temperature over a span of 6 h.

The characterization of the samples was carried out by X-ray diffraction (XRD), using a Siemens D-500 diffractometer with CuKα radiation. Figure 1 shows the XRD pattern of the sample. It is clear from Fig. 1 that both the Bi-2223 and Bi-2122 phases are present in the sample. Lines corresponding to the 2223 phase are denoted by H while those of 2122 phase are denoted by L. The a.c. susceptibility was measured by a Lake-Shore susceptometer. The sample was cooled in a low field through its transition temperature while X' and X'' were measured while warming up slowly. The absolute temperature is measured by a silicon diode (DT-470) thermometer with an accuracy of 0.2 K Figure 2 shows the a.c. susceptibility of the sample. It can be seen that there is a step like temperature dependence which suggests the presence of both the Bi-2223 and Bi-2122 phases with the superconductivity onset at 103 and 92 K, respectively. The volume fraction of Bi-2223 phase can be roughly estimated to be 40%. The off-line experiments of T_c ($R = 0$) were carried out using the conventional four probe

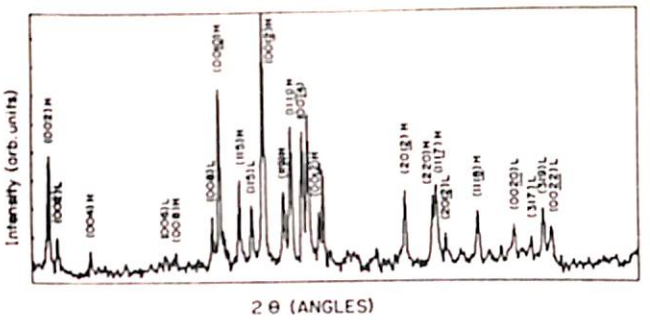

Fig. 1. X-ray diffraction pattern of $Bi_{1.7}Pb_{0.35}Sr_2Ca_2Cu_3O_{10+x}$. Lines corresponding to 2223 phase are denoted by *H* and those of 2122 phase are denoted by *L*.

technique. The sample was mounted on a copper plate with a well calibrated platinum resistance thermometer (PRT). This plate was vertically moved over the level of liquid nitrogen in a dewar.

The irradiation was done at the Nuclear Science Center, New Delhi. A 16 UD Tandem accelerator of the Van de Graff type was used for the implantation of 75 MeV ^{58}Ni with charge state +5 in the sample. The well collimated high energy heavy ion beam of diameter 3 mm was used to irradiate at near perpendicular incidence. The dimension of the sample was approximately $4 \times 1.5 \times 0.5\,mm^3$.

The on-line *in-situ* resistivity measurements were made with the conventional four probe technique by using a Keithley constant current source and a nanovoltmeter. The direction of the current was changed during the process of taking the readings and each resistivity value represents the average of two readings. Initially the beam current was adjusted to 0.2 pnA and found that due to thermal heating arising out implantation the resistivity changed with time. Thus the readings were recorded by stopping the beam at definite intervals and allowing the resistivity to reach a steady state. When the beam current was increased

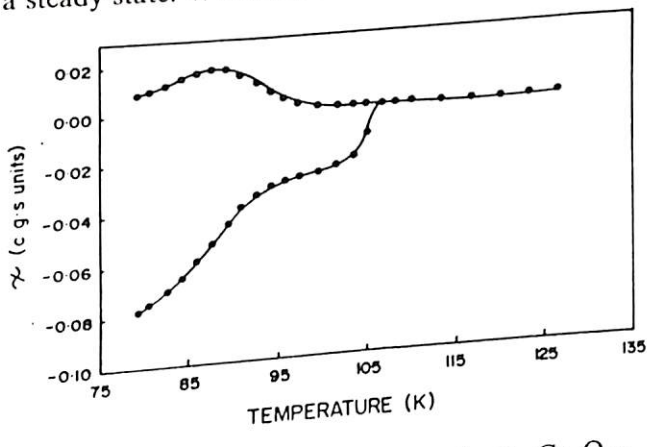

Fig. 2. A.c. susceptibility of $Bi_{1.7}Pb_{0.35}Sr_2Ca_2Cu_3O_{10+x}$ before irradiation.

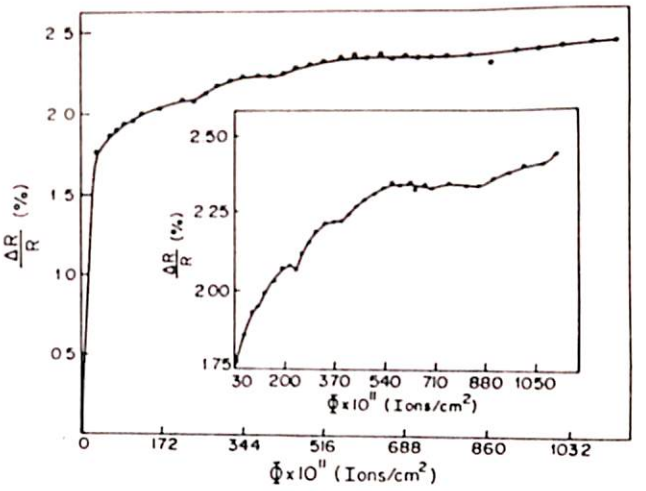

Fig. 3. Normalized electrical resistivity measured *in-situ* at room temperature as a function of ^{58}Ni fluence and the inset shows the details of the variation in resistivity at low fluence.

to 0.4 pnA, the time of stabilization was also increased.

3. RESULTS AND DISCUSSION

The variation of normalized resistivity with fluence is shown in Fig. 3. A sharp increase in the normalized resistivity (1.75%) was observed with a low fluence of 32.4×10^{11} ions cm^{-2}. The expanded details of increase in the normalized resistivity with fluence is shown is the inset to Fig. 3. Although comparatively small from the sharp increase, a monotonous increase in normalized resistivity was observed up to 500×10^{11} ions cm^{-2}. On close observation, the data clearly reveals at least three local minima at fluences of 250, 400 and 570×10^{11} ions cm^{-2} respectively. However, beyond 800×10^{11} ions cm^{-2}, we find that there is no substantial increase in the normalized resistivity which tends to saturate. The beam current was then increased to 0.4 pnA and we find a relatively small increase in normalized resistance, but this change is not as substantial as has been observed with the fluence less than 400×10^{11} ions cm^{-2} with a beam current of 0.2 pnA. It may be mentioned here that the sample thickness is 0.5 mm and when the particle beam impinges on the sample it heats up the sample and as the beam current is increased, the temperature will further increase. This can be clearly seen from the time dependent resistivity as soon as the beam is stopped for noting down the reading. Although as mentioned we have given equal 2 min interval for all the readings with a beam current of 0.2 pnA and 5 min interval for 0.4 pnA. We assume that a 5 min interval of 0.4 pnA obtains the same thermal state as that obtained by 2 min interval of 0.2 pnA.

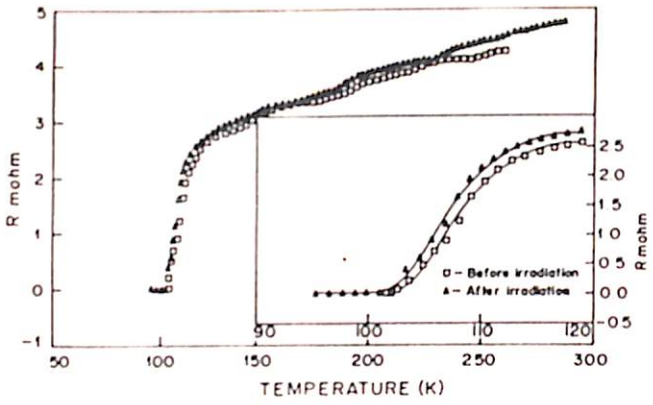

Fig. 4. Off-line measurement of the resistance of the sample as a function of temperature before and after irradiation. Inset shows the details of the data in the temperature range 120 to 90 K.

Figure 4 shows the off-line experiment of resistance of the sample as a function of temperature before irradiation and after irradiation. As can be seen from the figure, an overall fluence of 1139.5×10^{11} ions cm^{-2} increases the normalized resistivity by 2.5% but the T_c which was 103 K before irradiation does not change appreciably. The inset to Fig. 4 presents the data in the temperature range 90 to 120 K, this reveals that although the width of the transition does not change appreciably as a result of the irradiation, a shift of the curve can be observed to lower T_c.

We are not in a position to explain these results as the exact mechanism of creation of defects in these high T_c superconductors is not known. However, it has generally been observed that the bombarding ion while traversing through the crystal, loses its energy either by electronic excitations or nuclear collisions. In case of nuclear collisions, it will transfer energy to the target atoms, with maximum transfer to those atoms whose atomic mass are of the same order as that of the projectile ion (here it is ^{58}Ni ions). Thus, the radiation effect on the specimen depends on primarily knock-on atom spectrum. As a result, there will be a formation of defect cascades which are reported to be important for the enhancement of J_c (critical current) in high T_c superconductors [10]. The atomic radius of Cu ions is of the same order as that of Ni, and moreover, it has been observed that Ni ions can be easily substituted chemically at the copper site [11]. Therefore, the implantation of Ni ions could produce similar site substitution as has been observed by chemical substitutions. This is further supported by our observation that T_c does not change at this fluence. The transition temperature is dependent on the density of electron states which in turn reflects the copper–oxygen coordination [12]. As this has not appreciably changed, substitution of Cu by Ni is a likely possibility. From Fig. 4, the systematic change of resistivity of the irradiated sample through the entire temperature range of study clearly indicates that the defects which are created at room temperature, are of the same nature at all temperatures. It is probable that these are vacancy interstitial Frenkel pairs. The saturation of resistivity at higher fluence may be explained as due to the formation of stable Frenkel pairs which shows an exponential build up [13]. Secondly, in this sample both the 2223 phase and the 2122 phase are present, it is possible that the displaced atoms will interact with the local surroundings and preferably will try to achieve a state where its free energy is minimum. The appearance of a local minima in the on-line resistivity measurement may be the indicative of such a process.

In conclusion, we find appreciable changes in electrical transport properties of high T_c materials even at low ion fluences. To our knowledge this is the first detailed resistivity study at low ion exposures which has raised a few questions. Firstly, apart from ion induced damage, do we have a substitutional effect. If so, then what are their site symmetries. And secondly, the origin of the defects which seems to anneal.

Acknowledgement – One of us (N.S) thanks the CSIR pool scheme for financial support. We thank Prof. G.K. Mehta for encouraging this research. We also thank D. Kanjilal for assistance during irradiation. The authors are grateful to Prof. E.S. Rajagopal, for his keen interest in the work.

REFERENCES

1. A. Iwase, N. Watanabe, T. Iwata & T. Nihira *Jpn. J. Appl. Phys.* **28,** L1939 (1989).
2. A.D. Marwick, G.J. Clark, D.S. Yee, R.B. Laibowitz, G. Coleman & J.J. Cuomo, *Phys. Rev.* **B39,** 9061 (1989).
3. P. Vasek, L. Smrcka, J. Dominec, M. Pesek, O. Smreckova & D. Sykorova, *Solid State Commun.* **69,** 23 (1989).
4. T. Kato, N. Watanabe, Y. Kajumata, H. Naramoto, T. Iwata, Y. Ikeda, H. Maekawa & T. Nakamura, *Jpn. J. Appl. Phys.* **27,** 2097 (1988).
5. J. Bohandy, J. Suter, B.F. Kim, K. Moorjani & F.J. Adrian, *Appl. Phy. Lett.* **51,** 2161 (1987).
6. K. Shiraishi, H. Itoh & T. Kato, *Jpn. J. Appl. Phys.* **30,** L894 (1991).
7. T. Ishibashi, N. Inuishi & O. Yoda, *Jpn. J. Appl. Phys.* **30,** L1250 (1991).
8. P. Muller, H. Gerstenberg, M. Fischer, W. Schindler, J. Strobl, G. Sacmann-Ischenco & H. Kammermeier, *Solid State Commun.* **65,** 223 (1988).
9. J.R. Cost, J.O. Willis, J.D. Thompson & D.E.

Peterson, *Phys. Rev.* **B37,** 1563 (1988).
10. Y. Li, C. Ren, G. Chen & S. Zou, *J. Appl. Phys.* **69,** 7915 (1991).
11. A.V. Narlikar, in *International Conference on Superconductivity – ISCSC Jan 10–14, 1990, Bangalore, India* (Edited by S.K. Joshi, C.N.R. Rao & S.V. Subramanyam), p. 103, Singapore, World Scientific (1990).
12. J.G. Bednorz & K.A. Müller, *Rev. Mod. Phys.* **60,** 585 (1988).
13. B.L. Oxengendler & Yu. M. Tsipenyuk in *Progress in High Temperature Superconductors* Vol. 21, p. 373 (Edited by V.L. Aksenov, N.N. Bogolubov & N.M. Plakida), Singapore, World Scientific (1990).

Supercond. Sci. Technol. 8 (1995) 745–750. Printed in the UK

Effect of Fe substitutions on the magnetism and superconductivity of $YBa_2Cu_3O_{7-y}$ system with variable oxygen content

V P S Awana†§, R Lal†, Deepak Varandani†, A V Narlikar† and S K Malik†

† National Physical Laboratory, Dr K S Krishnan Road, New Delhi-110012, India
‡ Tata Institute of Fundamental Research, Homo Bhabha Road, Colaba, Bombay-400 005, India

Received 13 April 1995

Abstract. Magnetic and superconducting behaviours of fully oxygenated and oxygen-deficient $YBa_2Cu_{3-x}Fe_xO_{7-y}$ systems have been studied for $x = 0$, 0.09 and 0.21. With increasing Fe content, orthorhombic distortion of fully oxygenated samples ($y = 0.1$) decreases, while it recovers partially for oxygen-deficient samples ($y = 0.37$). In the normal state, the effective paramagnetic moment per Fe is found to be 4.65 μ_B ($x = 0.09$) and 4.05 μ_B ($x = 0.21$) in fully oxygenated samples and 2.93 μ_B ($x = 0.09$) and 1.93 μ_B ($x = 0.21$) in the case of oxygen-deficient samples. The T_c depression rate with Fe substitution is found to be retarded from about 5 K/at.% to about 3 K/at.% when oxygen is depleted from fully oxygenated samples. Oxygen iodometry results indicate that in both cases, the effective copper valence of the system decreases with increasing Fe content. It has been argued that the magnetic moment of Fe in different samples arises from the competition of the $3d_{x^2-y^2}$–$3d_{3z^2-r^2}$ energy separation with the interactions which lead to Hund's rules. The magnetic moment of Fe does not appear to be the main source of T_c degradation in the present case. Hole filling and direct suppression of the pairing interaction are perhaps the dominant factors in T_c degradation.

1. Introduction

Site substitutional studies in high temperature cuprate superconductors are of considerable interest from both theoretical and experimental considerations [1]. Of all the cationic sites, Cu sites are thought to be of prime importance as superconductivity is primarily supposed to reside in the CuO_2 planes. For substitutions at Cu sites, 3d metallic elements possess certain favourable features due to their compatible ionic sizes and closer orbital structures to that of copper [1, 2]. Further, incorporation of magnetic 3d elements provides an interesting prospect of the possible interplay of magnetism and superconductivity occuring in the doped materials. In this paper, we study the effect of the Fe substitution in the $YBa_2Cu_{3-x}O_{7-y}$ (Y-123) system.

Of the 3d elements, Ni and Zn substitute mainly at the Cu(2) site of the CuO_2 planes of the Y-123 unit cell, while trivalent Fe, Co and Ga substitute mainly at the Cu(1) site of Cu–O chains [1, 3, 4]. Fe substitutes at the Cu(1) site in its trivalent state and, as a result, in the case of an optimally oxygenated sample, increases the oxygen content of the parent system and thus causes a decrease in the orthorhombicity and carrier concentration of the component [5, 6].

The orthorhombicity of Y-123 i.e. the measure of difference between the a and b lattice parameters is known to be due to the missing oxygen atoms at 05 sites along the a direction orthogonal to the Cu–O chains [7, 8]. With Fe substitution, 05 sites start to get filled and the system tends to become tetragonal [6] with a relatively enlarged a axis [9, 10]. In the case of the oxygen-deficient Y-123 system, apart from the vacancy at the 05 position, there also arises a vacancy at the 01 site, thereby reducing the lattice parameter b, or equivalently, decreasing the orthorhombic character. Thus, like Fe substitution, oxygen deficiency also reduces the orthorhombic character of the Y-123 system. The difference in the two situations is that, while in the case of Fe substitution reduction of orthorhombic character is due to an increase in the a parameter (b fixed), in the case of oxygen deficiency, it is due to a decrease in the b parameter (a fixed). It would therefore be interesting to study how these two different effects combine when both oxygen deficiency and Fe substitution are present simultaneously in the Y-123 system.

§ Now at TIFR, Bombay.

0953-2048/95/100745+06$19.50

The the other interesting aspect which we have studied in the present investigation relates to the effects of the above factors on the magnetic moment at the Fe sites. This, we hope, may provide some insight into the mechanism of T_c degradation in the Fe-doped Y-123 system. For this purpose we have investigated the effects of Fe substitution in both fully oxygenated and oxygen-depleted Y-123 samples.

2. Experimental details

Samples of Y-123 were prepared by the conventional solid-state reaction route with the ingredients Y_2O_3, $BaCO_3$, CuO and Fe_2O_3 of better than 4N purity. Samples prepared in the normal fashion i.e. oxygenated after several calcinations at 930 °C for 24 hours and then furnace cooled to room temperature with an intervening annealing for 12 hours at 600 °C are denoted as set I.

To make oxygen-deficient samples, the above samples from set I were further heated at 400 °C for 12 hours in flowing argon and subsequently furnace cooled to room temperature; these samples are denoted as set II. All the samples were characterized for their phase purity, and their lattice parameters were determined at room temperature using a JEOL x-ray diffractometer using Cu Kα radiation. For superconducting properties, the samples were characterized with a SQUID magnetometer in a dc field of 50 G in both field-cooled and zero-field-cooled conditions. For the magnetism part, samples were further studied in their normal state, i.e. above T_c in an applied dc field of 5000 G. The effective copper valence was determined by the conventional iodometric titration technique [11, 12]. The oxygen content was then calculated, assuming Y to be in 3^+, Ba in 2^+ and Fe in 3^+ valence states.

3. Results and discussion

Before describing our results, it is worth mentioning recent findings of Fe substitution in Y-123, where it is shown that Fe migrates to planes from chains, when the samples are reduced and subsequently reoxidized [13]. For this, the reduction is carried out at around 800 °C and reoxidation at 400 °C. In our case, however, we have neither reduced the samples at such a high temperature nor reoxidized them, and thus the possibility of migration of Fe from Cu–O chains to Cu–O planes is expected to be remote. Consequently, in the case of both fully oxygenated and oxygen-deficient samples, Fe is believed to substitute mainly in the Cu–O chains.

3.1. Orthorhombicity

XRD patterns revealed the single-phase nature of all the samples in sets I and II. Lattice parameters were obtained by a least-squares analysis of the observed distances between crystal planes. The orthorhombic distortion of all the samples from sets I and II is depicted in figure 1. In the case of set I, the orthorhombic distortion decreases with an increase in Fe concentration, which is in good agreement with various other reports [3, 5, 9]. It may be observed

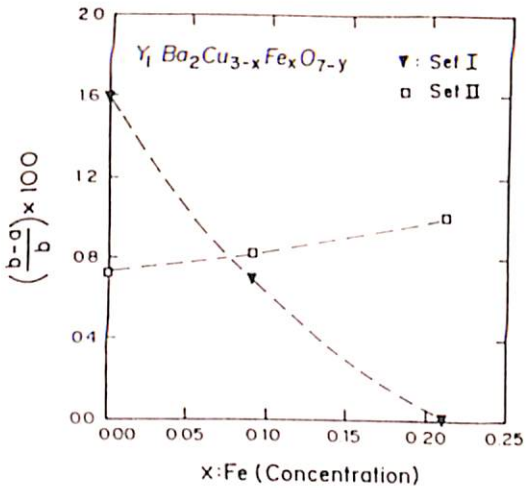

Figure 1. Orthorhombic distortion versus Fe concentration for both set I and set II samples.

that the orthorhombic distortion persists up to 7 at.% Fe. As already mentioned, the decrease in orthorhombicity of this set of samples is due to the filling of the empty 05 site [4, 9]. In the case of the oxygen-deficient samples of set II (see table 1), which have, besides 05, some of the 01 sites vacant, the pure compound ($x = 0.0$) (of set II) is known to be less orthorhombic in comparison with the pristine compound of set I, in agreement with other reports [8, 9, 14, 15]. The values of the orthorhombic distortions for the two sets of samples are also listed in table 1. When Fe is substituted into an oxygen-deficient sample, it increases its oxygen content and as a result, some of the vacant 01 sites in the Cu–O chains are filled. Consequently, the orthorhombicity of the oxygen-deficient pristine compound increases with Fe doping. However, the increase in the orthorhombicity with Fe doping in set II samples is much smaller than its decrease due to oxygen deficiency. In fact, the Fe-doped sample of set II remains less orthorhombic than the pure sample of set I. This shows an interesting interplay between the effect of oxygen deficiency and Fe doping. Although, separately, both significantly reduce the orthorhombic distortion, when both the effects are present together, the orthorhombicity is, relatively, affected less.

3.2. Magnetism

We have carried out dc magnetization measurements on all samples to check the paramagnetic moment of the Fe ions in the system; these are shown in figures 2–5. For all the samples, a dc field of 5000 G was applied to them in their normal state. In figure 2, the normal state dc susceptibility is shown for samples from set I. The dc susceptibility of the pristine sample from set I is not shown in the figure; in fact, it is an order of magnitude lower than that observed for Fe-doped samples of the same set, and was found to be nearly temperature independent. The behaviour of the dc susceptibility shown in figure 2 can be well fitted to the Curie–Weiss behaviour given by

$$\chi = \chi_0 + \frac{C}{T + \theta}. \qquad (1)$$

Table 1. Orthorhombicity $[(b - a)/b] \times 100$, transition temperature (T_c) magnetic parameters (θ, χ_0, C), Fe moment, effective Cu valence and oxygen content for the different samples.

Sample	$[(b - a)/b] \times 100$	T_c (dia) (K)	θ (K)	χ_0 (10^{-4} emu/mole)	C	Effective paramagnetic moment (μ_B)	Effective Cu valence	Oxygen content
Set I								
$x = 0.0$	1.590	90	—	—	—	—	2.27	6.90
$x = 0.09$	0.686	78	1.5	3.0	2.72	4.65/Fe	2.25	6.92
$x = 0.21$	0.000	54	9.5	1.3	2.06	4.05/Fe	2.22	6.96
Set II								
$x = 0.0$	0.721	48	1.8	1.73	0.06	0.71/Cu	2.09	6.63
$x = 0.09$	0.821	42	9.2	1.99	1.08	2.93/Fe	2.07	6.65
$x = 0.21$	1.007	25	9.7	5.92	0.47	1.94/Fe	2.06	6.67

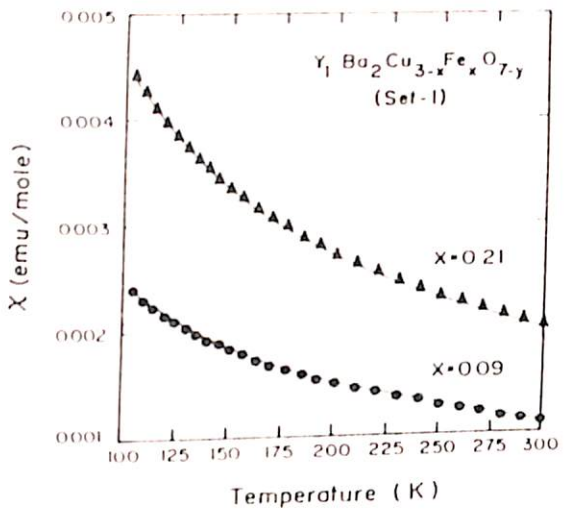

Figure 2. dc susceptibility χ versus temperature of Fe-doped Y-123 samples in their normal states for set I.

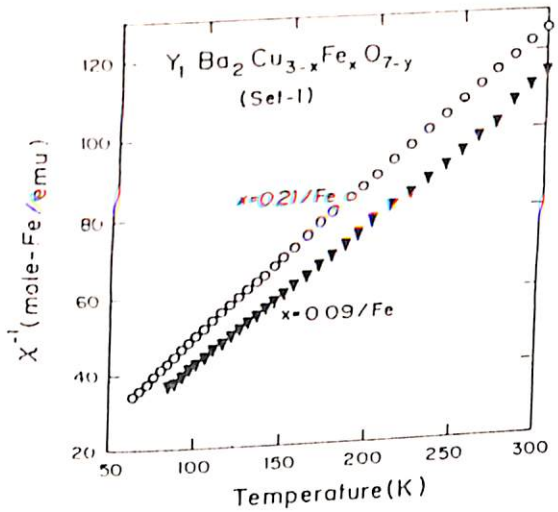

Figure 3. Inverse of dc susceptibility, $1/\chi$, versus temperature for set I samples in their normal states.

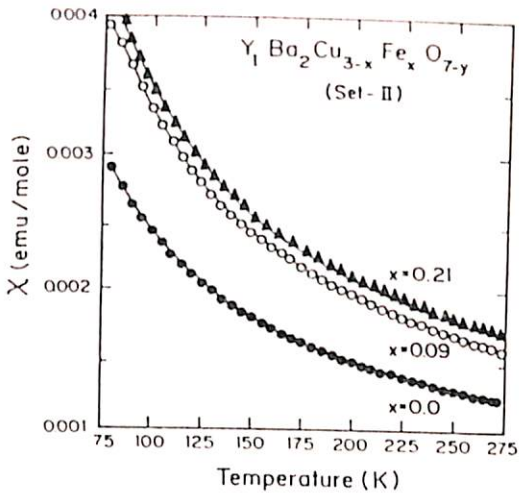

Figure 4. dc susceptibility χ versus temperature for Fe-doped Y-123 samples in their normal states for set II.

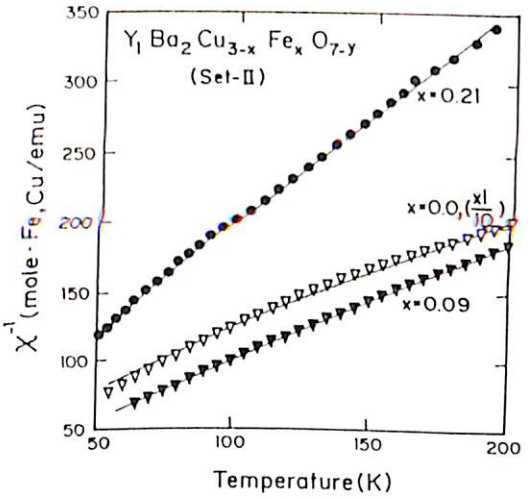

Figure 5. Inverse of dc susceptibility, $1/\chi$, versus temperature for set II samples in their normal states.

Before fitting the data of figure 2 to the above equation, we first corrected it for the molar susceptibility of the pure sample ($x = 0.0$) and then calculated the contribution per Fe in the formula unit. Subsequently, the fitting parameters were obtained for both $x = 0.09$ and $x = 0.21$ samples through a standard curve-fitting program, and these parameters are listed in table 1. The effective moment calculated for Fe in these samples was found to be 4.65 μ_B per Fe for the Fe 3 at.% sample and 4.05 per Fe for the 7 at.% Fe-doped sample. The temperature-independent part of the dc susceptibility, i.e. χ_0 was found to be in the range of 10^{-4} for both the samples (cf table 1). The value of θ was found to be lower for the Fe 3 at.% sample (1.5 K) and higher for the 7 at.% (9.5 K) sample. $1/\chi$ (corrected for

per Fe) versus temperature behaviour for these two samples from set I is shown in figure 3.

In figure 4 we show the variation of χ with temperature for the set II samples. While the dc susceptibility of the $x = 0.0$ sample of set I was found to be nearly temperature independent, the same sample after annealing in Ar at 400 °C (set II) shows a temperature dependence given by (1). For Fe-doped samples, a similar temperature dependence is also observed. After making all the corrections made for the set I samples, we obtained the fitting parameters for these samples: χ_0 is found to be of the order of 10^{-4}, and θ is found to increase with x. While the temperature-independent part χ_0 is of the same order as the set I samples, its magnitude is found to increase from $x = 0.0$ to $x = 0.21$. Effective Cu moment calculated for the $x = 0.0$ sample is found to be 0.71 μ_B per copper ion, while in the same sample of set I the Cu moment is found to be nonmagnetic. The fitting parameters i.e. C, θ, χ_0 and the effective moment per Fe or per Cu ion, are listed in table 1 for all the samples of set II.

From the values of the Fe moments (table 1) we draw the following conclusions:

(i) The magnetic moment of Fe decreases with x in both the set of samples.

(ii) The magnetic moment of Fe is significantly less in the oxygen deficient samples (set II) than in the fully oxygenated samples (set I) of the same Fe concentration.

(iii) The values of θ are small for all the samples compared to the temperature taken in the observations ($T > T_c$). Also, the values of θ for different samples are comparable with each other.

In order to understand the above findings, we may first note that in the crystalline environment the magnetic moment of Fe^{2+} (Fe^{3+}) is 5.4 μ_B (5.9 μ_B) [16]. It is supposed that the crystal field quenches the orbital angular momentum [16]. The magnetic moment estimated in the present case (table 1) is smaller than these values. Since the values of θ are similar in the cases of the samples of the two sets, we cannot attribute the large reduction of Fe moment in set II to the effects of the Cu moments.

In order to find a reasonable source of the reduction of Fe moments in the oxygen-deficient samples, we note that when the interaction leading to Hund's rules, say I_H, is larger than the energy separation between the $3d_{x^2-y^2}$ and $3d_{3z^2-r^2}$ states [17], say E_d, the spin of the Fe^{2+} (Fe^{3+}) impurity will be $S = 2$ (5/2). This leads to an Fe moment closer to 5.4 (5.9) [16]. Now, suppose the energy difference E_d increases and becomes much larger than I_H. Then Hund's rules will no longer apply, and the Fe moment will be governed by the spin, determined on the basis of the occupancy of the $3d_{x^2-y^2}$ and $3d_{3z^2-r^2}$ (and $3d_{xy}$) states. For Fe^{2+}, there will be two holes in each of the $3d_{x^2-y^2}$ and $3d_{3z^2-r^2}$ states. Since Hund's rule applies no longer, the two holes pair with opposite spins in the $3d_{x^2-y^2}$ and $3d_{3z^2-r^2}$ states so that finally $S = 0$ (1/2) for Fe^{2+} (Fe^{3+}). This corresponds to a reduction of the moment on Fe.

In view of the above, we may say that the reduction of Fe moments in the Fe-doped Y-123 samples is due to competition between the interaction I_H and energy E_d. The more E_d competes with I_H, the less the Fe moment will be. On the basis of figure 1, the different samples of Fe-doped Y-123 (from sets I and II) correspond to different degrees of orthorhombic distortion. But orthorhombic distortion will change the energy separation E_d: on the basis of figure 1, we expect E_d to change in the following order: E_d (7% Fe, set I) < E_d (3% Fe, set I) < E_d (3% Fe, set II) < E_d (7% Fe, set II). Then, since in view of the above, the Fe moment will decrease with increasing E_d, we find that the Fe moment p will vary in the order: p (7% Fe set I) > p (3% Fe set I) > p (3% Fe, set II) > p (7% Fe, set II). Except for the 7% Fe (set I) sample, this qualitative variation agrees with the experimental results of table 1. This shows that orthorhombic distortion plays a significant role in determining the Fe moment. However, because there is disagreement with the Fe moment of the 7% set I sample, there should be some other factor influencing the Fe moment. This may be ascribed to the greater proportion of oxygen in the 7% Fe (set I) sample, leading to the Fe 3d–0 2p hybridization, which reduces the interaction I_H so that effectively E_d will be greater than that for the 3% (set I) sample. If this is so, the moment of the 7% Fe (set I) sample is expected to be less than that of the 3% Fe (set I) sample.

3.3. Superconductivity

In order to see the implications of the behaviour of the magnetic moment of Fe, we consider the transition temperature of various samples of sets I and II. The T_c values are estimated from the dc susceptibility data. Figure 6 depicts the dc susceptibility in (emu/g) for some of the set I and II samples, obtained in a dc field of 50 G in both zero-field-cooled and field-cooled conditions. For the sake of brevity, plots for each and every sample are not shown: the T_c defined as the onset of diamagnetism is plotted in figure 7 for all the samples. While the T_c depressions are not exactly linear either in set I or II, it is interesting to note from figure 7 that the average rate of T_c depression defined as dT_c/dx is less in the case of set II than in set I. In the case of set I it is nearly 1.5 times

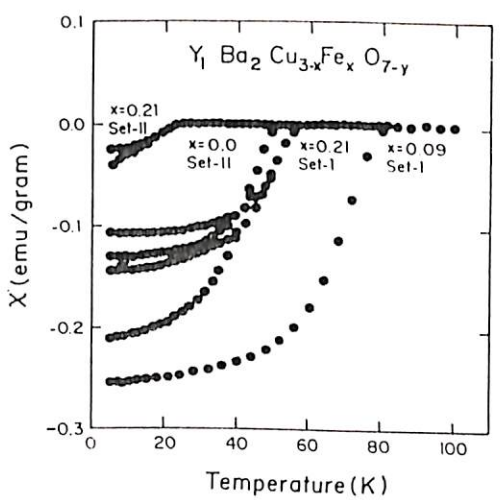

Figure 6. dc susceptibility versus temperature for both set I and set II samples. Applied dc field is 50 G.

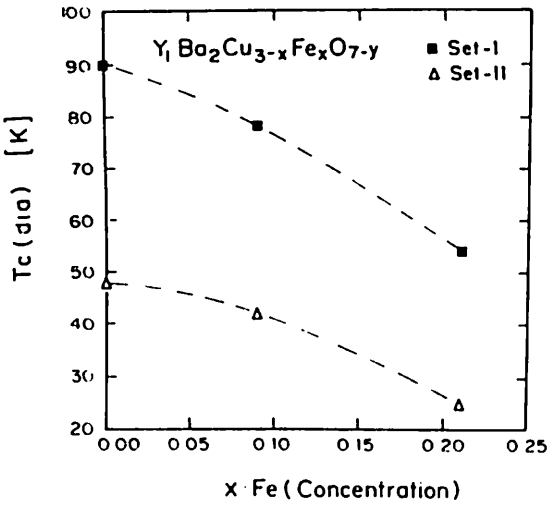

Figure 7. T_c(dia) versus Fe concentration for both set I and set II samples.

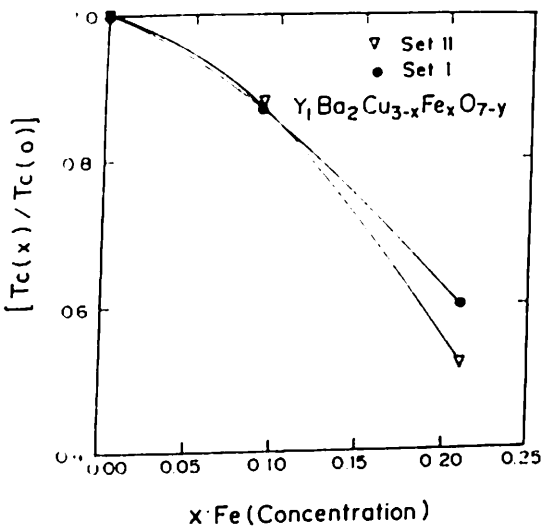

Figure 8. Reduced T_c (T_c/T_{co}) versus Fe concentration plot for both set I and set II samples.

larger than for set II (see table 1). It is again interesting to note that while T_c depression rates are different for the two sets of samples, the reduced T_c versus x plot for both sets lies on the same curve (see figure 8). Except for a little difference for the $x = 0.21$ samples, the data of both sets lie on the same curve. This means that the relative depression of T_c is similar in both sets of samples.

Let us compare the effect of Fe in causing T_c depression with that due to other dopants such as Ga and Al which, like Fe, also substitute at the Cu(1) site of the 1-2-3 structure. Nonmagnetic Ga and magnetic Fe substitute at the Cu(1) site with nearly the same effect on the number of holes and orthorhombicity, but comparatively the effect of Fe is more drastic on superconductivity [1, 15]. As far as Al substitution is concerned, the situation is not so transparent. Tarascon *et al* [9] have shown that Al has a less deleterious effect on T_c than Fe, while Xu *et al* [10] reported that both Al and Fe have comparable effects. In any case, the criterion for the pair breaking effect does apparently not relate to the possible magnetic (as for Fe) and nonmagnetic states (as for Al) of these two cations. Furthermore, the present results reveal that the magnetic moment of Fe decreases with χ, and interestingly for both the sets of samples, T_c decreases faster in the concentration range of $x = 0.09$ to $x = 0.21$ than in the range of $x = 0.0$ to $x = 0.09$. Consequently, the magnetic pair breaking seems unlikely to be the main cause of the T_c depression. Moreover, since the disorder effect of Fe will be stronger in the oxygen-deficient samples where the suppression of T_c with χ is comparatively less, the localization or mean-free-path effects also do not appear to be the main reasons for the suppression of T_c. The other possibilities of T_c depression could be either hole filling or direct suppression of the effective pairing interaction. Recent studies of T_c degradation in the Fe- (and Ni-)doped $YBa_2Cu_4O_8$ system [18], and also in some other cuprate superconductors [19], provide a credence to the contention of direct suppression of the effective pairing interaction by these dopants. Our previously reported work using XANES [20] and XPS [21] on Fe- and Ni-doped Bi-2212 system seems to corroborate this view as the results indicate a decrease in the density of states (DOS) at E_f with Fe and Ni substitutions which cause depression in T_c.

4. Conclusions

In summary, the magnetism and superconductivity of the Fe-doped Y-123 system is studied with variable oxygen content. While the orthorhombic distortion of the parent compound decreases in the case of fully oxygenated Fe-doped Y-123, it gains partial recovery in the oxygen-deficient Fe-doped samples. All Fe-doped samples, both oxygenated and oxygen-reduced, follow the Curie–Weiss paramagnetism from which the free Fe moment has been calculated, which to the first approximation appears to decrease in the oxygen-deficient samples. Also, the moment of Fe decreases with its concentration in both sets of samples. A possible cause of this appears to be the competition between the $3d_{x^2-y^2}$–$3d_{3z^2-r^2}$ energy separation and the interaction leading to Hund's rules. The values of the estimated magnetic moment of Fe in different samples rule out the possibility of pair breaking as a source of T_c degradation. Hole filling and/or direct suppression of the pairing interaction turn out to be possible sources of the T_c decrease manifested in the Fe-doped system. The process of the moment formation of Fe seems to correlate indirectly with the mechanism of T_c degradation.

Acknowledgments

The authors at NPL thank Professor S K Joshi, Director-General, CSIR and the President, Indian National Science Academy, New Delhi for his continued interest and encouragement in our superconductivity work.

References

[1] Narlikar A V, Agarwal S K and Narasimha Rao C V 1989 *Studies of High Temperature Superconductors* ed A Narlikar vol I (New York: Nova) p 343

[2] Xio G, Cieplak M Z, Garvin A, Streitz F H, Chien C L, Rhyne J J and Gotaas J A 1988 *Nature* **332** 238

[3] Tarascon J M, Barboux P, Miceli P F, Green L H, Hull G W, Eibschultz M and Sunshine S A 1987 *Phys. Rev.* B **36** 8393
[4] Takayama-Muromachi E, Uchida Y and Kato K 1987 *Japan. J. Appl. Phys.* **26** L2087
[5] Xu Y, Suenaga M, Tafto J, Sabatini R L, Moodenbough A R and Zolliker P 1989 *Phys. Rev.* B **39** 6667
[6] Gio G, Streitz F H, Garvin A, Du Y W and Chien C L 1987 *Phys. Rev.* B **35** 8782
[7] Calastini G and Rizzoli C 1987 *Nature* **328** 606
[8] Ourmazd A, Renteschler J A, Spence J C H, Keeffe M O, Grahm R J, Johnson Jr D W and Rhodes W W 1988 *Nature* **328** 606
[9] Tarascon J M and Bagley B G 1993 *Chemistry of High T_c Materials* ed A Vanderaha (NJ: NOYES) p 310
[10] Xu Y, Sabatini R L, Moddenbaugh A R, Zhu Y, Shyu S G, Suenaga M, Dennis K W and McCallum R W 1990 *Physica* C **169** 205
[11] Harris D C and Hewston T A 1987 *J. Solid State Chem.* **69** 182
[12] Nazzal A I, Lee V Y, Engler E M, Jacowitz R D, Tokura Y and Goodenough J B 1988 *Physica* C **153–155** 1367
Harris D C 1993 *Chemistry of High T_c Materials* ed T A Vanderaha (NJ: NOYES) p 609
[13] Qiu Z Q, Du Y W, Tang H and Walker J C 1989 *J. Magn. Magn. Mater.* **78** 359
Katsuyama S, Ueda Y and Kosuge K 1990 *Physica* C **165** 404
[14] Cava R J, Hewat A W, Hewat E A, Batlogg B, Marezio M, Rabe K M, Karjewski J J, Peck Jr W F and Rupp L W 1990 *Physica* C **165** 419
[15] Jorgenson J D, Veal B W, Paulikas A P, Nowicki L J, Crabtree G W, Claus H and Kwok W K 1991 *Phys. Rev.* B **41** 1863
[16] Kittel C 1976 *Introduction to Solid State Physics* 5th edn (New York: Wiley) p 443
[17] Pickett W E 1989 *Rev. Mod. Phys.* **61** 433
[18] Lal R, Awana V P S, Pandey S P, Yadav V S, Varandani D, Narlikar A V, Chikara A and Gmelin E 1995 *Phys. Rev.* B **51** 539
[19] Lal R 1995 *Phys. Rev.* B at press
[20] Rao K V R, Garg K B, Agarwal S K, Awana V P S and Narlikar A V 1992 *Physica* C **192** 419
[21] Kulkarni P, Kulkarni S K, Nigavekar A S, Agarwal S K, Awana V P S and Narlikar A V 1990 *Physica* C **166** 530